

STRUCTURE AND ENZYMOLOGY OF THE CHEMOTAXIS HISTIDINE KINASE, CHEA

A Dissertation

Presented to the Faculty of the Graduate School

of Cornell University

In Partial Fulfillment of the Requirements for the Degree of

Doctor of Philosophy

by

Anna Rusch Greenswag

January 2015

© 2015 Anna Rusch Greenswag

STRUCTURE AND ENZYMOLOGY OF THE CHEMOTAXIS HISTIDINE KINASE, CHEA

Anna Rusch Greenswag, Ph. D.

Cornell University 2015

Bacterial chemotaxis enables changes in motility via response to the surrounding chemical environment and is noted for its high signal gain, range, and sensitivity. The efficacy of the bacterial chemotaxis signaling pathway is highly dependent on the propagation of the extracellular chemical signal through a hexagonal array comprised of: methyl-accepting chemotaxis protein receptors, histidine kinase CheA, and coupling protein CheW. CheA is the principal enzyme in the chemotaxis pathway and is composed of five domains (P1-5). Initiation of the phospho-relay by CheA ends in rotational switching of the flagellar rotor. CheA only achieves a broad range of autophosphorylation activity when associated with chemoreceptors.

This dissertation focuses on the structural and biochemical changes during the CheA autophosphorylation event. The propensity of *Thermotoga maritima* CheA to naturally undergo trans autophosphorylation was elucidated and strategic mutations enabled generation of disulfide-locked CheA variants to further probe protein dynamics. Employing small-angle x-ray scattering (SAXS), the resting state of CheA was determined to be globular. Where upon nucleotide addition the protein transitioned to a dynamic state as a result of the movement of P1 and P4 domains to facilitate transfer of the γ -phosphate. Coupling crystallographic and biochemical data, a model was generated of CheA that is able to account for variances in enzymatic activity, incorporating key structural features to the functional response of signal

transduction. To further the understanding the influence the receptors impart to CheA, chemoreceptor cytoplasmic kinase-control modules based on the *E. coli* aspartate receptor, Tar, were covalently fused into a dimer and trimerized by a foldon domain (Tar_{FO}). SAXS, multi-angle light scattering, and pulsed-dipolar electron paramagnetic resonance spectroscopy of spin-labeled proteins indicate that the Tar_{FO} is soluble, monodisperse, and assembles into homogenous trimers wherein the protein interaction regions closely associate at the opposite ends of the foldon domain. The Tar_{FO} activates CheA autophosphorylation to the same degree as membrane integrated receptors and stabilizes a planar conformation of the kinase consistent with current array models for the assembly state of the ternary complex. Overall, these studies illuminate a planar CheA active structure and provide a more in depth investigation of the CheA autophosphorylation event.

BIOGRAPHICAL SKETCH

Anna grew up in Roseville, Minnesota with parents Linda Rusch and Douglas Greenswag along with an older sister Kari Greenswag. She graduated from Roseville Area High School with an interest in science and a desire to live on the west coast. Matriculating at Willamette University, she quickly chose to major in Chemistry and minor in Mathematics. She joined multiple clubs including Angles-Queer-Straight Alliance, Chemistry Club, and 2009 Class Council to expand her impact on the university. Angles organized group events to support multiple ways of life both on and off campus. Chemistry Club would perform demonstrations at local elementary schools to increase interest in science. Class Council organized events for the 2009 class to improve interactions between students in different disciplines.

Anna spent the summer of 2007 working for Dr. Sarah Kirk in the Science Collaborative Research Program (SCRIP) at Willamette University generating tetracaine derivatives to specifically interact with cyclic nucleotide gated ion channels. To expand on this work, she continued this project in the summer of 2008 as a Murdock Scholar at Oregon Health and Science University (OHSU) with Dr. Jeffery Karpen. This work allowed her to present at multiple conferences within Oregon. As a result, Dr. Sarah Kirk nominated her to receive the Portland Section ACS James G. Anderson scholarship for her senior year. The tetracaine project became her undergraduate thesis. After graduation, Anna matriculated at Cornell University for more synthetic experience.

While at Cornell University she initially worked for Dr. Chad Lewis on biomimetic catalysts. After passing her candidacy exam, she wanted to focus on biochemistry, and joined Dr. Brian Crane's lab, focusing on protein behavior and interactions. After graduation, Anna will begin a postdoctoral position with NIBR in Cambridge, MA.

For Sidney Greenswag.

ACKNOWLEDGMENTS

First and foremost, I want to thank Dr. Brian Crane for his support, consideration, and guidance throughout graduate school. He is an amazing advisor and person that made it possible for me to obtain my degree. I would also like to recognize my former and current committee members, Dr. David Collum, Dr. William Dichtel, Dr. Hening Lin and, Dr. Richard Cerione, for always supporting my work and giving advice over the years.

I would like to thank the Crane lab group members for being very welcoming to a newcomer to the field: Xiaoxiao and Ria for mentoring me. Thomas and Sarah for helping me as part of the morning shift and answering lots of questions. Camille, Nattakan, and Alise for being great office mates. Karen was always a resource for modeling and crystal processing questions. Estella Yee and I could always reminisce about our time at Willamette University. Greg, Dipanjan, and Craig were always good for a laugh along with instrument help. Sophie Ruff was fun to have around lab. Finally, our newest lab members, Mike and Angela, were a joy to be around. And a special thank you to Mike and Alise for helping edit my thesis.

Dr. Richard Gillian and others at CHESS and APS were always a great help for collecting and processing data. So many others in the chemistry department have lent a hand, specifically Clint in the Cerione group. My thanks also to all the staff in the chemistry department because they made my days better and always loved my baking, especially Dave and Larry.

Finally, I would like to thank my family for supporting me in every decision I have made both personally and professionally.

TABLE OF CONTENTS

Biographical Sketch	iii
Dedication	iv
Acknowledgements	v
List of Figures	x
List of Tables	xiii
Abbreviations	xiv
Chapter 1: Introduction	
1.1: Chemotaxis Background	1
1.2: The Histidine Kinase, CheA	3
1.3: Coupling Protein, CheW	8
1.4: Methyl-accepting chemotaxis protein receptor, MCP/chemoreceptor and Signal Feedback	9
1.5: MCP receptor array	12
1.6: CheY and phosphatases	13
1.7: The Flagellar motor	14
1.8: Summary	15
References	17
Chapter 2: A preformed soluble chemoreceptor complex that mimics cellular assembly states and activates CheA	
2.1: Introduction	24
2.2: Materials and Methods	26
2.2.1: Construction and cloning of the trimer-of-dimers mimetics	26

2.2.2: Cloning, mutagenesis, and spin labeling of proteins	28
2.2.3: Multi-angle light scattering (MALS)	28
2.2.4: Small-angle x-ray scattering (SAXS)	29
2.2.5: Protein interactions by pull-down	29
2.2.6: CheA autophosphorylation assay	30
2.2.7: Pulsed-dipolar EPR spectroscopy	31
2.2.8: Quantification of flagellar rotation patterns	32
2.2.9: Methylation status of recombinant Tar variants	32
2.3: Results	33
2.3.1: Oligomerization state of the Tar _{FO} mimetics	34
2.3.2: Globularity of the Tar _{FO}	35
2.3.3: The MCP PIRs associate in Tar _{FO}	36
2.3.4: CheA kinase activation by Tar _{FO}	37
2.3.5: Interactions of Tar variants with CheA:CheW	42
2.3.6: Effects of Tar _{FO} on CheA conformation	43
2.3.7: Cellular activities of Tar _{FO}	46
2.4: Discussion	47
2.4.1: Structural considerations of soluble receptor mimics	47
2.4.2: Effects of Tar variants on CheA activity	48
References	51
Chapter 3: Probing the dynamics of <i>Thermotoga maritima</i> histidine kinase CheA to determine domain interactions that regulate autophosphorylation activity	
3.1: Introduction	56

3.2: Materials and Methods	58
3.2.1: Construction and cloning of Δ P2 variants	58
3.2.2: Heterodimer formation and analysis	59
3.2.3: Autophosphorylation activity of Δ P2 variants	60
3.2.4: Disulfide cross linking	61
3.2.5: Small-angle x-ray scattering (SAXS)	61
3.2.6: Circular dichroism	62
3.2.7: ATP-TNP binding assay by fluorescence enhancement	62
3.3: Results	62
3.3.1: Generation of the Δ P2 variants	62
3.3.2: Activity of Δ P2 versus CheA _{FL}	63
3.3.3: Generation of CheA heterodimers to test for trans phosphorylation	64
3.3.4: P1 and P4 domain interactions as a probe of kinase activity	66
3.3.5: ATP causes dramatic changes to the dynamics of P1-P2 within CheA _{FL}	67
3.4: Discussion	73
3.4.1: Trans autophosphorylation by CheA	73
3.4.2: CheA _{FL} and 41AA dimers	73
3.4.3: P1 and P4 interactions	74
3.4.4: Dynamics of the CheA P1-P2	75
References	78

Chapter 4: Structure and Activity of a CheA kinase variant that undergoes enhanced autophosphorylation

4.1: Introduction	81
4.2: Materials and Methods	82
4.2.1: Cloning and protein purification	82
4.2.2: Activity of CheA _{FL} and separated histidine phosphotransfer and kinase domains	82
4.2.3: Crystallization and Data collection	83
4.2.4: Modeling	83
4.3: Results	84
4.3.1: Separated P1+P3P4 has higher activity than CheA _{FL}	84
4.3.2: Structure of CheA P3P4	86
4.3.3: Comparison of P3P4 to the structure of P3P4P5	87
4.3.4: Extrapolating the P3P4 structure to a full length CheA:CheW complex	89
4.3.5: A full array model based on the P3P4 structure	91
4.4: Discussion	92
4.4.1: CheA activity	92
4.4.2: CheA Domain Flexibility	94
4.4.3: A molecular model for the chemoreceptor arrays	95
References	98
Appendix	
Conclusions	101
References	103

LIST OF FIGURES

Figure 1-1:	Movement of bacterium	1
Figure 1-2:	<i>E. coli</i> chemotaxis signal transduction pathway	2
Figure 1-3:	Cartoon depiction of CheA dimer	3
Figure 1-4:	Crystal structure of the P1 domain and active site	4
Figure 1-5:	Crystal structure of the P2 domain	5
Figure 1-6:	Crystal structure of the P3 domain	6
Figure 1-7:	Active site and crystal structure of the P4 domain	6
Figure 1-8:	Crystal structure of the P5 domain	7
Figure 1-9:	Crystal structure of CheW and P5/CheW ring with Tm14	8
Figure 1-10:	Cartoon depiction of MCP dimer	9
Figure 1-11:	Crystal structures of CheB and CheR	10
Figure 1-12:	Ternary complex	11
Figure 1-13:	EM image and cartoon of array	13
Figure 1-14:	Crystal structures of CheY, CheX, and CheZ	14
Figure 1-15:	EM image of the flagellar motor	15
Figure 2-1:	Ternary complexes	25
Figure 2-2:	Foldon motif from bacteriophage T4 fibrin	26
Figure 2-3:	Schemes for cloning the Tar _{FO}	28
Figure 2-4:	Schemes of Tar receptor variants generated	28
Figure 2-5:	MALS of the Tar variants	34
Figure 2-6:	SAXS plots and envelopes of Tar variants	35
Figure 2-7:	EPR plots and visual of distances on Tar trimer-of-dimers	37

Figure 2-8:	CheA phosphotransfer reactions	37
Figure 2-9:	Radioisotope gels of CheA activity with receptors	39
Figure 2-10:	CheA activity over time with receptors	41
Figure 2-11:	MALS of ternary complexes	42
Figure 2-12:	Pulldown of <i>T. maritima</i> CheA+CheW and receptors	43
Figure 2-13:	EPR probability density with activating and deactivating receptor	44
Figure 2-14:	Flagellar rotation patterns of <i>E. coli</i> cells transformed with Tar variants	45
Figure 3-1:	CheA	56
Figure 3-2:	Δ P2 variants	59
Figure 3-3:	Phosphorimages and bar plot of Δ P2 variants	63
Figure 3-4:	SEC profiles of CheA _{FL} and P3P4P5	64
Figure 3-5:	Phosphorimages and bar plots of CheA _{FL} and Δ P2 mutants	65
Figure 3-6:	Cross linked SDS-PAGE gels and bar plot of P1*+P3P4* and P1*+ P3P4P5* over temperature and with nucleotide	66
Figure 3-7:	Cross linked SDS-PAGE gels and bar plot of CheA _{FL} * and 41AA* over temperature and with nucleotide	67
Figure 3-8:	Bar plots of P1*+ P3P4P5*, CheA _{FL} *, and 41AA* with CheW and Tm14	69
Figure 3-9:	Kratky plots of P3P4P5 and Scattering plot of CheA _{FL}	69
Figure 3-10:	Kratky plots of CheA _{FL} and Δ P2 variants	71
Figure 3-11:	CheA _{FL} Kratky plot with nucleotide in <i>T. maritima</i> and <i>E. coli</i>	71
Figure 3-12:	Kratky plots and Fluorescence of CheA D449A mutant	72
Figure 3-13:	CD profiles of CheA _{FL} and 41AA with nucleotide	72

Figure 3-14	Model of 41AA variant	76
Figure 4-1:	Activity of CheA _{FL} and separated domains	84
Figure 4-2:	CheA _{FL} and separated domains activity over time	84
Figure 4-3:	Addition of ADP to CheA _{FL} and separated domains deplete P1-P	85
Figure 4-4:	P3P4 crystal structure	86
Figure 4-5:	Overlay of P3P4 kinase domain with existing crystal structures	88
Figure 4-6:	Electron density of nucleotide within the P4 domain	88
Figure 4-7:	Electron density of Linker	89
Figure 4-8:	Grafting P4 unto the P3P4 structure	90
Figure 4-9:	Grafting CheW onto the P3P4P5 structure	90
Figure 4-10:	Modeling the 41AA variant with intact P1 domain	91
Figure 4-11:	Planar vs. orthogonal CheW/P5 ring structures	92
Figure 4-12:	Depiction of the array <i>in vivo</i>	96

LIST OF TABLES

Table 2-1	Tar _{FO} constructs generated	33
Table 2-2:	Kinetic parameters for autophosphorylation assays	42
Table 3-1:	Description of Δ P2 variants	59
Table 3-2:	Cross linking mutants defined	66
Table 4-1:	Kinetic parameters for CheA autophosphorylation assays	86
Table 4-2:	Data collection and refinement statistics for the P3P4 structure	87

LIST OF ABBREVIATIONS

ADP	Adenosine diphosphate
ADPCP	α,β -methyleneadenosine 5'-triphosphate
ATP	Adenosine triphosphate
<i>B. subtilis</i>	<i>Bacillus subtilis</i>
CCW	Counterclockwise
CD	Circular dichroism spectroscopy
CHESS	Cornell High Energy Synchrotron Source
CW	Clockwise
DEER	Double electron electron resonance
DHP	Dimerization histidine phosphotransfer
DTT	Dithiothreitol
<i>E.c. or E. coli</i>	<i>Escherichia coli</i>
ECT	Electron cryotomography
EDTA	Ethylenediaminetetraacetic acid
EM	Electron microscopy
EPR	Electron paramagnetic resonance spectroscopy
FPLC	Fast protein liquid chromatography
HAMP	Histidine kinase, Adenylyl cyclase, Methyl-accepting protein, & Phosphatase
HEPES	2-[4-(2-hydroxyethyl)piperazin-1-yl]ethanesulfonic acid
IPTG	β -D-thiogalactopyranosidase
KCM	Kinase control module

MALS	Multi-angle light scattering
MCP	Methyl-accepting chemotaxis proteins
MTS-SL	<i>S</i> -(2,2,5,5-tetramethyl-2,5-dihydro-1H-pyrrol-3-yl)methyl methanesulfonate
MW	Molecular weight
Ni ²⁺ -NTA	Nickel-nitriloacetic acid
NMR	Nuclear magnetic resonance
PAGE	Polyacrylamide gel electrophoresis
PCR	Polymerase chain reaction
PDS	Pulsed dipolar spectroscopy
PIR	Protein interaction region
PMSF	Phenylmethanesulfonyl fluoride
RR	Response regulator
SAXS	Small-angle x-ray scattering
SDS	Sodium dodecyl sulfate
SEC	Size exclusion chromatography
<i>T.m.</i> or <i>T. maritima</i>	<i>Thermotoga maritima</i>
TNP-ATP	2',3'-O-(2,4,6-Trinitrophenyl) adenosine 5'-triphosphate
Tris	2-Amino-2-hydroxymethyl-propane-1,3-diol

CHAPTER 1: INTRODUCTION

1.1: Chemotaxis background

The bacterial chemotaxis systems of *Escherichia coli*, *Bacillus subtilis*, and *Salmonella typhimurium* have been extensively studied, and are known for their high sensitivity, signal gain, and sensing range.¹⁻⁵ *E. coli* has a sensing range of five orders of magnitude, with the limit of detection of some chemoeffectors in the nanomolar range.⁶ The chemotactic signal transduction pathway enables bacteria to adapt their motility to a varying chemical environment by altering the direction of flagella rotation. In *E. coli*, the flagella rotate in either a counterclockwise (CCW) or clockwise (CW) direction. CCW rotation promotes the flagella to oligomerize into a helical bundle to propel the bacteria forward smoothly. CCW rotation is disrupted via detection of repellants or decrease in attractants, resulting in separation of one or more flagellum from the bundle by rotating clockwise (CW), causing the bacterium to tumble.^{7,8} This allows the cell to reorient roughly 60° from the previously smooth swimming direction in solution,⁹ thus enabling the cell to swim away from the source of repellants or towards the attractants (Figure 1-1).¹⁰⁻¹² The thermophile *Thermotoga maritima* proteins behave similarly to the model organisms listed above, however, have an added advantage being high stability *in vitro*.

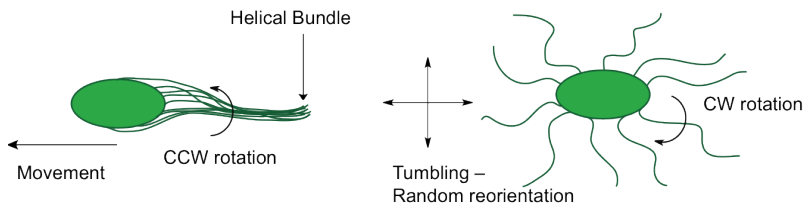


Figure 1-1: Movement of bacterium. Movement of the bacterium as a result of flagella rotation. The helical bundle formed for CCW rotation enables smooth forward swimming. CW rotation induces separation of the flagella bundle causing the bacterium to tumble and reorient.

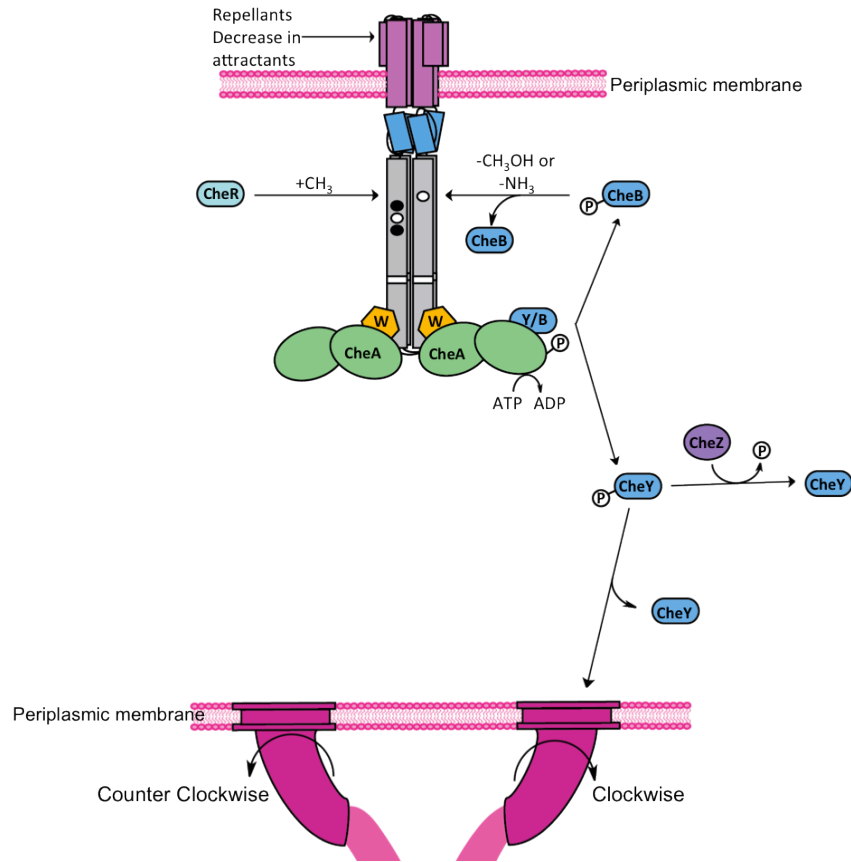


Figure 1-2: *E. coli* chemotaxis signal transduction pathway. All the proteins known to be involved in the pathway.

The bacterial chemotactic signaling cascade is defined as a two-component system^{2,13} that typically employs both a transmembrane sensor kinase and a subsequent response regulator. Together these components function cooperatively to propagate the chemoeffector signal downstream. The chemotaxis pathway is unique from other two-component systems, for the transmembrane sensor and kinase exist as distinct proteins that interact as the first component in the system. The transmembrane sensor is a methyl-accepting chemotaxis protein (MCP) with a bound cytoplasmic homodimeric histidine kinase, CheA and coupling protein CheW. In examining the transmembrane sensor component, the MCPs organize into a hexagonal honeycomb lattice¹⁴ located primarily at the pole of the cell,² where detection of a chemoeffector by the MCPs is transduced

intracellularly to CheA (Figure 1-2). The second component in the pathway is CheY, which is the primary response regulator (RR) for CheA. Subsequently, CheA interacts with CheY to facilitate the transfer of the inorganic phosphate (P) from CheA to a strictly conserved aspartate in CheY. Phosphorylated CheY (CheY-P) is then recruited to the cytoplasmic portion of the flagellar rotor.^{2,4,15-17} The 45 MDa flagellar motor is located on the lateral membrane in *E. coli*, or at the cell pole in *T. maritima*,⁵ and is the downstream output of the chemotaxis pathway.

Other components of the pathway include methyl-transferase CheR, methyl-esterase CheB (another CheA response regulator), and phosphatase CheZ. CheB and CheR are part of the signal feedback to reset the system back to pre-stimulus levels. CheZ regulates the CheY-P concentration that interacts with the flagella motor.

1.2: The Histidine Kinase CheA

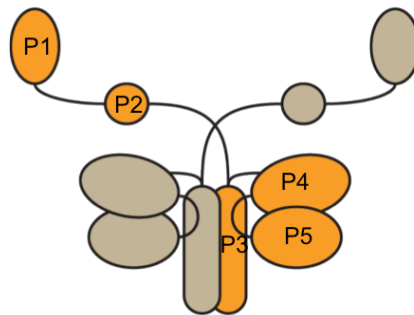


Figure 1-3: Cartoon depiction of CheA dimer. Homodimer depicted in gray and orange and the P1-5 domains labeled within one subunit.

Like most sensor histidine kinases in the GHKL (gyrase, Hsp90, histidine kinase, MutL) superfamily,¹⁸ CheA exists as a homodimer (Figure 1-3).¹⁹ Typically, sensor kinases contain a dimerization histidine phosphotransfer (DHP), kinase, HAMP (Histidine kinases, Adenylyl cyclases, Methyl-accepting chemotaxis proteins and Phosphatases), transmembrane, and ligand binding domains. CheA is unique with respect

to the GHKL superfamily as there is no transmembrane signaling domains and the histidine phosphotransfer and dimerization domains are separate, P1 and P3 respectively. In addition, the P2 is an uncommon domain that docks response regulators, CheB and CheY.

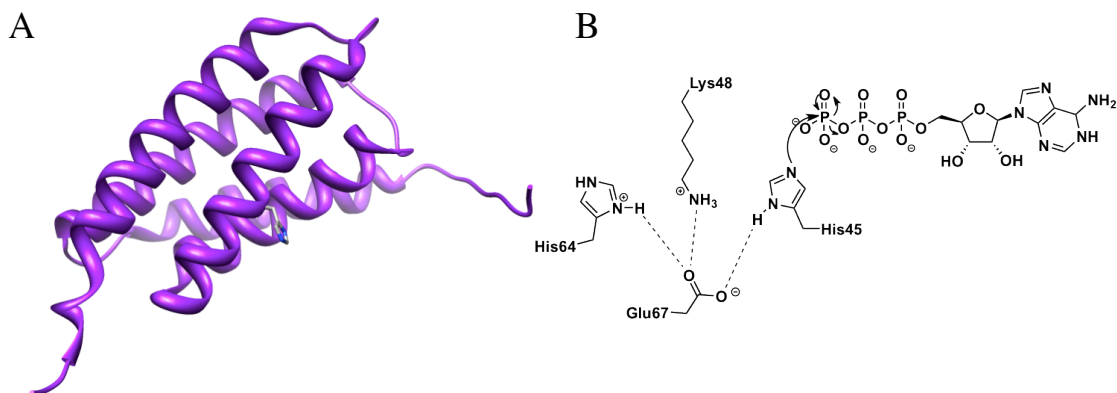


Figure 1-4: Crystal structure of the P1 domain and active site. A: NMR structure of the *E. coli* P1 domain, with His48 in gray (2LP4, purple).²⁰ **B:** *T. maritima* P1 active site interaction with ATP and subsequent stabilization of surrounding residues.²¹

The P1 domain is the histidine phosphotransfer domain. The structure is composed of four antiparallel α -helices (Figure 1-4A). Connecting the P1 and P2 domains is a linker comprised of approximately 75 residues. The first 25 residues of this linker form an α -helix that runs alongside the P1 domain.²⁰ The P1-P2 linker is quite long and flexible, enabling access to the opposing subunit's P4 domain to transfer the γ -phosphate of ATP to P1. This type of phosphotransfer is referred to as trans autophosphorylation. In *E. coli*, His48 (His45 in *T. maritima*) is responsible for accepting the γ -phosphate on its N_n position. This histidine is midway along a helix and highly solvent exposed and therefore readily accessible to the ATP substrate. This phosphorylated His (His-P) is subsequently stabilized by the residues Lys48, His64, and

Glu67 (Figure 1-4B).²¹ The P1 domain transfers the phosphate to the response regulator CheY.

The structure of the P2 domain (Figure 1-5: 1U0S)²² is composed of a beta sheet consisting of four antiparallel strands stabilized by adjacent α -helices. The P2 domain docks response regulators. CheY and CheB compete for interaction with the P2 domain and for subsequent contact with the P1 His-P.¹⁹ Both linkers on either side of the P2 domain are long and flexible,²³ thus allowing the P2 domain to move independently with respect to the rest of CheA.²⁴ Constructs without the P2 domain (Δ P2) are still able to transfer the phosphate to the response regulators,^{25,26} indicating that the presence of the P2 domain is not a requirement for phosphotransfer. Moreover, the Δ P2 variants exhibit similar autophosphorylation activity compared to native CheA *in vitro*. While P2 is known to increase CheA activity *in vivo*,²⁶ these results demonstrate that the P2 domain is not essential for CheA activity.

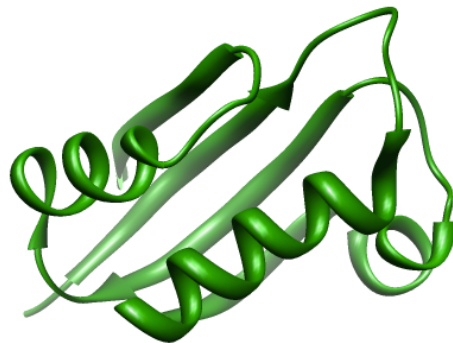


Figure 1-5: Crystal structure of the P2 domain. Crystal structure of the *T. maritima* P2 domain (1U0S, green).²²

The P3 domain is the dimerization domain of CheA that facilitates the formation of the active dimeric species. Like the P1 domain, P3 is entirely helical (Figure 1-6).²⁷ The P3 domain monomers interact via an anti-parallel coiled-coil motif to generate the

active CheA dimer (CheA₂).²⁸ While in sensor kinases, dimerization domain is also responsible for histidine phosphotransfer, for CheA these functions are separated into the P3 and P1 domains, respectively.

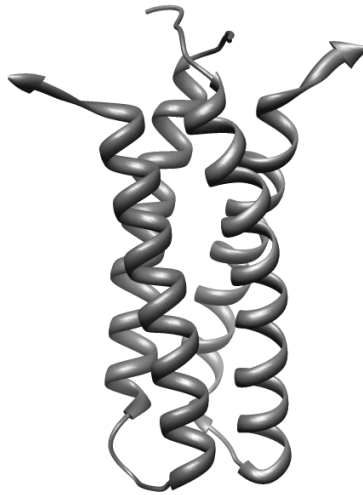


Figure 1-6: Crystal structure of the P3 domain. Crystal structure of the *T. maritima* P3 domain dimer (1B3Q, dark gray).²⁷

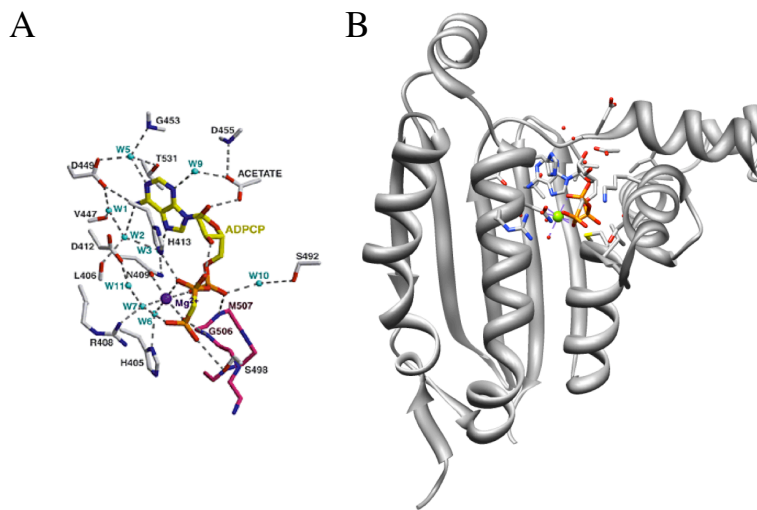


Figure 1-7: Active site and crystal structure of the P4 domain. **A:** Active site of the *T. maritima* P4 kinase with ADPCP bound. **B:** Crystal structure of the *T. maritima* P4 domain with ADPCP bound (1I58, gray).²⁹

The P4 domain binds ATP to transfer the γ -phosphate to the P1 domain (Figure 1-7A).²⁹ The nucleotide is anchored via the adenosine into the base of the active site so that the γ -phosphate that interacts with Mg^{2+} is solvent exposed. It has also been established that potassium must be present during autophosphorylation, although its explicit role is unknown. The structure of P4 (Figure 1-7B: 1I58 crystal of the P4)²⁹ contains a Bergerat-fold that is common in the class of ATPases in the GHKL family.¹⁸ A four-stranded β -sheet forms the back of the ATP binding pocket, with adjacent α -helices surrounding and stabilizing the bound nucleotide. Within the homodimer, the binding of the first ATP causes a negative allosteric cooperativity of a second ATP from being bound, which causes the K_d to increase three fold.³⁰

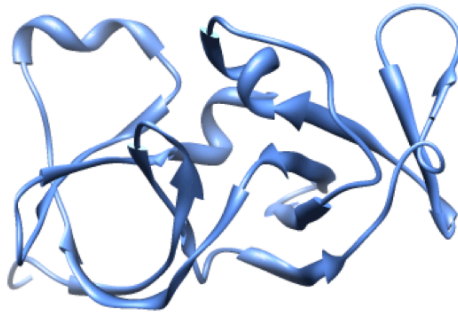


Figure 1-8: Crystal structure of the P5 domain. Crystal structure of the *T. maritima* P5 domain from (2CH4, pale blue).³¹

The P5 domain has two roles. The first is to anchor CheA to the lattice through interactions with the adaptor protein CheW and the MCPs. The second is to relay the signal from the MCPs to CheA domains. Although it is not known how this signal is transmitted, it has been elucidated that the P5 domain is required to facilitate an interaction between CheA and MCPs. Note, the structure of the P5 domain (Figure 1-8:

2CH4)³¹ is similar to CheW but differ in the flexible loop regions and length of the C-terminal α -helix in the P5 domain is shorter.

Sensor kinases are known to undergo either cis or trans phosphorylation in their homodimer.³² Crosslinking and NMR studies have shown that the *E. coli* P1 of one monomer interacts with the P4 of the other to undergo trans autophosphorylation.^{14,33,34} The structure and sequence of CheA is highly conserved across species,³⁵ yet it has not been determined if the trans autophosphorylation event is also conserved.

1.3: Coupling protein, CheW

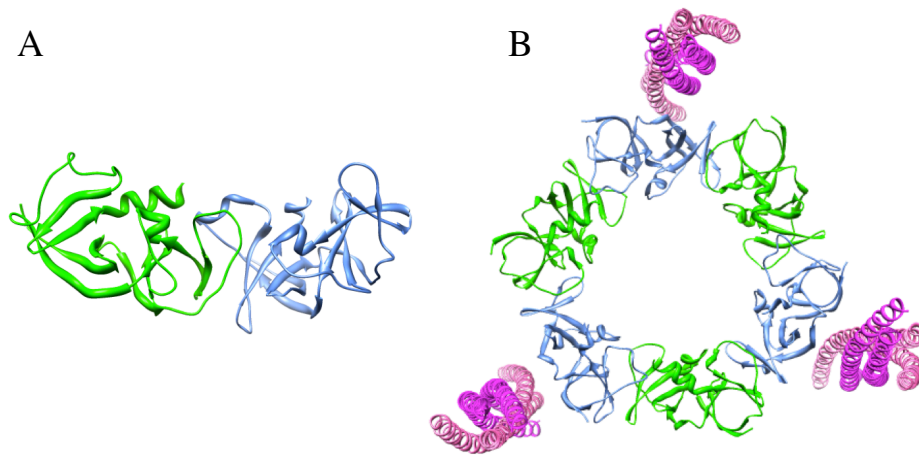


Figure 1-9: Crystal structure of CheW and P5/CheW ring with Tm14.
A: Crystal structure (4JPB) of CheW (green) and P5 domain (pale blue) bound. **B:** Crystal structure of the CheW/P5 hexagonal ring with receptor Tm14 (pink).³⁶

CheW is the coupling protein that interacts with MCPs and the CheA P5 domain. The secondary structure is very similar to the P5 domain of CheA with slight differences in the flexible loop regions and CheW has a longer C-terminal α -helix (Figure 1-9A: 4JPB).³⁶ CheW is also structurally necessary to form the hexagonal ring in the chemoreceptor lattice (Figure 1-9B: 4JPB ring).³⁶ A current opinion on the role of CheW

in vivo is that it forms a secondary CheW only ring to increase the stability of the lattice. However, as the concentration of CheW *in vivo* has the been shown to be similar to CheA,³⁷ this theory is unlikely to be correct due an insufficient amount of CheW to create a second CheW only ring. Furthermore, the MCPs impart minimal activation of CheA in the absence of CheW, where upon inclusion of CheW, activation increases dramatically thus its' role is more than just structural.

1.4: Methyl-accepting chemotaxis protein MCP/chemoreceptor and Signal Feedback

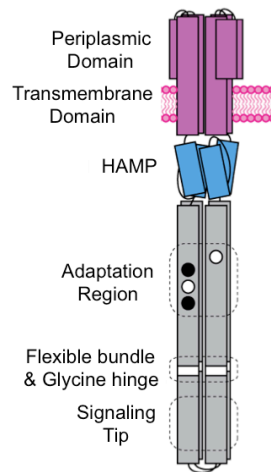


Figure 1-10: Cartoon depiction of MCP dimer with domains labeled.
 Depicted as a dimer with the KCM in gray.

The chemotaxis pathway in *E. coli* employs five different MCPs responsible for sensing different environmental cues: Tsr – serine; Tar – aspartate, maltose, and heavy metals; Tap – dipeptide and pyrimidines; Trg – ribose and galactose; Aer – redox state.³ The dimeric helical MCPs have six structural modules: the periplasmic domain for ligand binding, the transmembrane domain, a signal conversion module called the HAMP domain, the adaptation region, the glycine-rich flexible bundle, and the protein interaction region at the cytoplasmic tip¹ (Figure 1-10). The last three regions comprise the kinase-control module (KCM). Within the adaptation region, conserved glutamate

and glutamine residues undergo reversible methylation through action of the methyl-esterase, CheB (a CheA response regulator that is only active upon phosphorylation) and the methyl-transferase, CheR (Figure 1-11: 1A2O³⁸ and 1BC5³⁹).⁴⁰ All MCPs have six structural modules, except for Aer, which lacks the periplasmic domain, but in its place contains a flavin-binding PAS domain. For *E. coli* MCPs, methylation counters attractant binding by reactivating CheA and reducing ligand sensitivity.⁴¹ The time scale of this adaption is much slower than instigation of the pathway (minutes vs. milliseconds).⁴² For *E. coli*, methylation increases activity of CheA while demethylation diminishes activity.^{43,44} This regulation is not necessarily true across species as the methylation status in *B subtilis* and *T. maritima* causes changes to CheA activity that differ from that observed in *E. coli*. Substitution of the glutamate residues with glutamine residues mimics MCP glutamate methylation.⁴³⁻⁴⁷

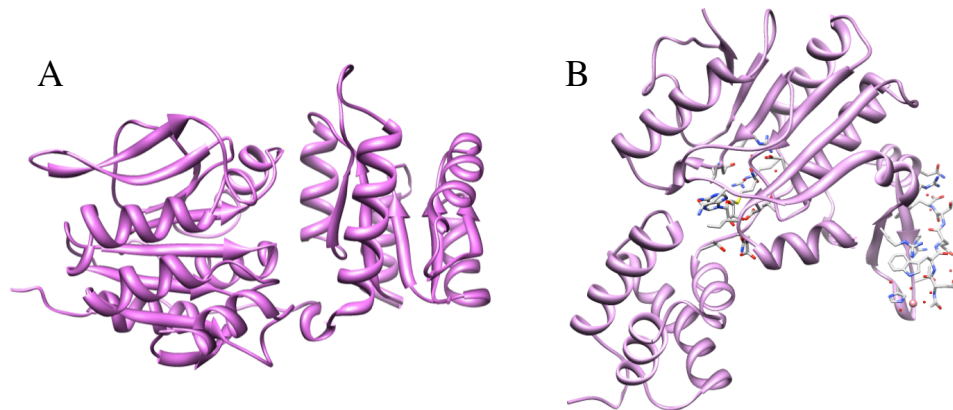


Figure 1-11: Crystal structures of CheB and CheR. A: Crystal structure of CheB from (1A2O, pale purple).³⁸ **B:** Crystal structure of CheR from (1BC5, pale pink).³⁹

The interaction of a ligand on the periplasmic domain initiates the signal, which is propagated through the membrane down the MCP cytoplasmic domain (300 Å) to the distal tip that interacts with the bound CheW and CheA. Ligands can vary from amino

acids and carbohydrates to metal ions, allowing the bacterium to sense multiple environmental cues simultaneously. However, only one binding site in a dimer can be occupied at once as a result of negative cooperativity.^{48,49} It is noted that *E. coli* can respond to a less than 1% change in the aspartate occupancy of the Tar MCP receptor.⁵⁰ These small changes can initiate a 14-fold increase in CheA kinase activity and downstream flagella rotation bias.⁵¹

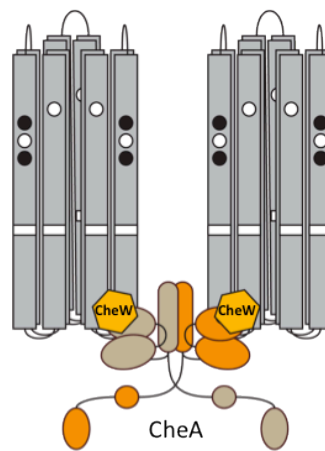


Figure 1-12: Ternary complex. Ternary complex, the smallest activating unit of the array, is composed of 6 MCP KCMs and 1 dimeric CheA:CheW.

The transmembrane portion is thought to transduce the signal through a piston-like movement that propagates downward through the membrane.^{48,52} The HAMP domain immediately follows the transmembrane portion and is a common structural motif in bacterial receptors. It is composed of two parallel α -helices, which when dimerized in an MCP dimer, form a tight parallel four helix bundle.^{53–56} HAMP oscillates between a dynamic and rigid structure to accommodate changes in receptor activity state. Following the HAMP is the adaptation region that contains conserved glutamine and glutamate residues that are subject to modification via either methylation or

demethylation/deamination by CheR and CheB. MCP modification provides feedback to keep a temporal record of ligand concentration. For *E. coli* Tar, methylation of these residues generates an activating MCP. Demethylation generates a decrease in activation of CheA, increasing the sensitivity range of the MCP in response to ligands. The flexible glycine-hinge is below the adaptation region and enables facile interconversion between the different MCP activation states.⁵⁷ The signaling tip is the highest conserved region of MCPs across species,⁵⁸ which enables clustering^{59,60} and interaction with CheA and CheW to form the ternary complex (Figure 1-12).^{24,31,61} This clustering initiates formation of the mixed trimer-of-dimers,^{3,62} which forms the higher-ordered lattice to enhance communication between the receptors.^{47,63,64}

Spatial changes along the MCP are translated into a chemical change through CheA autophosphorylation, but it is unknown how these actions are coupled. *In vivo* FRET experiments have shown that a single MCP can affect up to 36 kinases, but the mechanism underlying this coupling is unknown.⁴¹

1.5: MCP receptor array

The MCPs organize into hexagonal honeycomb arrays measuring 12 nm across,^{66,67} as visualized by electron microscopy (EM) and electron cryo-tomography (ECT).^{14,68} This configuration of the MCPs have been found in many bacteria and archaea (Figure 1-13).^{66,69} The array is composed of thousands of various types of MCPs⁷⁰ organized into mixed trimer-of-dimers⁷¹ that reside at each vertex in the hexagonal lattice. This diverse packing of different MCPs enables broad detection of ligand type and concentration, and subsequent rapid response.⁵⁸ Both the histidine kinase, CheA, and the coupling protein, CheW, are localized at the base of the array.⁷² The constrained nature of the lattice

enables immediate detection and response. The thermodynamic stability of the array is evident by the slow exchange of the lattice components (MCP, CheA, CheW) newly expressed cytoplasmic proteins *in vivo*.⁷³ There has been extensive work to determine the correct ratio of the components within the ternary complex (Figure 1-12), where it is currently thought that MCP:CheW:CheA ratio is 6 MCP subunits:1 CheW monomer:1 CheA monomer.

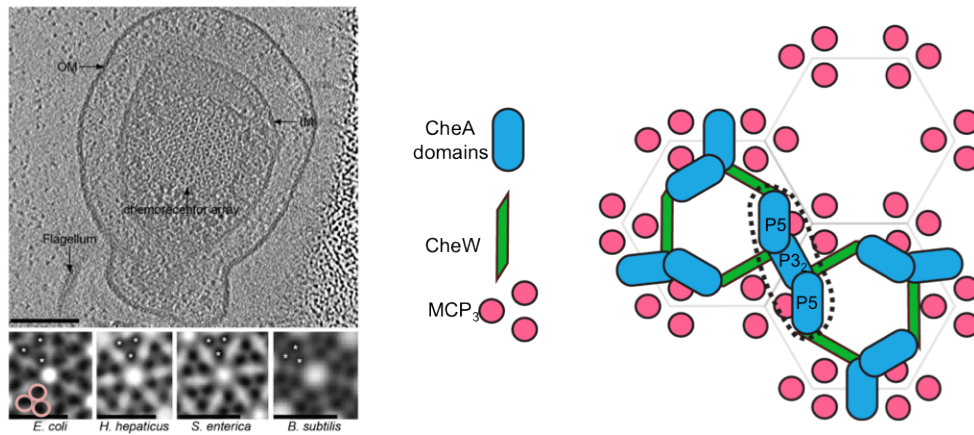


Figure 1-13: EM image and cartoon of the array. EM images of the array in several species and cartoon depiction of the array based upon EM and crystallography.^{36,65}

1.6: *CheY and phosphatases*

The secondary messenger protein, CheY, which accepts the γ -phosphate from the P1 domain of CheA, is primarily localized to the receptor arrays.^{5,74} The steady state concentrations of CheY are maintained such that CheY exists at a comparable intracellular concentration to that of CheA.³⁷ Phosphotransfer to CheY is rapid, and binding to the P2 domain induces interaction with the P1 domain.⁷⁵ The structure of CheY is similar to the P4 domain, containing a Bergerat-fold (Figure 1-14A: 1FFS). When phosphorylated, CheY diffuses through the cytosol to interact with the flagellar motor complex, specifically FliM. CheY can readily undergo autodephosphorylation

within 10 seconds, however this rate can be increased by the presence of phosphatase CheZ (*E. coli*) to 0.1 seconds.⁷⁶⁻⁷⁸ CheZ is a helical homodimer (Figure 1-14B: 1KMI) that governs the amount of CheY-P that interacts with the flagellar motor.⁴⁷⁻⁵⁰ Unlike *E. coli*, *T. maritima* contains additional phosphatases that are cytosolic (CheC/CheX) (Figure 1-13C: 1KXO) and associate directly to the flagellar motor (FliY).

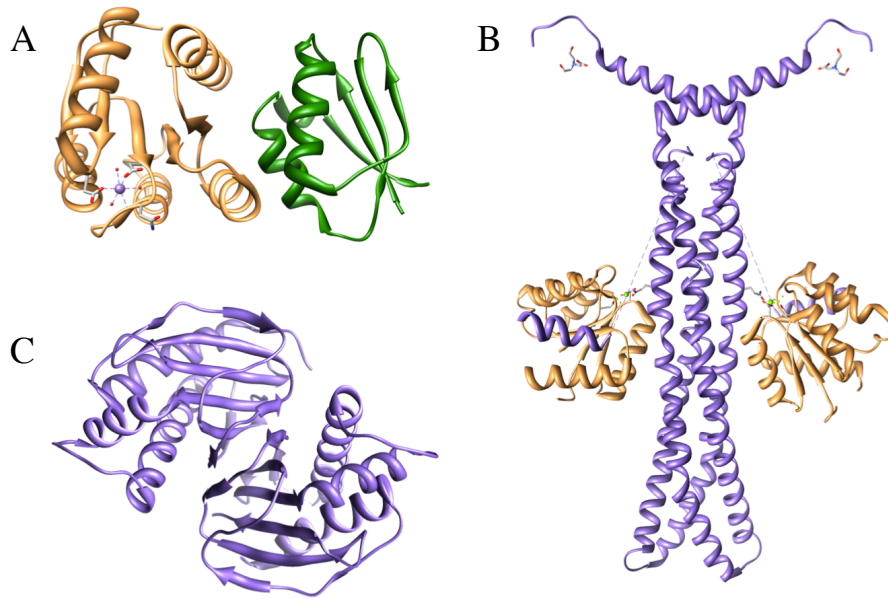


Figure 1-14: Crystal structures of CheY, CheX, and CheZ. **A:** Crystal structure of CheY (pale orange, 1FFS) bound to P2 (green). **B:** Crystal structure of CheZ (lavender) bound to CheY (1KMI). **C:** Crystal structure of CheX (1KXO, lavender).

1.7: The Flagellar motor

The flagellar motor is a complex nanomachine that converts chemical energy stored in the proton gradient spanning the inner membrane to mechanical work of rotational switching.^{10,80} For rapid response, the flagellar motor can start, stop, and change rotation almost instantly. In comparison to the array, the flagellar rotor has been shown to readily undergo exchange of stator and/or rotor proteins with their cytosolic counterparts.⁸¹⁻⁸³ Extensively studied in *E. coli* and *S. typhimurium*, the entire flagella

motor has been estimated to span 45-65 nm in diameter (Figure 1-15)⁸⁰ and can rotate several hundred Hertz with minimal friction or heat generation.¹⁰

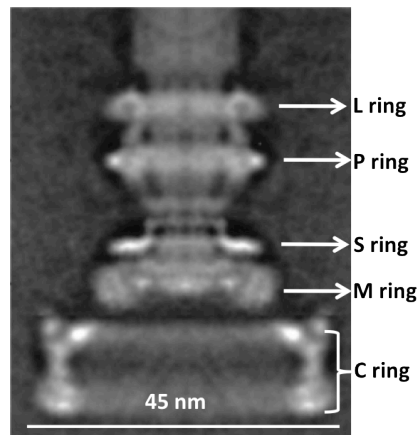


Figure 1-15: EM image of the flagellar motor. EM image of *S. typhimurium* of flagellar motor complex.⁸⁰

1.8 Summary

The interaction between the P1 and P4 domains that allows for initial phosphotransfer from ATP remains unclear. The interaction of these two domains is essential for chemotaxis, but the transient nature of their association, due to the dynamic nature of CheA, has made this critical process difficult to study. As histidine kinases occur primarily in prokaryotes,¹⁹ they are excellent candidates for drug targets for human infections by bacterial pathogens; considering CheA is necessary for infectivity of prokaryotic pathogens such as pathogenic spirochetes (lyme disease and syphilis),⁸⁴⁻⁸⁶ *Vibrio cholerae* (cholera),⁸⁷⁻⁸⁹ and *Helicobacter pylori* (stomach cancers and gastric ulcers).^{87,90-92}

It is pertinent to understand the underlying mechanism of signal transduction, phosphorylation, and subsequent downstream interactions to gain a more complete understanding of bacterial chemotaxis. In Chapter 2, through multi-angle light scattering (MALS) experiments, *in vitro* ternary complexes have been isolated when the receptors

are in a pre-formed trimer-of-dimer (Tar_{FO}). This exhibits a drastic effect on the formation of phosphorylated CheA (CheA-P) that is not translated to the production of high quantities of CheY-P. In Chapter 3, small angle x-ray scattering (SAXS) showed CheA is globular in its resting state with the P1 domains held close to the core. Upon activation, the P1 domains are released from the core, increasing the interaction between the P1 and P4 domains. However, circular dichroism (CD) shows no change in helical content upon activation indicating that the observed changes in the Kratky plots are not a result of partial unfolding. This P1-P4 interaction is additionally influenced by the receptors, determined by disulfide trapping assays of the active sites. In Chapter 4, radioisotope experiments demonstrated that the separated domains exhibit a higher affinity for one another. A model of the CheA structure in the array was based upon the planar separated P3P4 domains. Overall, these studies provide an in depth investigation of the CheA autophosphorylation event from a structural and biochemical perspective.

REFERENCES

- (1) Hazelbauer, G. L.; Falke, J. J.; Parkinson, J. S. *Trends Biochem. Sci.* **2008**, *33*, 9–19.
- (2) Wadhams, G. H.; Armitage, J. P. *Nat. Rev. Mol. Cell Biol.* **2004**, *5*, 1024–1037.
- (3) Hazelbauer, G. L.; Lai, W.-C. *Curr. Opin. Microbiol.* **2010**, *13*, 124–132.
- (4) Sourjik, V. *Trends Microbiol.* **2004**, *12*, 569–576.
- (5) Sourjik, V.; Armitage, J. P. *EMBO J.* **2010**, *29*, 2724–2733.
- (6) Mao, H.; Cremer, P. S.; Manson, M. D. *Proc. Natl. Acad. Sci.* **2003**, *100*, 5449–5454.
- (7) Turner, L.; Ryu, W. S.; Berg, H. C. *J. Bacteriol.* **2000**, *182*, 2793–2801.
- (8) Terashima, H.; Kojima, S.; Homma, M. In *International Review of Cell and Molecular Biology*; Kwang W. Jeon, Ed.; Academic Press, 2008; Vol. Volume 270, pp. 39–85.
- (9) Mora, T.; Bai, F.; Che, Y.-S.; Minamino, T.; Namba, K.; Wingreen, N. S. *Phys. Biol.* **2011**, *8*, 024001.
- (10) Berg, H. C. *Annu Rev Biochem* **2003**, *72*, 19–54.
- (11) Kojima, S.; Blair, D. F. *Int Rev Cytol* **2004**, *233*, 93–134.
- (12) Sowa, Y.; Berry, R. M. *Q Rev Biophys* **2008**, *41*, 103–132.
- (13) Briegel, A.; Ames, P.; Gumbart, J. C.; Oikonomou, C. M.; Parkinson, J. S.; Jensen, G. J. *Mol. Microbiol.* **2013**, *89*, 831–841.
- (14) Zhang, P.; Khursigara, C. M.; Hartnell, L. M.; Subramaniam, S. *Proc. Natl. Acad. Sci.* **2007**, *104*, 3777–3781.

- (15) Lee, S.-Y.; Cho, H. S.; Pelton, J. G.; Yan, D.; Henderson, R. K.; King, D. S.; Huang, L.; Kustu, S.; Berry, E. A.; Wemmer, D. E. *Nat. Struct. Mol. Biol.* **2001**, *8*, 52–56.
- (16) Dyer, C. M.; Vartanian, A. S.; Zhou, H.; Dahlquist, F. W. *J. Mol. Biol.* **2009**, *388*, 71–84.
- (17) Sarkar, M. K.; Paul, K.; Blair, D. *Proc. Natl. Acad. Sci.* **2010**, *107*, 9370–9375.
- (18) Dutta, R.; Inouye, M. *Trends Biochem. Sci.* **2000**, *25*, 24–28.
- (19) Grebe, T. W.; Stock, J. B. *Adv. Microb. Physiol.* **1999**, *41*, 139–227.
- (20) Mo, G.; Zhou, H.; Kawamura, T.; Dahlquist, F. W. *Biochemistry* **2012**, *51*, 3786–3798.
- (21) Quezada, C. M.; Hamel, D. J.; Grădinaru, C.; Bilwes, A. M.; Dahlquist, F. W.; Crane, B. R.; Simon, M. I. *J. Biol. Chem.* **2005**, *280*, 30581–30585.
- (22) Park, S. Y.; Beel, B. D.; Simon, M. I.; Bilwes, A. M.; Crane, B. R. *Proc Natl Acad Sci U A* **2004**, *101*, 11646–11651.
- (23) Zhou, H.; McEvoy, M. M.; Lowry, D. F.; Swanson, R. V.; Simon, M. I.; Dahlquist, F. W. *Biochemistry* **1996**, *35*, 433–443.
- (24) Bhatnagar, J.; Borbat, P. P.; Pollard, A. M.; Bilwes, A. M.; Freed, J. H.; Crane, B. R. *Biochemistry* **2010**, *49*, 3824–3841.
- (25) Stewart, R. C.; Jahreis, K.; Parkinson, J. S. *Biochemistry* **2000**, *39*, 13157–13165.
- (26) Jahreis, K.; Morrison, T. B.; Garzón, A.; Parkinson, J. S. *J. Bacteriol.* **2004**, *186*, 2664–2672.
- (27) Bilwes, A. M.; Alex, L. A.; Crane, B. R.; Simon, M. I. *Cell* **1999**, *96*, 131–141.

- (28) Surette, M. G.; Levit, M.; Liu, Y.; Lukat, G.; Ninfa, E. G.; Ninfa, A.; Stock, J. B. *J. Biol. Chem.* **1996**, *271*, 939–945.
- (29) Bilwes, A. M.; Quezada, C. M.; Croal, L. R.; Crane, B. R.; Simon, M. I. *Nat. Struct. Mol. Biol.* **2001**, *8*, 353–360.
- (30) Eaton, A. K.; Stewart, R. C. *Biochemistry* **2009**, *48*, 6412–6422.
- (31) Park, S.-Y.; Borbat, P. P.; Gonzalez-Bonet, G.; Bhatnagar, J.; Pollard, A. M.; Freed, J. H.; Bilwes, A. M.; Crane, B. R. *Nat. Struct. Mol. Biol.* **2006**, *13*, 400–407.
- (32) Nishiyama, S.; Garzón, A.; Parkinson, J. S. *J. Bacteriol.* **2014**, *196*, 257–264.
- (33) Miller, A. S.; Kohout, S. C.; Gilman, K. A.; Falke, J. J. *Biochemistry* **2006**, *45*, 8699–8711.
- (34) Hamel, D. J.; Zhou, H.; Starich, M. R.; Byrd, R. A.; Dahlquist, F. W. *Biochemistry* **2006**, *45*, 9509–9517.
- (35) Wuichet, K.; Zhulin, I. B. *Sci Signal* **2010**, *3*, ra50.
- (36) Li, X.; Fleetwood, A. D.; Bayas, C.; Bilwes, A. M.; Ortega, D. R.; Falke, J. J.; Zhulin, I. B.; Crane, B. R. *Biochemistry* **2013**, *52*, 3852–3865.
- (37) Li, M.; Hazelbauer, G. L. *J. Bacteriol.* **2004**, *186*, 3687–3694.
- (38) Djordjevic, S.; Goudreau, P. N.; Xu, Q. P.; Stock, A. M.; West, A. H. *Proc Natl Acad Sci U S A* **1998**, *95*, 1381–1386.
- (39) Djordjevic, S.; Stock, A. M. *Nat. Struct. Biol.* **1998**, *5*, 446–450.
- (40) Springer, W. R.; Koshland, D. E. *Proc. Natl. Acad. Sci.* **1977**, *74*, 533–537.
- (41) Sourjik, V.; Berg, H. C. *Proc. Natl. Acad. Sci.* **2002**, *99*, 123–127.
- (42) Sagawa, T.; Kikuchi, Y.; Inoue, Y.; Takahashi, H.; Muraoka, T.; Kinbara, K.; Ishijima, A.; Fukuoka, H. *Biophys. J.* **2014**, *107*, 730–739.

- (43) Sourjik, V.; Berg, H. C. *Nature* **2004**, *428*, 437–441.
- (44) Borkovich, K. A.; Alex, L. A.; Simon, M. I. *Proc. Natl. Acad. Sci.* **1992**, *89*, 6756–6760.
- (45) Dunten, P.; Koshland, D. E. *J. Biol. Chem.* **1991**, *266*, 1491–1496.
- (46) Aizawa, S.-I.; Harwood, C. S.; Kadner, R. J. *J. Bacteriol.* **2000**, *182*, 1459–1471.
- (47) Li, G.; Weis, R. M. *Cell* **2000**, *100*, 357–365.
- (48) Milburn, M. V.; Prive, G. G.; Milligan, D. L.; Scott, W. G.; Yeh, J.; Jancarik, J.; Koshland, D. E.; Kim, S. H. *Science* **1991**, *254*, 1342–1347.
- (49) Tatsuno, I.; Homma, M.; Oosawa, K.; Kawagishi, I. *Science* **1996**, *274*, 423–425.
- (50) Jasuja, R.; Yu-Lin; Trentham, D. R.; Khan, S. *Proc. Natl. Acad. Sci.* **1999**, *96*, 11346–11351.
- (51) Segall, J. E.; Block, S. M.; Berg, H. C. *Proc. Natl. Acad. Sci.* **1986**, *83*, 8987–8991.
- (52) Falke, J. J.; Erbse, A. H. *Structure* **2009**, *17*, 1149–1151.
- (53) Airola, M. V.; Watts, K. J.; Bilwes, A. M.; Crane, B. R. *Structure* **2010**, *18*, 436–448.
- (54) Airola, M. V.; Sukomon, N.; Samanta, D.; Borbat, P. P.; Freed, J. H.; Watts, K. J.; Crane, B. R. *PLoS Biol* **2013**, *11*, e1001479.
- (55) Buron-Barral, M. D.; Gosink, K. K.; Parkinson, J. S. *J. Bacteriol.* **2006**, *188*, 3477–3486.
- (56) Dunin-Horkawicz, S.; Lupas, A. N. *J. Mol. Biol.* **2010**, *397*, 1156–1174.
- (57) Coleman, M. D.; Bass, R. B.; Mehan, R. S.; Falke, J. J. *Biochemistry* **2005**, *44*, 7687–7695.
- (58) Alexander, R. P.; Zhulin, I. B. *Proc. Natl. Acad. Sci.* **2007**, *104*, 2885–2890.

- (59) Sourjik, V.; Berg, H. C. *Mol. Microbiol.* **2000**, *37*, 740–751.
- (60) Skidmore, J. M.; Ellefson, D. D.; McNamara, B. P.; Couto, M. M.; Wolfe, A. J.; Maddock, J. R. *J. Bacteriol.* **2000**, *182*, 967–973.
- (61) Boukhvalova, M. S.; Dahlquist, F. W.; Stewart, R. C. *J. Biol. Chem.* **2002**, *277*, 22251–22259.
- (62) Ames, P.; Studdert, C. A.; Reiser, R. H.; Parkinson, J. S. *Proc. Natl. Acad. Sci.* **2002**, *99*, 7060–7065.
- (63) Endres, R. G.; Wingreen, N. S. *Proc. Natl. Acad. Sci. U. S. A.* **2006**, *103*, 13040–13044.
- (64) Li, M.; Hazelbauer, G. L. *Mol. Microbiol.* **2005**, *56*, 1617–1626.
- (65) Briegel, A.; Li, X.; Bilwes, A. M.; Hughes, K. T.; Jensen, G. J.; Crane, B. R. *Proc. Natl. Acad. Sci.* **2012**, *109*, 3766–3771.
- (66) Briegel, A.; Ortega, D. R.; Tocheva, E. I.; Wuichet, K.; Li, Z.; Chen, S.; Müller, A.; Iancu, C. V.; Murphy, G. E.; Dobro, M. J.; Zhulin, I. B.; Jensen, G. J. *Proc. Natl. Acad. Sci.* **2009**, *106*, 17181–17186.
- (67) Briegel, A.; Ding, H. J.; Li, Z.; Werner, J.; Gitai, Z.; Dias, D. P.; Jensen, R. B.; Jensen, G. J. *Mol. Microbiol.* **2008**, *69*, 30–41.
- (68) Liu, J.; Hu, B.; Morado, D. R.; Jani, S.; Manson, M. D.; Margolin, W. *Proc. Natl. Acad. Sci.* **2012**, *109*, E1481–E1488.
- (69) Gestwicki, J. E.; Kiessling, L. L. *Nature* **2002**, *415*, 81–84.
- (70) Falke, J. J. *Proc. Natl. Acad. Sci.* **2002**, *99*, 6530–6532.
- (71) Khursigara, C. M.; Wu, X.; Subramaniam, S. *J. Bacteriol.* **2008**, *190*, 6805–6810.

- (72) Greenfield, D.; McEvoy, A. L.; Shroff, H.; Crooks, G. E.; Wingreen, N. S.; Betzig, E.; Liphardt, J. *PLoS Biol* **2009**, *7*, e1000137.
- (73) Schulmeister, S.; Ruttorf, M.; Thiem, S.; Kentner, D.; Lebedez, D.; Sourjik, V. *Proc. Natl. Acad. Sci.* **2008**, *105*, 6403–6408.
- (74) Vaknin, A.; Berg, H. C. *J. Mol. Biol.* **2007**, *366*, 1416–1423.
- (75) Segall, J. E.; Manson, M. D.; Berg, H. C. *Nature* **1982**, *296*, 855–857.
- (76) Guhaniyogi, J.; Wu, T.; Patel, S. S.; Stock, A. M. *J. Bacteriol.* **2008**, *190*, 1419–1428.
- (77) Sourjik, V.; Berg, H. C. *Proc. Natl. Acad. Sci.* **2002**, *99*, 12669–12674.
- (78) Silversmith, R. E.; Guanga, G. P.; Betts, L.; Chu, C.; Zhao, R.; Bourret, R. B. *J. Bacteriol* **2003**, *185*, 1495–1502.
- (79) Schuster, M.; Silversmith, R. E.; Bourret, R. B. *Proc. Natl. Acad. Sci.* **2001**, *98*, 6003–6008.
- (80) Thomas, D. R.; Francis, N. R.; Xu, C.; DeRosier, D. J. *J. Bacteriol.* **2006**, *188*, 7039–7048.
- (81) Bray, D.; Levin, M. D.; Morton-Firth, C. J. *Nature* **1998**, *393*, 85–88.
- (82) Duke, T. *Proc. Natl. Acad. Sci. U. S. A.* **2002**, *99*, 6521–6523.
- (83) Delalez, N. J.; Berry, R. M.; Armitage, J. P. *mBio* **2014**, *5*, e01216–14.
- (84) Burgdorfer, W.; Barbour, A. G.; Hayes, S. F.; Benach, J. L.; Grunwaldt, E.; Davis, J. P. *Science* **1982**, *216*, 1317–1319.
- (85) Motaleb, M. A.; Miller, M. R.; Bakker, R. G.; Li, C. H.; Charon, N. W. In *Two-Component Signaling Systems, Pt A*; Simon, M. I.; Crane, B. R.; Crane, A., Eds.; Methods in Enzymology; 2007; Vol. 422, p. 421 – +.

- (86) Li, C. H.; Bakker, R. G.; Motaleb, M. A.; Sartakova, M. L.; Cabello, F. C.; Charon, N. W. *Proc. Natl. Acad. Sci. U. S. A.* **2002**, *99*, 6169–6174.
- (87) Schweinitzer, T.; Josenhans, C. *Arch. Microbiol.* **2010**, *192*, 507–520.
- (88) Antunez-Lamas, M.; Cabrera-Ordóñez, E.; Lopez-Solanilla, E.; Raposo, R.; Trelles-Salazar, O.; Rodríguez-Moreno, A.; Rodríguez-Palenzuela, P. *Microbiol.-Sgm* **2009**, *155*, 434–442.
- (89) Spagnuolo, A. M.; DiRita, V.; Kirschner, D. *J. Theor. Biol.* **2011**, *289*, 247–258.
- (90) Howitt, M. R.; Lee, J. Y.; Lertsethtakarn, P.; Vogelmann, R.; Joubert, L. M.; Ottemann, K. M.; Amieva, M. R. *Mbio* **2011**, *2*.
- (91) Rader, B. A.; Wreden, C.; Hicks, K. G.; Sweeney, E. G.; Ottemann, K. M.; Guillemin, K. *Microbiol.-Sgm* **2011**, *157*, 2445–2455.
- (92) Rolig, A. S.; Carter, J. E.; Ottemann, K. M. *Proc. Natl. Acad. Sci. U. S. A.* **2011**, *108*, 19749–19754.

CHAPTER 2: PREFORMED SOLUBLE CHEMORECEPTOR TRIMERS THAT MIMIC CELLULAR ASSEMBLY STATES AND ACTIVATE CHEA AUTOPHOSPHORYLATION

2.1: Introduction

Electron microscopy studies of gold labeled MCPs in whole cells indicated that chemoreceptors cluster at the cell poles.¹ It has subsequently become clear that a highly-ordered molecular arrangement based on trimeric receptor dimers underlies clustering. The trimer-of-dimers arrangement of MCPs was first observed in the crystal structure of the serine sensing receptor Tsr in *E. coli*.² The trimerization contact residues are clustered in the signaling tip of the MCPs and has the highest degree of sequence identity among receptors from the same and different bacteria.^{3,4} Substitution of the trimerization contact residues produce defective chemotaxis *in vitro*.⁵ *In vivo* crosslinking experiments by a trivalent reagent supported the existence of MCP trimer-of-dimers in cells.^{5,6} Electron microscopy (EM) and electron cryotomography (ECT) revealed a trimeric architecture that is widely conserved in across different bacterial species (Figure1-13).^{3,7-10} ECT studies show the trimer-of-dimers arrange in an edge-on-edge arrangement to produce a honeycomb lattice of receptors, CheA, and CheW.^{9,10}

Trimerization of MCPs plays a pivotal role in CheA kinase activation. MCPs associated into nanodisks only activate CheA when there are at least three parallel receptors in the same disk.¹¹ Furthermore, the minimum stoichiometry for kinase activation involves two such nanodisks (i.e. two trimers-of-dimers) per CheA dimer.^{12,13} This assembly state is consistent with that of the extended lattice model (which has a stoichiometry of 6 MCP subunits: 1 CheW monomer: 1 CheA monomer) proposed from a combination of crystallographic and ECT data.¹⁰

In the lattice model, a receptor dimer contacts either CheW or CheA through the same interface (Figure 2-1) to generate a honeycomb arrangement.^{4,14}

Certain MCPs do not contain transmembrane regions, yet they also appear to assemble into soluble honeycomb lattices.^{15,16} Nonetheless, recombinant MCP cytoplasmic kinase control modules (KCMs) generally do not produce trimers in solution. In some cases, individual MCP KCMs inhibit CheA activity, where in other cases they are activating.^{15,17} However, if the KCMs are templated to lipid vesicles,¹⁸⁻²⁰ or treated with osmolytes,²¹ trimers capable of activating CheA appear to form. Addition of leucine zipper domains²²⁻²⁴ and surrogate HAMP modules N-terminal of the KCMs²⁵ have also been proven effective at activating CheA *in vitro* and *in vivo*. However, in these and other cases, the oligomeric states and homogeneity of active species are difficult to assess.

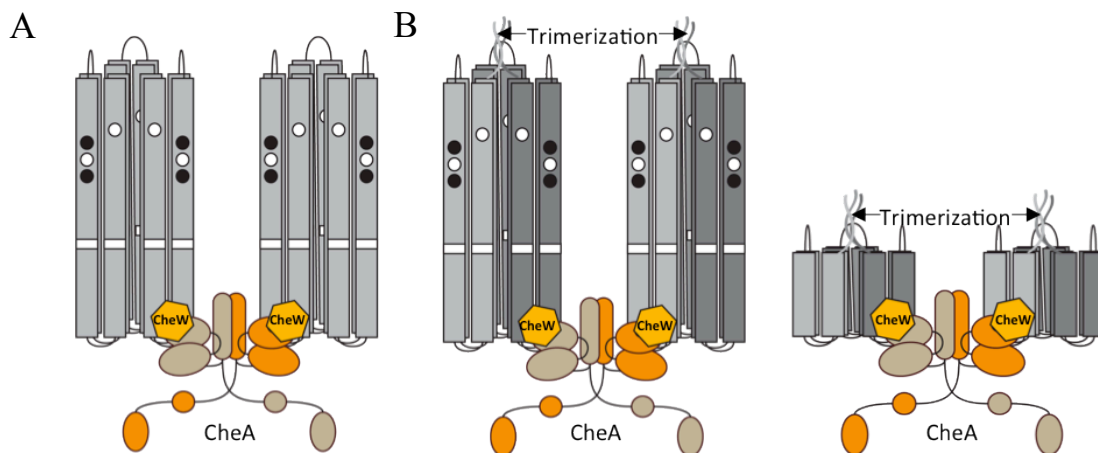


Figure 2-1: Ternary complex. A: Ternary complex composed of six MCP KCMs and 1 dimeric CheA:CheW is the smallest activating unit of the array. **B:** Trimerized MCP dimers with and without the adaptation region.

In order to generate homogenous complexes of MCPs with CheA and CheW in activated states the engineering of chemoreceptor mimetics that pre-form the trimer-of-dimer module in solution was pursued. Fusions of receptor KCMs were created with naturally occurring trimerization motifs, such as engineered Leu zipper proteins and the foldon from bacteriophage

T4 fibrin.²⁶⁻²⁸ Despite its small size, the foldon forms a stable β -propeller trimer with each of three intertwined β -hairpins supplied from each subunit (Figure 2-2).²⁶⁻²⁸ The foldon subunits trimerize rapidly and have been previously used to oligomerize fused proteins.²⁶ Single chain variants (fused dimers) of chemoreceptor KCMs were produced with C-terminal foldon tags assemble into soluble trimers (Tar_{FO}) with interacting tips that are capable of increasing CheA autophosphorylation to a degree similar to that observed in membrane arrays. Furthermore, pulsed dipolar EPR measurements on spin-labeled proteins reveal that CheA bound to a trimer-of-dimers mimetic assumes a conformation that matches expectations from the modeled cellular receptor arrays.

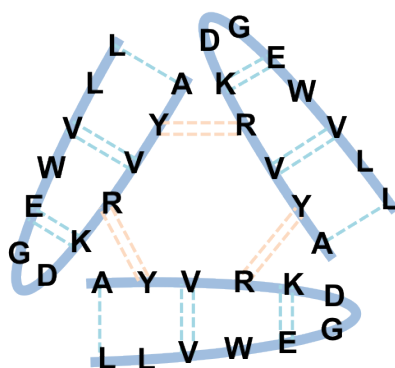


Figure 2-2: Foldon motif from bacteriophage T4 fibrin. Trimeric foldon motif from bacteriophage T4 fibrin forms a β -propeller from three β -hairpins, dotted lines represent backbone hydrogen bonds.

2.2: Materials and Methods

2.2.1: Construction and cloning of the trimer-of-dimers mimetics. The KCM of the aspartate receptor Tar plus a sequence that encodes for a seven amino acid peptide GASGGTG at the 3' end was cloned into pET28a between 5' NdeI and 3' BamHI restriction sites. A second Tar fragment was then cloned in frame into the same vector between 5' BamHI and 3' HindIII restriction sites. The NdeI-Tar_C-BamHI-Tar_C'-stop-HindIII construct encodes a Tar_{SC} covalent "dimer". The foldon trimerization motif was introduced through PCR cloning from the GP67

vector template (a gift from the laboratory of Gary Whittaker, Cornell University) with introduced restriction sites for fusion onto the C-terminus of Tar_{SC} (5' HindIII and 3' Xho I), or for fusion onto the N-terminus (5' NheI and 3' NdeI). Constructs of the general formulation NcoI-foldon-NdeI-Tar_C-BamHI-Tar_C'-HindIII or NdeI-Tar_C-BamHI-Tar_C'-HindIII-foldon-stop-XhoI produced variants of the Tar foldon (Tar_{FO}) with different Tar subunit lengths and foldon linkages (Figure 2-3). The Tar_{FO}, short construct is produced via NdeI-Tar₃₅₃₋₄₂₄-BamHI-SpeI-Tar₃₅₃₋₄₂₄-ScaI-foldon-stop-NotI-XhoI. For N-terminal-fused foldons, an N-terminal 6-His-tag plus thrombin cleavage site was retained on the foldon fragment for purification; for C-terminal-fused foldons, the His-tag plus thrombin site was removed prior to Tar fusion by PCR cloning the foldon unit alone into the vector pET28a and then transferring the fragment into the Tar-containing vector. Tar_{FO} was grown in LB media, inoculated at 37 °C with 2 mL of kanamycin (50 mg/mL) and overnight culture. Cells were grown until the optical density reached A₆₀₀ = 0.6, the temperature was then lowered to 17 °C before inducing with 2 mL of IPTG (35 mg/mL) and subsequent overnight growth. During purification, all buffers included 10% glycerol to improve stability. 10 mM PMSF was added to lysis buffer (50 mM Tris [pH 7.5], 150 mM NaCl, 5 mM imidazole, 10% glycerol) for sonication prior to centrifugation to limit proteolysis. The lysate was then run over Ni²⁺-NTA affinity resin to extract the Tar_{FO} which was then eluted with 50 mM Tris [pH 7.5], 150 mM NaCl, 200 mM imidazole, 10% glycerol after wash with buffer containing 20 mM imidazole. Thrombin was added and incubated overnight to cleave the His₆-tag. The sample was eluted over a Sephadex 200 SEC prep column run with gel filtration (GF) buffer (50 mM Tris [pH 7.5], 150 mM NaCl, 10% glycerol) before further concentration (to 12 mg/mL) with a 50 kDa MW concentrator (Figure 2-4).

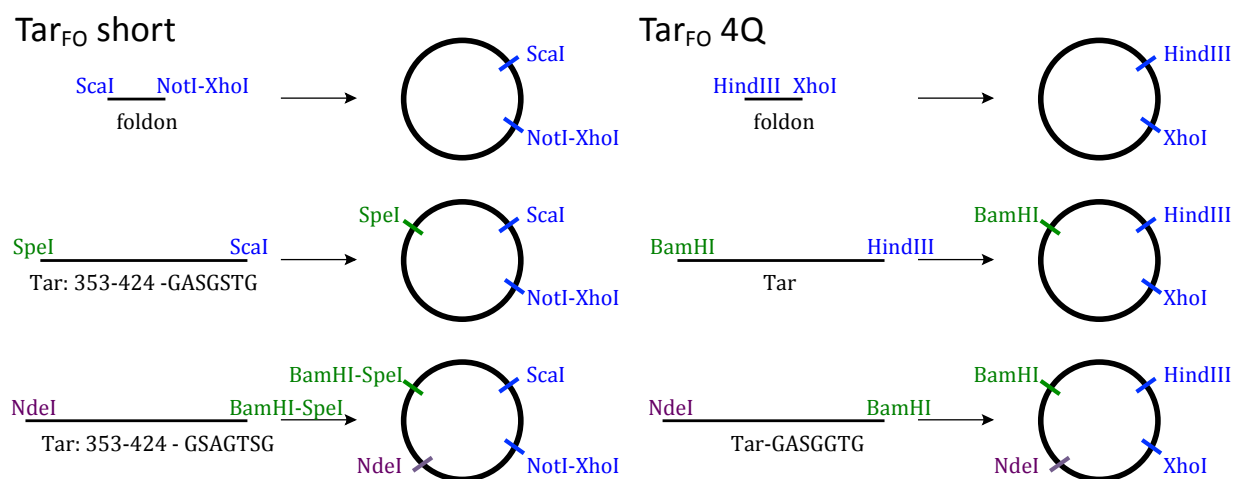


Figure 2-3: Schemes for cloning the Tar_{FO}. Cloning strategies for the Tar_{FO} constructs (not to scale)

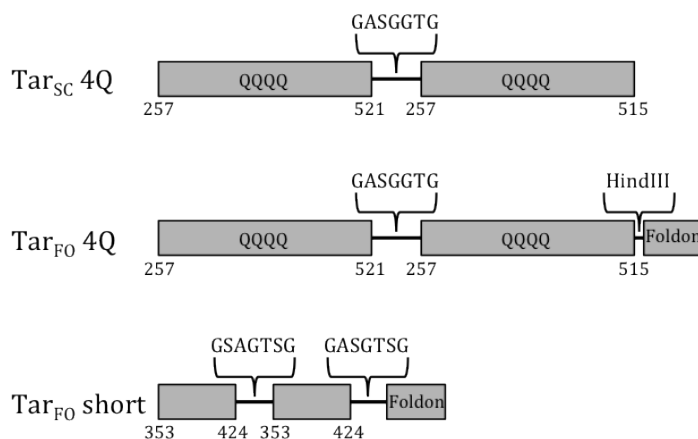


Figure 2-4: Schematic of Tar protein variants generated. Description of the Tar protein variants used in this chapter with description of the linkers.

2.2.2: *Cloning, mutagenesis, and spin labeling of proteins.* Two Glu residues in the adaptation site of Tar (E302, E491) were mutated to Gln with Quikchange mutagenesis (Agilent Technologies). For site-specific spin labeling, Glu389 was changed to Cys (Quikchange, Stratagene) and spin-labeled as previously described.²⁹ Tar_{FO} is otherwise Cys free.

2.2.3: *Multi-angle light scattering (MALS).* A 5 mg/mL monomeric BSA (Sigma) control was injected onto a Phenomenex Bio Sep-SEC-s 300 column that had been equilibrated in GF buffer served to normalize the light scattering detectors and act as a data quality control. Then purified

protein samples (1 mg/mL to 10 mg/mL) were injected onto the same column. The SEC is coupled to a static 18-angle light scattering detector (DAWN HELEOS-II), and a refractive index detector (Optilab T-rEX; Wyatt Technology), and dynamic light-scattering device (WyattQELS). Data were collected every second at the flow rate of 1 mL/min for 30 minutes at 25 °C. The ASTRA V software was used to extract the molar weight distribution, RMS radius, radius of hydration, and the polydispersity of each resolved peak.

2.2.4: Small-angle x-ray scattering (SAXS). Protein buffer was exchanged to 50 mM HEPES pH 7.5, 150 mM NaCl, 2 mM DTT, and 5% glycerol. Three concentrations were prepared at 4, 3, and 2 μ M for Tar_{FO} 4Q and Tar_{SC} 4Q. For the Tar_{FO} short three concentrations were prepared at 31, 15, and 7 μ M. The samples were centrifuged at 13,000 rpm for 20 minutes, and kept in a 4 °C chilling tray prior to data collection. Data was collect at the G1 of CHESS with Pilatus 100K detector.³⁰ Samples were exposed to x-rays for 2 sec per frame for 10 frames. During exposures 30 μ L of sample is continuously oscillated through the illuminated volume (0.125 μ L) at 2-4 μ L s⁻¹, thereby reducing the absorbed dose by two orders of magnitude.³¹ The programs RAW³² and Primus³³ were used to generate Guinier and Kratky plots. Molecular weight prediction was based upon a standard of 3 mg/mL glucose isomerase (173 kDa). Envelope reconstructions was calculated using ATSAS³⁴⁻³⁶ programs. A total 10 independent models were generated and averaged using Damaver then combined into one envelope.

2.2.5: Protein interactions by pull-down. Binding affinities of untagged Tar_{FO} 4Q, Tm14, and Tm CheW to His-tagged CheA Δ 289 (P3P4P5) were tested via pull-down assays. Proteins were incubated together with 30 μ L Ni²⁺-NTA affinity resin (equilibrated with 50 mM HEPES (pH 7.5), 150 mM NaCl, 5 mM imidazole, 10 % glycerol) and rocked for 1 hour at room temperature. Samples were microcentrifuged and resuspended several times in wash buffer (50 mM HEPES

(pH 7.5), 150 mM NaCl, 50 mM imidazole, 10 % glycerol) to remove non-specifically bound proteins. To quench the reaction, 30 μ L of SDS Coomassie loading dye was added to the sample, which was then heated at 90 °C for 5 min prior to running on a denaturing Nu-PAGE gel. Gel bands were quantified by densitometry and analyzed with ImageJ software. Non-specific binding of target proteins to Ni²⁺-NTA resin was determined and subtracted from values obtained with the His₆-tagged CheA bait.

2.2.6: CheA autophosphorylation assays. CheA monomer (1-2.5 μ M), CheW (1-2.5 μ M), and Tar_{FO} 4Q or short (1-2.5 μ M) or Tar_{SC} 4Q (3-6 μ M) was incubated for 1 hour at room temperature with TKEDM buffer (50 mM KCl, 10 mM MgCl₂, 0.5 mM DTT, 0.5 mM EDTA, 5 mM Tris pH 7.5). Concentrations for CheW and MCP variants were optimized to 1 CheA monomer:1 CheW:3 MCP dimers. Then 2 μ L of 2.3 mM cold ATP and 3-8 μ L of [γ -³²P] ATP (3000 Ci/mmol, 10 mCi/mL, Perkin Elmer) solution was added to the sample made up to a total volume of 25 μ L. After incubation times of 10 seconds up to 12 minutes, the sample was quenched with 25 μ L of 3 \times SDS with 50 mM EDTA pH 8.0 and then subjected to gel electrophoresis on a 4-20% gradient Tris-Glycine gel. The gel was stained with Coomassie blue, destained with water, and then dried with GelAir dryer. The dry gel was placed in a cassette and imaged with a Storm phosphoimager (GE Healthcare) for at least 24 hrs. The resulting band intensities were analyzed with ImageJ and the kinetic data was fit to the first order expression $P_t = A_0(1 - e^{-kt})$.

ADP/ATP chase. CheA monomer (1 μ M), CheW (1 μ M), and Tar_{FO} 4Q or short (1 μ M) or Tar_{SC} 4Q (3 μ M) samples were prepared and exposed as described previously. After 6 minutes of incubation with 2 μ L of hot solution, 2 μ L of 2 mM nucleotide (ADP or ATP) was added and subsequently quenched after 3 to 30 minutes.

Phosphate Transfer to CheY. CheA monomer (1 μM), CheW (1 μM), CheY (25 μM), and Tar_{FO} 4Q or short (1 μM) or Tar_{SC} 4Q (3 μM) samples were prepared and exposed as described previously then quenched after 30 seconds.

Comparison to Membrane array. The membrane array solution sent by Kene Piasta and Joseph Falke (University of Colorado, Boulder)^{15,37} contained: CheA (5 μM), CheW (10 μM), and Tsr receptors (6.7 μM). The samples were spun down 13000 rpm for 7 minutes, supernatant removed and resuspended in 15 μL of 1x TKEDM buffer. In each sample contained 5 μL of the washed arrays, 5 μL of the CheY solution (80 μM stock). The assays contained CheA (2.5 μM), CheW (5 μM), CheY (40 μM), and Tsr receptors (3.4 μM) were supplemented with 1 μL of ATP hot solution as described previously then quenched after 30 seconds

2.2.7: Pulsed-dipolar EPR spectroscopy. Cysteine variants were expressed in *E. coli* as described above. Cell lysates were applied to a Ni²⁺-NTA column to bind the His₆-tagged target proteins then 5-10 mM MTS-SL nitroxide spin-label (1-Oxyl-2,2,5,5-tetramethylpyrroline-3-methyl)methanethiosulfonate; Toronto research, Toronto, ON) was added to the column, incubated at room temperature for 4 hours and then overnight at 4 °C. Reaction with the free Cys thiol yields the nitroxide side chain commonly known as R1. Samples were eluted after a subsequent overnight incubation with thrombin to remove the His₆-tag. Proteins were further purified on a size-exclusion column (Superdex 200; Pharmacia Biotech) and concentrated in GF buffer (50 mM TRIS [pH 7.5], 150 mM NaCl). PDS measurements: Four pulse DEER experiment were conducted at 60 K on a 17.3 GHz FT EPR spectrometer, which is modified to perform PDS experiments.³⁸⁻⁴¹ The baseline used for data processing was approximated by a linear polynomial. Distance distributions of spin separations within the sample were calculated by the Tikhonov method⁴² and refined by the Maximum Entropy Regularization Method

(MEM).⁴³ Several PDS experiments reported in this thesis were performed by Dr. Xiaoxiao Li and Dr. Peter Borbat.

2.2.8: Quantification of flagellar rotation patterns. Tar_{FO} and Tar_{SC} constructs were transferred using NdeI and HindIII sites to the vector pKG116, which contained a salicylate inducible promoter. Plasmids were transferred into host strains (UU2612) CheRB⁺ or (UU2610) CheRB⁻ (generously provided by J. S. Parkinson). Direct measurements of flagellar rotation patterns were carried out using a tethered cell assay similar to that published by Parkinson and Slocum.⁴⁴ Specifically, *E. coli* cells harboring Tar_{FO}, Tar_{SC}, full-length/KCM Tar-containing plasmids, or pKG116, were grown in tryptone broth, induced for 1 hour with 2 μ M sodium salicylate, washed in KEP buffer (10 mM potassium phosphate, 0.1 mM EDTA, pH 7.0), and resuspended in tethering buffer (KEP buffer with 75 mM NaCl). Flagella were sheared in a Waring commercial blender for 15 sec. Bacteria with sheared flagella were added to anti-flagellin antibody (abcam, 1:500 final dilution), placed onto a microscope slide and then visualized by dark-field microscopy. The rotation patterns of 50-100 cells were observed for 10 sec each and recorded as exclusively CW or CCW, predominantly CW or CCW, or frequently reversing. This experiment was performed with assistance from Dr. Kylie Watts from Loma Linda University.

2.2.9: Methylation status of recombinant Tar variants. *E. coli* UU2612 expressing Tar_{FO}, Tar_{SC}, full-length Tar, Tar-KCM, and UU2610 expressing full-length Tar, were grown in Luria-Bertani broth and induced for 3.5 hours with 2 μ M sodium salicylate. Bacteria were washed in chemotaxis buffer (100 μ M potassium-EDTA, 10 mM potassium phosphate, pH 7.0, 10 mM sodium lactate, 1 mM magnesium sulfate, and 1 mM ammonium sulfate) before protein synthesis was stopped with 500 μ g/ml spectinomycin. Methylation was carried out as described by Kort *et al.*⁴⁵ with modifications. Specifically, methylation was initiated by adding 10 μ Ci/ml L-(methyl-

³H)methionine (82 Ci mmol⁻¹, Perkin Elmer) and reactions were stopped by adding formaldehyde. Tar/UU2612 methylation was also tested by adding 5 mM aspartate after L-(methyl-³H)methionine. After SDS-PAGE, gels were soaked for 30 min in Fluoro-hance™ (RPI Corp.), then dried and exposed to autoradiography film at -80°C for at least three days. The steady-state expression level of each methylated protein was determined by Western blot using 1:100,000 anti-Tsr antibody (generously provided by J. S. Parkinson). This experiment was performed with assistance from Dr. Kylie Watts from Loma Linda University.

	Methylation States	N-/C-foldon	1st Tar KCM (residue numbers)	2nd Tar KCM (residue numbers)
1	QEQE	n/a	257-521	257-521
2	QEQE	N	257-521	257-521
3	QEQE	N	263-515	263-553
4	QEQE	N	263-515	263-515
5	QEQE	N	GGGGG-263-515	263-515
6	QEQE	N	263-515	263-515-NWETF
7	QEQE	C	GGGGG-263-515	263-515
8	QEQE	C	263-515	263-515
9	QEQE	C	263-515	263-521
10	QEQE	C	257-521	263-515
11	QEQE	C	257-521	257-521
12	QEQE	C	257-521	257-515
13	QQQQ	n/a	257-521	257-521
14	QQQQ	C	257-521	257-515
15	QQQQ	C	257-521	257-521
16	QQQQ	C	257-521	257-528
17	n/a	C	353-424-GSAGTSG	353-424-GASGSTG

Table 2-1: Tar_{FO} constructs generated. Tar_{FO} constructs generated by Dr. Xiaoxiao Li and Joanne Widom.

2.3: Results

To develop a soluble MCP trimer-of-dimers mimetic, first the cytoplasmic kinase control module (KCM) or the *E. coli* aspartate receptor Tar was engineered into a single-chain module (Tar_{SC}) that included either: 1) the entire KCM with the adaptation and protein interaction regions (PIR),

but not the unstructured tail, or 2) just the PIR (Figure 2-1). In each case, the C-terminus of the first repeated module was joined to the N-terminus of another through a GASGGTG peptide linker (Table 2-1, Figure 2-3). A foldon trimerization motif was then fused onto either the N-terminus or the C-terminus of the Tar_{SC}. The length of the linker between the Tar_{SC} dimer and foldon motif was varied to optimize the stability of the variants and their trimerization. Two additional Gln substitutions were introduced in the adaptation region of each “subunit” to produce the “QQQQ” state, which mimics complete methylation (and hence maximal kinase activation). As an alternative strategy, a coiled-coil based trimerization motif (LLVWEGDKRVYA)⁴⁶ was also employed in substitution of the foldon, but the recombinant expression of such variants were far inferior to the foldon fusions and were thus not pursued.

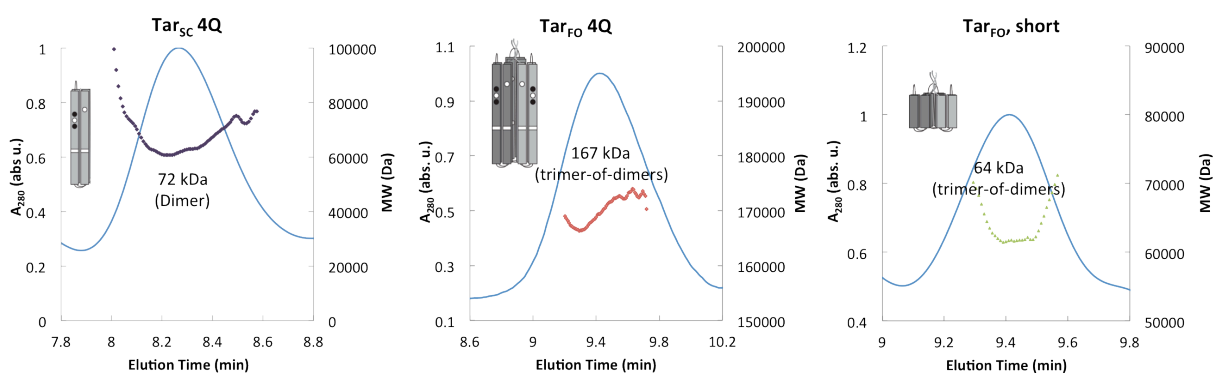


Figure 2-5: MALS of Tar variants. MALS-SEC data of the Tar_{SC} and Tar_{FO} variants. Based on molecular weight predictions, the Tar_{SC} is a monomer both Foldon variants are trimers when injected at 5 mg/mL.

2.3.1: Oligomerization state of the Tar_{FO} mimetics. Different variants of the trimer-of-dimer MCPs exhibited a range of expression levels and varied proteolytic sensitivities. Nevertheless, MALS analysis of the expressed proteins generally indicated a trimeric association state (Figure 2-5), and smaller amounts of higher molecular weight (MW) aggregates. The most stable protein, Tar_{FO} 4Q 515 (number 14 in Table 2-1; and hereafter referred to Tar_{FO} 4Q), produced the highest

levels of expression and was hence subjected to subsequent analysis. Subsequently, a shorter construct employing only the protein interaction region (PIR) of the receptor was also generated. The resulting Tar_{FO}, short (number 17 in Table 2-1) was also well-behaved and further investigated.

MALS-SEC analysis indicates that about 88% of the chromatographed mass of Tar_{FO} 4Q has an average MW of 168 kDa, roughly the expected 171 kDa molecular weight of the trimeric Tar_{FO} 4Q (3 x 59 = 177 kDa, Figure 2-5). Whereas 11% of the calculated mass has an average MW of 209 kDa, which may represent a minor tetrameric state similar to that found for the recombinant MCP Tm14.⁴ The Tar_{SC} produced only a dimer in solution, as predicted with an expected 60 kDa molecular weight. Although the Tar_{FO}, short was more prone to aggregation, however the primary elution peak had the expected MW of 63 kDa (Figure 2-5).

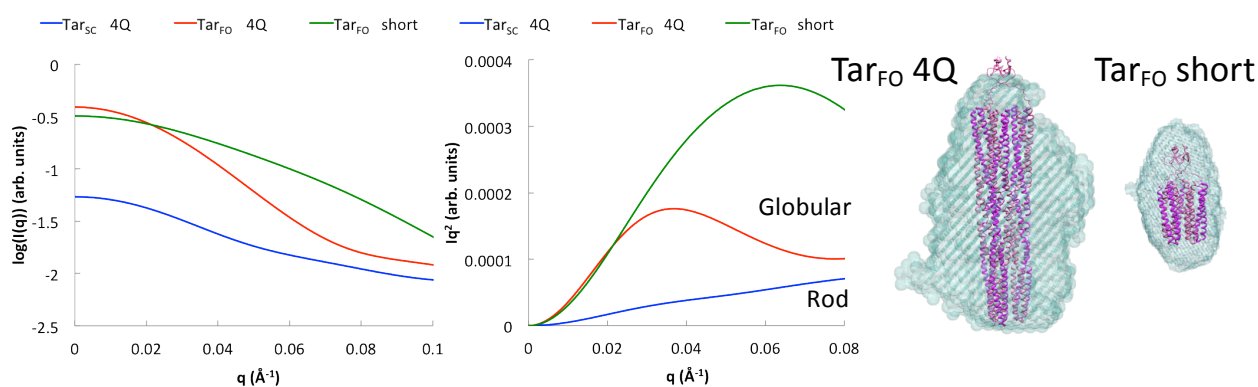


Figure 2-6: SAXS plots and envelopes of Tar variants. SAXS intensity (left) and Kratky plots (right) of Tar_{SC}, Tar_{FO} 4Q, and Tar_{FO} short at 1 mg/mL. A plateau in the Kratky plot at large q indicates rod-like structure⁴⁷⁻⁴⁹, whereas a decrease in Iq^2 indicates a globular polymer. Molecular envelopes calculated with ATSAS and Damaver are superimposed on models of the Tar_{FO} 4Q and Tar_{FO} short based on the fitting of cryo-EM electron density from native receptor arrays to known KCM crystal structures (right).⁹

2.3.2: *Globularity of the Tar_{FO}.* SAXS data reports on the overall shapes and conformational properties of biological macromolecules. For polymers, the shape of the Kratky plot ($I(q)q^2$ vs. q ,

where q represents the scattering vector, $\frac{4\pi \sin(\theta)}{\lambda}$) will distinguish globular structures ($I(q)q^2$ attenuates at high q) from rod-like shapes ($I(q)q^2$ plateaus at high q) and Gaussian chains ($I(q)q^2$ has a positive slope at high q). SAXS data indicates that dimeric KCMs and their single-chain counterparts produce rod-like structures in solution (Figure 2-6). In contrast, the Tar_{FO} 4Q and Tar_{FO} short produce more globular structures. Calculated molecular envelopes for the Tar_{FO} variants generally fit the expected dimension of the respective species (Figure 2-6). The expanded width of the envelope relative to the tightly packed model likely reflects some flexibility of the subunits.

2.3.3: The MCP PIRs associate in Tar_{FO}. Pulsed Dipolar EPR spectroscopy (PDS) was used to monitor the interaction of the PIRs within Tar_{FO}. Nitroxide spin labels were introduced at the very tip of the receptor by substituting Glu389 in the first MCP KCM repeat with cysteine and then reacting the variant with MTS-SL to form the nitroxide side-chain R1. There are no other Cys residues in Tar_{FO}, and the native protein does not react with MTS-SL. Due to the symmetry of the Tar_{SC} a label can potentially reside at six positions within the trimer. However, it seems likely that the foldon linkage to the C-terminus of the second KCM repeat will favor the labeled KCM at either the “inner” or “outer” position within the trimer, effectively yielding three spin-label positions per trimer related by three-fold symmetry (Figure 2-7). If the receptor tips are associated, as in the membrane arrays, the inter-subunit separations should produce distances in the range of ~30-45 Å, depending on label conformational flexibility. Indeed, PDS measurements on the spin-labeled Tar_{FO} reveal a wide, but well defined distance distribution for spin-spin separations of 28-35 Å with a lesser peak at ~45 Å (Figure 2-7). Thus, the receptor tips, which reside ~200 Å from the trimerization motif, must be closely associated. The ~45 Å spin-spin separation may represent some expansion or minor fraying of the tips, but even so, the Tar_{FO}

oligomerization is remarkably structured given that the Tar_{SC} units have little tendency to trimerize on their own at these concentrations.

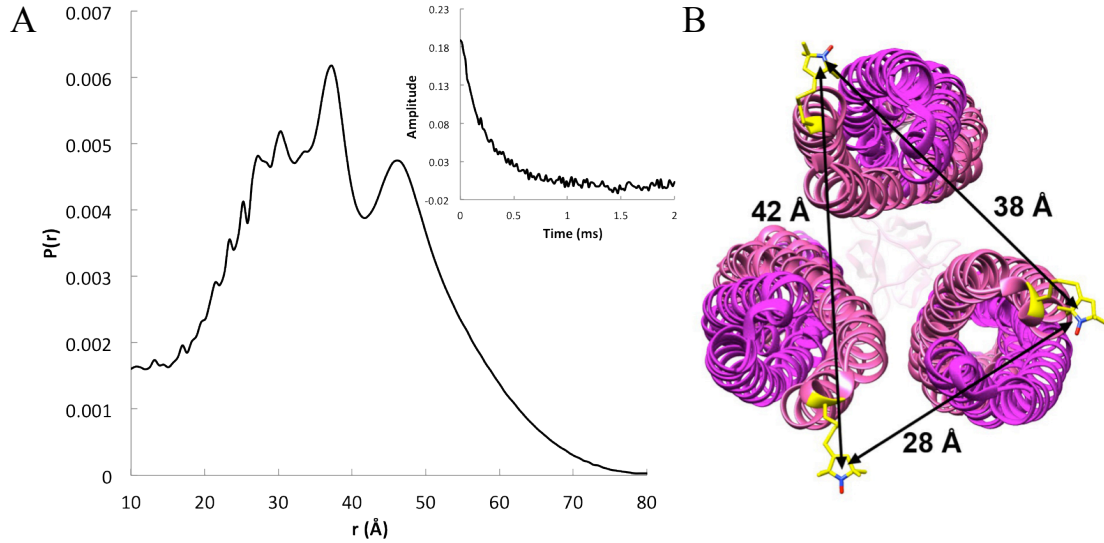


Figure 2-7: EPR plots and visual of distances on Tar trimer-of-dimers. A: PDS analysis of Tar_{FO} DEER spin-separation distance distribution $P(r)$ and time domain data (inset) for Tar_{FO} 4Q 515 E389C-spin (50 μ M) shows a broad distribution with multiple peaks corresponding to the various distances of the nitroxide spin labels at the receptor tips. PDS Data collected by Dr. Xiaoxiao Li. **B:** Model of Tar_{FO} 4Q viewed from the tip toward the Foldon. Distance separations generated by plausible spin label conformers generally agree with the distribution shown in (A).

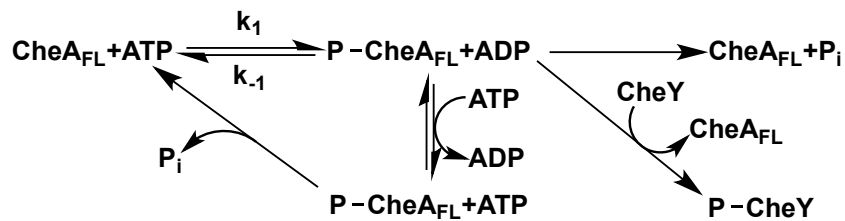


Figure 2-8: CheA phosphotransfer reactions. After CheA autophosphorylation the phosphate group can be transferred from the P1 histidine residue to CheY, back to ADP or undergo hydrolysis. Bimolecular binding of ATP to CheA is assumed fast relative to autophosphorylation under conditions of excess ATP.⁵⁰

2.3.4: *CheA kinase activation by Tar_{FO}.* Autophosphorylation of CheA (Figure 2-8) was monitored by phospho-His (CheA-P) production after reaction with $[\gamma\text{-}^{32}\text{P}]$ ATP, gel

electrophoresis and phosphorimage analysis. Autophosphorylation activity was studied in the presence and absence of CheW and either Tar_{SC}, Tar_{FO} 4Q, or Tar_{FO} short (Figure 2-9). During CheA autophosphorylation phosphate transfer equilibrates between the substrate histidine and ADP.⁵¹ Net His phosphorylation is then a first-order approach to this equilibrium whose endpoint depends on both forward and reverse rate constants (Figure 2-8). However, fast nucleotide exchange (~ seconds)^{50,52,53} competes with the internal equilibration between phospho-His and ATP. Thus, under conditions of saturating of excess ATP, the reverse reaction should be minimal. Nevertheless, ATP preparations can contain contaminating ADP in appreciable amounts and hence alter the endpoint of the autophosphorylation assay.^{50,54} Thus, we monitored the loss of CheA-P after quenching with excess cold ATP. No appreciable change in CheA-P was seen over 30 minutes after addition of 2 mM cold ATP (note that this experiment also then measures the stability of CheA-P, whose $t_{1/2} \gg 30$ min). Given these considerations, CheA autophosphorylation was treated as a first order process and fit to the standard expression (See Methods). In contrast, chasing free CheA with excess cold ADP (2 mM) favors the back reaction and thereby depletes CheA-P over the course of minutes (Figure 2-10B). There appears to be two phases to this response: a fast initial decay and then a slower prolonged decrease. The presence of CheW or Tar variants had little effect on the back reaction with ADP, but addition of the Tar_{FO} and Tar_{SC} species largely removed the fast phase of the CheA-P depletion. In these and subsequent autophosphorylation reactions proteins were pre-incubated for 10 minutes to 1 hour with CheW and the Tar variants to facilitate complex formation. All reactions were run under conditions of excess ATP.

When complexed with CheW and the Tar_{FO} variants CheA autophosphorylation increases, but the progress curves had unexpected time dependencies. Under our conditions,

CheW alone increases CheA autophosphorylation somewhat at early time points (~30 seconds). Nonetheless, the measured k_1 value for the first-order CheA:CheW autophosphorylation (1.2 min^{-1}) is similar to that measured previously for CheA alone (1.5 min^{-1}).⁵⁰ The Tar variants without CheW generally inhibit autophosphorylation, but with CheW present, autophosphorylation increases to a level that exceeds that of CheW alone (Figure 2-10, Table 2-2). Maximum activation was observed when the complexes were preformed at least 1 hour prior to ATP addition.

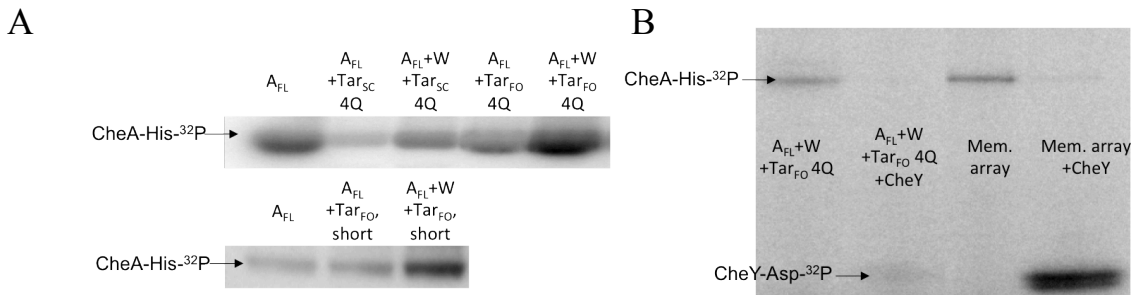


Figure 2-9: Phosphorimage of gels of CheA activity with receptors. Phosphorimage PAGE gel of *E. coli* CheA autophosphorylation with receptor variants \pm CheW. All the receptors increase CheA activity only if CheW is present. *E. coli* CheA ($2.5 \mu\text{M}$), CheW ($2.5 \mu\text{M}$), and Tar_{FO} ($5 \mu\text{M}$) or Tar_{SC} ($15 \mu\text{M}$) and CheY ($40 \mu\text{M}$) were incubated at 25°C for 1 hour prior to exposure for 30 seconds. **A:** *E. coli* CheA-P with receptors \pm CheW. All the receptors increase CheA activity only if CheW is present. **B:** PAGE gel comparing CheA activity with the Tar_{FO} 4Q versus membrane (Mem.) array comprised of CheA ($2.5 \mu\text{M}$), CheW ($5 \mu\text{M}$) and Tsr receptors ($3.4 \mu\text{M}$).

Autophosphorylation at < 30 seconds appeared increased with addition of the Tar variants (Figure 2-9 and 2-10), but quantitative comparisons proved difficult at short times. At longer times phosphorylated CheA-P accumulated in the presence of variants, reaching plateau values that far exceed that of CheA:CheW alone (Figure 2-10A, Table 2-2). This reactivity is accentuated greatest by the Tar_{FO} short which produces saturation levels of CheA-P ~20-fold greater than that of CheA:CheW alone after 12 minutes (Figure 2-10A, Table 2-2). All the progress curves could be fit reasonably well to a first order expression, with the resulting

prefactors and rate constants dominated by the plateau behavior at long times (Table 2-2). The Tar_{FO} short showed some indication of a faster phase < 1.5 minutes, but this was difficult to resolve in biexponential fits (Figure 2-10A). The initial rates of the time course (k_1A_0) for CheA:CheW alone, Tar_{SC}, Tar_{FO} 4Q, Tar_{FO} short are all relatively similar (Table 2-2). Notably, the amount of CheA-P produced with the Tar_{FO} 4Q is commensurate with that observed in native membrane arrays that contain a similar amount of CheA (Figure 2-10B) (Membrane arrays were kindly provided by Kene Piasta and Joseph Falke, University of Colorado, Boulder). Previous studies of CheA activation on receptor binding gave changes in plateau CheA-P values on the order of 5-10-fold, but in these cases CheA-P saturation usually occurred within a few minutes.^{18,23,51,54-56} Interestingly, the species with the largest prefactors, have rate constants that are much *less* than that for autophosphorylation by isolated CheA:CheW. This slower process likely represents conversion from an inactive to active form of CheA facilitated by the Tar variants. After conversion, fast autophosphorylation builds up CheA-P, which is then stable over the assay time course.

Although the Tar variants increase autophosphorylation yields, they do not activate subsequent CheY transfer to the extent observed in the membrane arrays (Figure 2-10B, D), where activity can change more than 100 fold.^{12,13,55,57} This is despite the fact that CheY completely dephosphorylates similar amounts of CheA-P in the membrane arrays or in complex with the foldon species (Figure 2-10). Tar_{FO} 4Q does produce a moderate increase in phosphotransfer to CheY, but surprisingly the Tar_{FO} short shows no increase at all (Figure 2-10D). One possibility for this behavior is that, exchange between the inactive and active forms of CheA, facilitated by the Tar variants, still greatly favors the inactive kinases and thus, little CheA-P is available on the time scales of CheY phosphotransfer and the stability of CheY-P.

Alternatively, CheA may have the capability of being activated at two levels, one that increases autophosphorylation and a second that increases CheY-phosphotransfer. The Tar_{FO} variants then only achieve the former. Higher concentrations of Tar_{SC} and Tar_{FO} do not further increase CheA autophosphorylation nor CheY phosphotransfer, probably because most Tar_{FO} species associate with CheA:CheW under conditions of the assay (Figure 2-11) and more Tar variant will compete CheW away from CheA.^{18,58}

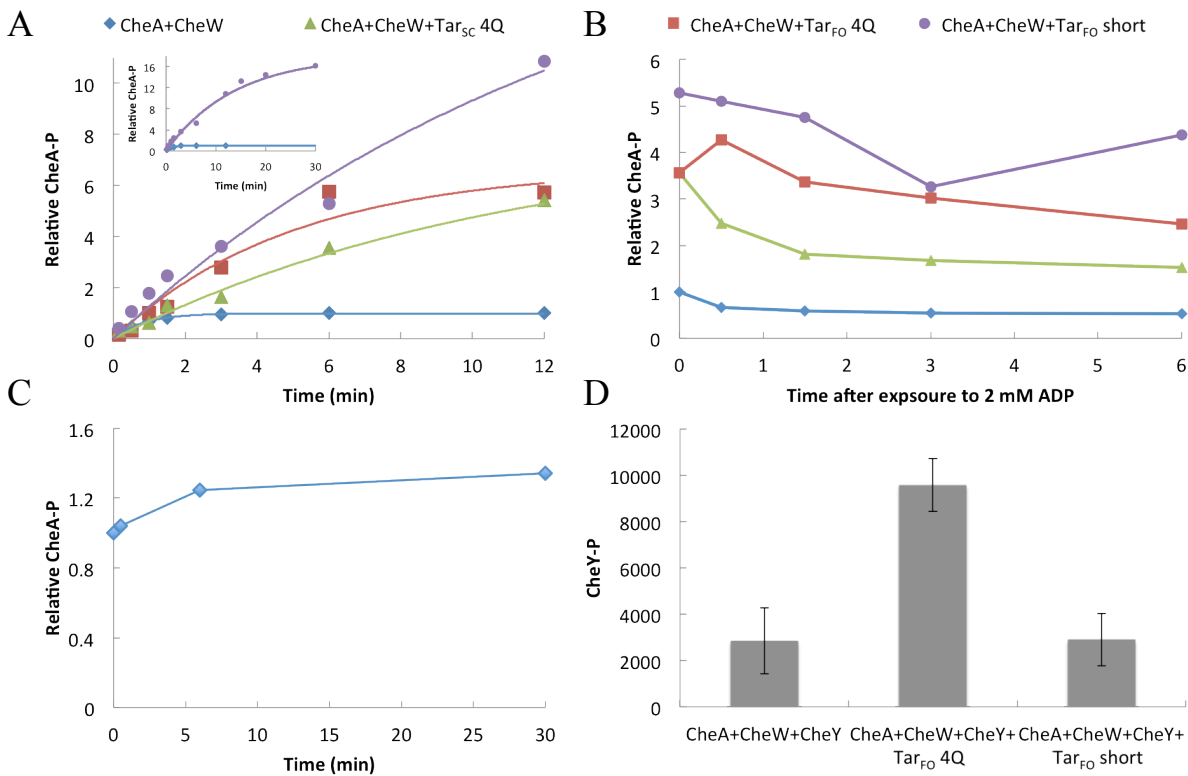


Figure 2-10: CheA activity over time with receptors. In all assays *E. coli* CheA (1 μ M), CheW (1 μ M), and Tar_{FO} 4Q and short (1 μ M) or Tar_{SC} (3 μ M) incubated at 25 °C for 1 hour prior to exposure for the indicated time points. Each data point represents an average over 2-4 assays. **A:** CheA-P formation over time in the presence of CheW and Tar variants. Inset shows CheA-P buildup in the Tar_{FO} short at long times compared to CheA:CheW. **B:** Addition of cold ADP to CheA+CheW \pm Tar variants after autophosphorylation for 6 minutes. **C:** Addition of cold ATP to CheA+CheW 6 minutes after incubation with γ -³²P-ATP. **D:** Transfer to CheY in the presence of CheA+CheW \pm Tar_{FO} 4Q and short. Error bars represent standard error of the mean (SEM) calculated from three independent experiments (n = 3).

Components	A_0 (P1-P formation)	k_1 (minutes ⁻¹)	R^2
CheA+CheW	0.99 ± 0.01	1.18 ± 0.05	0.99
CheA+CheW+Tar _{SC} 4Q	8 ± 1	0.08 ± 0.02	0.98
CheA+CheW+Tar _{FO} 4Q	6 ± 1	0.20 ± 0.03	0.94
CheA+CheW+Tar _{FO} short	21 ± 9	0.05 ± 0.03	0.96

Table 2-2: Kinetic parameters for autophosphorylation assays. Prefactor and rate constant values from activity vs. time fits. Addition of receptor increases the prefactor value and decreases the rate constant. Relative rates (k_1A_0) were determined.

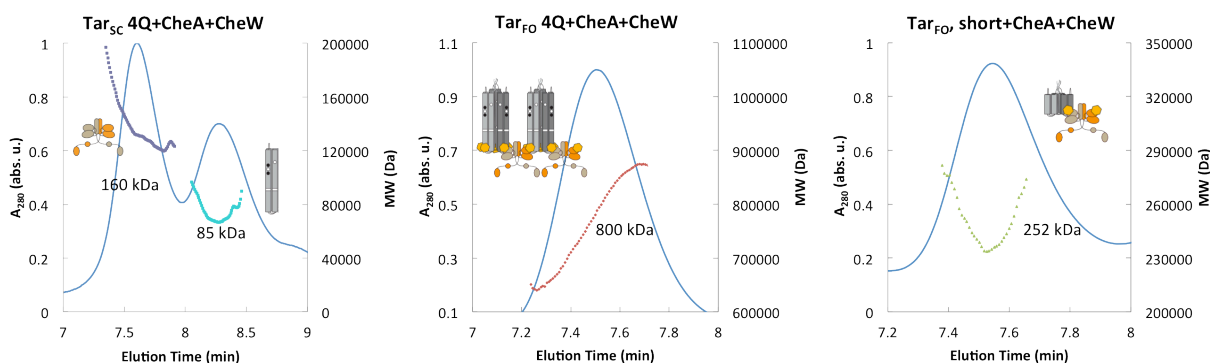


Figure 2-11: MALS of ternary complexes. MALS-SEC traces of CheA:CheW complexes with Tar variants. The Tar_{FO} complexes produced well-defined SEC elution profiles containing high molecular weight complexes. The Tar_{FO} 4Q complex had a greater polydispersity than the Tar_{FO} short complex, which was highly monodisperse. In contrast, the Tar_{SC} shows only monodisperse peaks corresponding to CheA dimer and Tar_{SC}. Cartoon representations of hypothetical complexes corresponding to the average molecular weights are shown. Samples were incubated at 25 °C for 1 hour prior to injection with CheA:CheW:Tar_{SC} in a 1:1:6 subunit ratio and CheA:CheW:Tar_{FO} in a 1:1:2 subunit ratio. Samples were run at a total protein concentration of 5 mg/mL.

2.3.5: *Interactions of Tar variants with CheA:CheW.* MALS-SEC was used to examine the interactions between the Tar variants and CheA:CheW. Mixtures of Tar_{SC} and CheA:CheW showed little complex formation on MALS-SEC, even after an hour of precubincubation; however, both the Tar_{FO} 4Q and the Tar_{FO} short produced large complexes that were reasonably monodisperse (Figure 2-11). In the case of Tar_{FO} short, the average MW corresponded to that of one CheA:CheW dimer and one Tar_{FO} short; whereas in the case of the Tar_{FO} 4Q, the complex was larger, more heterogeneous and likely involved at least two copies of the Tar_{FO} and

CheA:CheW. MW and radius of gyration analyses of the elution peaks indicated primarily a single species for CheA:CheW complexes with Tar_{FO} short, but more heterogeneity for the Tar_{FO} 4Q.

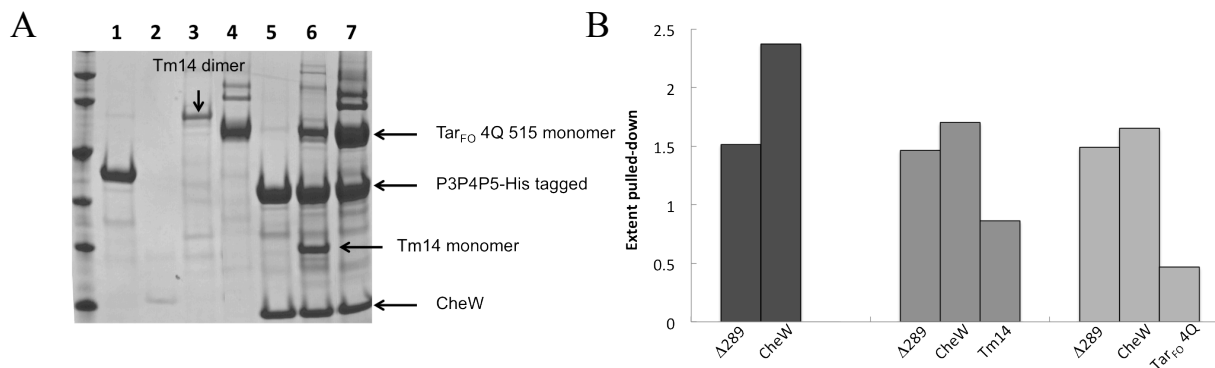


Figure 2-12: Pulldown of *T. maritima* CheA+CheW and receptors. Pulldown assay for interactions between Tar variants and CheA:CheW. **A:** Lane 1: His-tagged CheA P3P4P5 (75 μM), lane 2-5: Ni²⁺-NTA bead interaction with untagged CheW (2), Tm14 which runs primarily as a dimer (3), and Tar_{FO} 4Q (4) which shows non-specific binding to Ni²⁺-NTA. Lanes 5-7, pull-downs by CheA P3P4P5-His of CheW (5), CheW+ Tm14 (6), CheW+ Tar_{FO} 4Q (7). All interacting proteins at 100 μM except Tar_{FO} 4Q at a 74-90 μL of 7 μM and Tm14 at 74-90 μL of 49 μM. **B:** Bar plot of pulldown to account for non-specific binding.

2.3.6: *Effects of Tar_{FO} on CheA conformation.* The structure of the ternary complex between the *T. maritima* CheA:CheW complex and an inhibitory KCM from the *T. maritima* receptor Tm14 (previously denoted MCP_C, residues 41-254) has been previously investigated by spin-labeling and PDS.⁵⁹ The arrangements of the regulatory CheA P5 domains in this inhibitory complex were different than those predicted from modeling the CheA:CheW complex into the ECT maps of intact receptor arrays, wherein CheA P5 and CheW polymerize into planar interlocking ring structures.⁹ Thus, it was investigated whether the effect of the Tar_{FO} 4Q on a spin-label reporter site of the *T. maritima* CheA/CheW P5 complex known to be sensitive to receptor binding (residue 545, *T. maritima*).⁵⁹ A pulldown assay confirmed that Tar_{FO} 4Q and Tm14 bind to *T. maritima* P3P4P5 and CheW with similar affinities (Figure 2-12). Subsequent DEER

measurements on CheA:CheW spin-labeled at position 545 reveals that the Tar_{FO} induces a ~7 Å increase in the separation of the P5 domains relative to that observed with Tm14 (Figure 2-13). In addition, the spin-spin distribution has greater breadth compared with that of the inhibitory receptor and retains a minor distance peak at the position seen with Tm14. The longer distances with Tar_{FO} 4Q are consistent with conversion to the more planar P5 arrangement needed to accommodate the larger trimeric assembly of receptors found in the membrane arrays. The broadness of the distribution may reflect flexibility in the absence of the extended ring structures of the arrays.

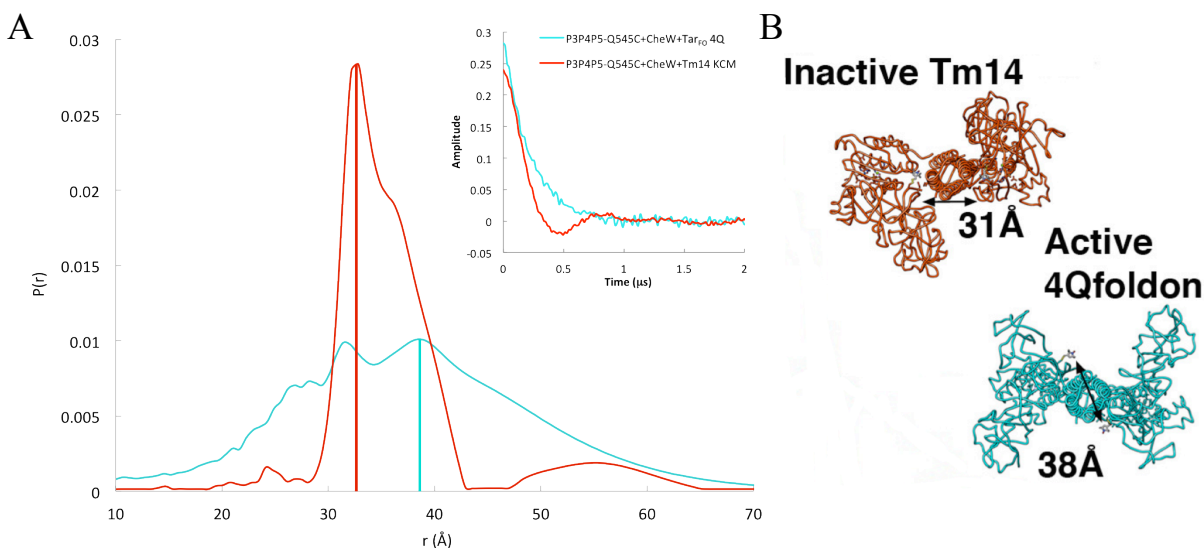


Figure 2-13: EPR probability density with activating and deactivating receptor. **A:** Distance distributions (left) and background-corrected time-domain data (right) of spin separations in *T. maritima* CheA P3P4P5 (Δ 289) Q545C (38 μ M) + CheW (55 μ M) with Tm14 KCM (138 μ M) and Tar_{FO} 4Q (100 μ M). **B:** Structural prediction of distance between the spin labels in the inhibited form of CheA (red) and an active form with planar P5 domains (cyan). PDS data obtained by Dr. Xiaoxiao Li.

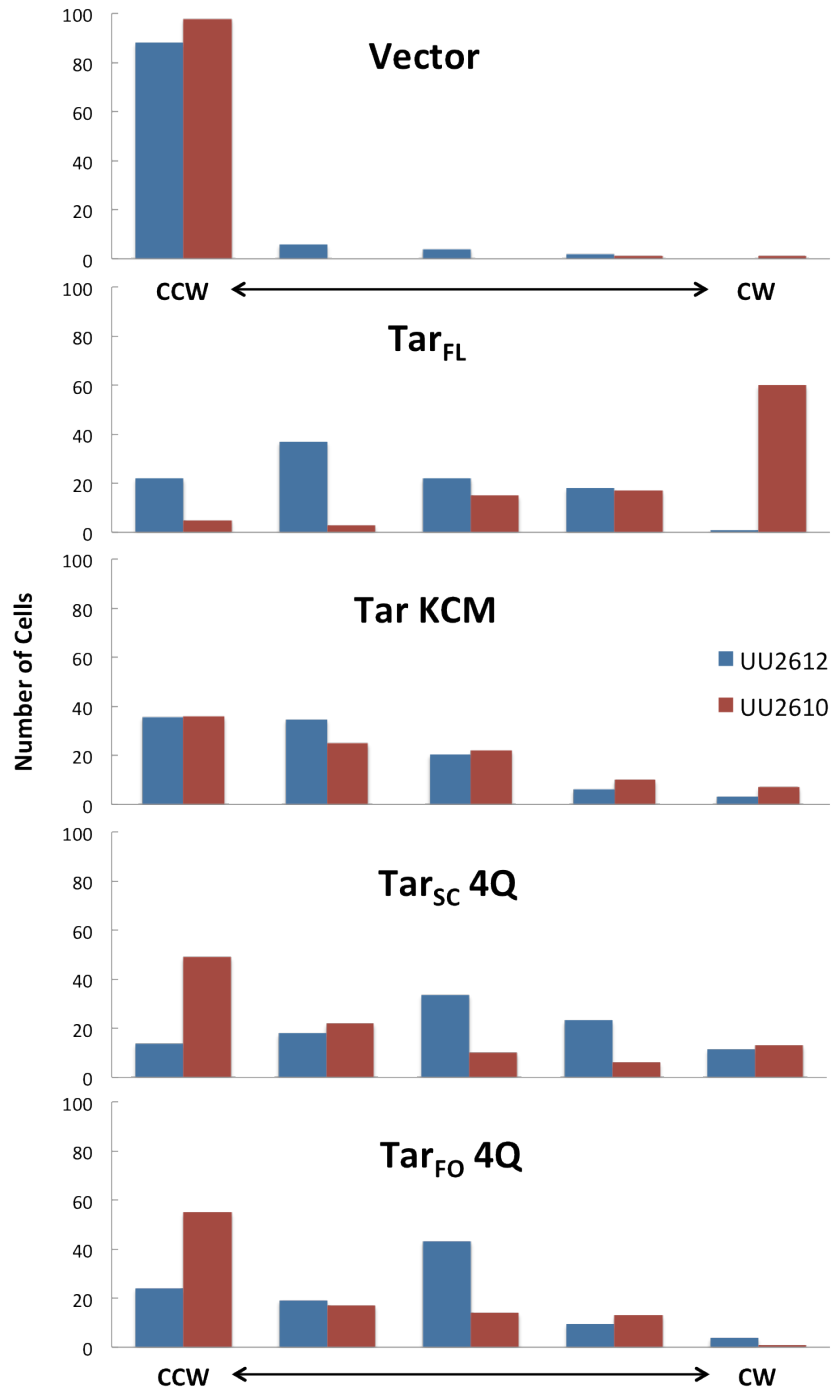


Figure 2-14: Flagellar rotation patterns of *E. coli* cells transformed with Tar variants. Rotation patterns were determined in the absence (UU2610) or presence (UU2612) of the methylation system (CheB/R). Both strains lacked all native chemoreceptors. Each histogram summarizes the behavior of rotating cells as (from left to right): exclusively CCW, predominantly CCW, frequently reversing with no overall directional bias, predominantly CW, and exclusively CW. Data obtained with assistance from Dr. Kylie Watts, Loma Linda University.

2.3.7: *Cellular activities of Tar_{FO}*. To test the function of Tar_{FO} *in vivo* we introduced Tar_{FO} 4Q into an *E. coli* strain devoid of all other chemoreceptors and monitored flagella rotation in a tethered cell assay. Of the two foldon species, Tar_{FO} 4Q was chosen because it shows the greatest ability to activate phosphotransfer to CheY. In these assays, CheA inhibition causes CCW flagella rotation, whereas CheA activation causes CW flagella bias. Flagella rotation biases were determined for cell populations containing full-length membrane incorporated Tar, the dimeric Tar KCM, Tar_{SC} and Tar_{FO}; all in the absence (strain UU2610) and presence (strain UU2612) of the methylation system (CheR and CheB). Introduction of full-length Tar causes a strongly CW phenotype in CheRB- cells (UU2610) that adapts back toward CCW in the presence of the methylation system (UU2612) (Figure 2-14). The Tar signaling domain alone (KCM) produces much less CW bias, and is largely unaffected by the methylation system. This degree of CheA activity is less than that seen with cytoplasmic receptor domains when an activating HAMP domain is fused to their N-terminus.²⁵ In CheRB- cells both Tar_{FO} and Tar_{SC} similarly increase CW bias (Figure 2-14). For Tar_{FO} 4Q and Tar_{SC} CW bias increases further in the presence of the methylation system to an extent that exceeds that of full-length Tar. This result is somewhat surprising because the methylation sites are coded as all-Gln in each case, and hence no further activation by CheR should be possible. Indeed, although all of the proteins were well expressed, Tar_{SC} or Tar_{FO} were not methylated in *E. coli*. The increased kinase activity of Tar_{FO} 4Q and Tar_{SC} in CheRB+ cells may reflect stabilization of the Tar_{FO} and Tar_{SC} kinase assemblies by binding of the methylation enzymes. CheR presumably binds to more dynamic adaptation regions, which the Tar_{FO} may possess in the absence of membrane association. Alternatively, CheB-mediated deamination may alter the Tar_{FO} conformation in a manner that produces an inverted response. Similar effects have been observed with HAMP domain point mutations and

generally speak to the conformational sensitivity of the signaling complex.^{25,60,61} Unfortunately, the QEQE versions of the Tar_{FO} were not sufficiently stable to evaluate their *in vivo* properties. Unfortunately, the QEQE versions of the Tar_{FO} were not sufficiently stable to evaluate their *in vivo* properties.

2.4: Discussion

A soluble chemoreceptor module that mimics the trimer-of-dimers assembly state found in membrane arrays was developed to study the effect of receptor trimerization on kinase activity and structure. Fusing KCM subunits together into a single-chain “dimer” and then trimerizing the resulting units with a surrogate foldon domain produces a surprisingly homogeneous and globular structure with associated PIRs. Additionally, conversion to the all Gln state (4Q), which stabilizes the adaptation region by removing negative charge,^{25,62,63} aids in better expression levels and stability.

2.4.1: Structural considerations of soluble receptor mimics. Several approaches have been taken to study the interaction of CheA:CheW complexes with simplified receptor species. Leucine-zipper dimerization and HAMP domains have been used to stabilize chemoreceptor cytoplasmic domains and form stable complexes with CheA.¹⁵⁻²⁵ KCM fragments also show honeycomb structures when expressed with CheA and CheW and treated with osmolytes.¹⁵⁻²⁵ KCM fragments templated on lipid bilayers produce hexagonal symmetries and give large degrees of CheA activation.^{18,20,64} Nanodisk-incorporated receptors show native-like behaviors and also allow the assessment of different assembly states, but the quantities of activated complexes obtained are relatively small.^{11-13,65,66} All of these aforementioned CheA:receptor assemblies are heterogeneous and many also involve lipid components. The Tar_{FO} variants developed here produces homogeneous, well-defined ternary complexes that bind CheA, increase

autophosphorylation and can be studied by biophysical methods such as pulsed EPR, SAXS, single particle EM and crystallography. The globular nature of the Tar_{FO} from SAXS and PDS distance restraints demonstrate the tendency for the PIRs to associate in the absence of other factors, provided that they are held in close proximity. Moreover, the receptor tips trimerize even though the foldon associates the KCM N-termini more closely than is found in the natural arrays, where they tend to spread apart as they approach the membrane.⁹ The trimeric nature of the Tar_{FO} 4Q is also reflected in the conformation of bound CheA. Compared to when CheA binds a single KCM (e.g. Tm14), the P5 domains are spread farther apart across the CheA dimer interface to accommodate the larger trimeric species. The P5 domains are then placed in a planar arrangement, which is the conformation needed to template the hexagonal receptor arrays (Figure 1-13). These results also match expectations from recent molecular dynamics simulations that implicate a planar arrangement of P5 as a preferred conformation for the kinase.⁶⁷

2.4.2: Effects of Tar variants on CheA activity. Pulldown assay, PDS experiments, and activity assays demonstrate that the Tar_{FO} species interact with CheA and CheW. The degree of CheA autophosphorylation observed with Tar_{FO} and CheW compares favorably with receptor mediated CheA autophosphorylation in membrane arrays^{18,23,51,54-56,68}, albeit the kinetics differ. As in these other experiments, the Tar_{FO} species primarily increase the prefactor terms and hence the level of CheA-P at saturation. One explanation for such behavior is that receptors alter the position of the equilibrium (k_1 and/or k_{-1}) between forward phosphorylation of substrate His and reverse phosphorylation of ADP (Figure 2-8). However, in the presence of saturating ATP, nucleotide exchange will out-complete the reverse reaction, and thus His phosphorylation should proceed to completion. Furthermore, a 10-fold change in total CheA-P production would imply large changes to the k_1 and k_{-1} that are not indicated under conditions of cold ADP chase. A second

rationale for the increase in peak autophosphorylation is that the fraction of kinase capable of autophosphorylation increases in the Tar_{FO} complexes, i.e. the CheA has an inactive and active form and the receptor variants increase access to an active conformation of the kinase. For free CheA, a large fraction of kinase is inactive, and this form exchanges slowly with the active fraction on the time scale of the experiment. The Tar variant complexes produce more active CheA, but exchange from the inactive form is also accelerated so that much greater levels of CheA-P accumulate. The rate constant for exchange is less than that for autophosphorylation. The lower activation numbers with Tar_{SC} likely reflect the higher entropic cost of assembling the active form, which is circumvented in Tar_{FO} by the preformed foldon trimer.

Unlike CheA autophosphorylation, CheY phosphotransfer activity is not substantially increased by the Tar_{FO} variants. With all receptor preparations tested, CheY fully dephosphorylates CheA within 10 seconds; yet only with the membrane arrays do large amounts of CheY-P accumulate. One possibility for this difference is that the Tar variants do not lock in the active state of CheA to the same degree as the membrane arrays. Exchange to the active form occurs more readily than with free CheA, but it is slow relative to CheY phosphotransfer. With the Tar variants, the rate constant k_1 largely represents this exchange rate. Consistent with this view, the Tar_{FO} 4Q, which has the largest k_1 value of the variants also shows the greatest increase in CheY phosphotransfer. Alternatively, there could be two steps to CheA activation, one involving autophosphorylation and the other net phosphotransfer to CheY, with the variants only affecting the former (Figure 2-8). The phospho-His is more labile in the activated form of membrane associated CheA compared to the inhibited state due to enhanced reaction with ADP.⁵⁶ Interestingly, Tar_{FO} associated-CheA does not show this enhanced exchange with ADP, and if anything, the back reaction diminishes in these complexes. Thus, low phosphate exchange

with ADP correlates with low phosphotransfer to CheY. Nonetheless the Tar_{FO} 4Q variant does increase CheY phosphotransfer to some extent and this is reflected by increased CW-biased flagellar rotation when Tar_{FO} 4Q in the presence of the methylation system. Notably, the Tar_{FO} variants do not achieve the same degree of activation *in vivo* as Tar cytoplasmic domains that are fused to activating HAMP domains.²⁵ Apparently, the specific conformation of each receptor dimer, set by HAMP, is critical to achieve a high degree of CheA activation, even in the context of trimeric receptors.

In conclusion, Tar_{FO} variants demonstrate that constrained receptor PIRs will trimerize and that these species will bind CheA and CheW to form defined complexes in the absence of membranes or other components. Thus, the Tar variants provide a useful tool for studying how receptor engagement affects the structure and activity of the CheA:CheW complex. Importantly, the trimer mimetics stimulate CheA autophosphorylation by increasing the fraction of active kinase and facilitating conversion from the inactive form. The active and inactive conformations of CheA when bound to these PIR trimers may represent the activity states modulated by chemoattractant in native membrane arrays. Further investigations will be aimed at understanding what molecular features influence the stability of these states and hence the accumulation of phosphorylated CheY by these complexes.

REFERENCES

- (1) Maddock; Shapiro, L. *Science* **1993**, *259*, 1717–1723.
- (2) Kim, K. K.; Yokota, H.; Kim, S.-H. *Nature* **1999**, *400*, 787–792.
- (3) Briegel, A.; Ortega, D. R.; Tocheva, E. I.; Wuichet, K.; Li, Z.; Chen, S.; Müller, A.; Iancu, C. V.; Murphy, G. E.; Dobro, M. J.; Zhulin, I. B.; Jensen, G. J. *Proc. Natl. Acad. Sci.* **2009**, *106*, 17181–17186.
- (4) Li, X.; Fleetwood, A. D.; Bayas, C.; Bilwes, A. M.; Ortega, D. R.; Falke, J. J.; Zhulin, I. B.; Crane, B. R. *Biochemistry (Mosc.)* **2013**, *52*, 3852–3865.
- (5) Ames, P.; Studdert, C. A.; Reiser, R. H.; Parkinson, J. S. *Proc. Natl. Acad. Sci.* **2002**, *99*, 7060–7065.
- (6) Studdert, C. A.; Parkinson, J. S. *Proc. Natl. Acad. Sci. U. S. A.* **2004**, *101*, 2117–2122.
- (7) Zhang, P.; Khursigara, C. M.; Hartnell, L. M.; Subramaniam, S. *Proc. Natl. Acad. Sci.* **2007**, *104*, 3777–3781.
- (8) Briegel, A.; Ding, H. J.; Li, Z.; Werner, J.; Gitai, Z.; Dias, D. P.; Jensen, R. B.; Jensen, G. *J. Mol. Microbiol.* **2008**, *69*, 30–41.
- (9) Briegel, A.; Li, X.; Bilwes, A. M.; Hughes, K. T.; Jensen, G. J.; Crane, B. R. *Proc. Natl. Acad. Sci.* **2012**, *109*, 3766–3771.
- (10) Liu, J.; Hu, B.; Morado, D. R.; Jani, S.; Manson, M. D.; Margolin, W. *Proc. Natl. Acad. Sci.* **2012**, *109*, E1481–E1488.
- (11) Boldog, T.; Grimme, S.; Li, M.; Sligar, S. G.; Hazelbauer, G. L. *Proc. Natl. Acad. Sci.* **2006**, *103*, 11509–11514.
- (12) Li, M.; Hazelbauer, G. L. *Proc. Natl. Acad. Sci.* **2011**, *108*, 9390–9395.

- (13) Li, M.; Khursigara, C. M.; Subramaniam, S.; Hazelbauer, G. L. *Mol. Microbiol.* **2011**, *79*, 677–685.
- (14) Piasta, K. N.; Ulliman, C. J.; Slivka, P. F.; Crane, B. R.; Falke, J. J. *Biochemistry (Mosc.)* **2013**, *52*, 3866–3880.
- (15) Pollard, A. M.; Bilwes, A. M.; Crane, B. R. *Biochemistry (Mosc.)* **2009**, *48*, 1936–1944.
- (16) Briegel, A.; Ladinsky, M. S.; Oikonomou, C.; Jones, C. W.; Harris, M. J.; Fowler, D. J.; Chang, Y.-W.; Thompson, L. K.; Armitage, J. P.; Jensen, G. J. *eLife* **2014**, *3*, e02151.
- (17) Ames, P.; Parkinson, J. S. *J Bacteriol* **1994**, *176*, 6340–6348.
- (18) Asinas, A. E.; Weis, R. M. *J. Biol. Chem.* **2006**, *281*, 30512–30523.
- (19) Besschetnova, T. Y.; Montefusco, D. J.; Asinas, A. E.; Shrout, A. L.; Antommattei, F. M.; Weis, R. M. *Proc. Natl. Acad. Sci.* **2008**, *105*, 12289–12294.
- (20) Shrout, A. L.; Montefusco, D. J.; Weis, R. M. *Biochemistry (Mosc.)* **2003**, *42*, 13379–13385.
- (21) Seeley, S. K.; Weis, R. M.; Thompson, L. K. *Biochemistry (Mosc.)* **1996**, *35*, 5199–5206.
- (22) Francis, N. R.; Wolanin, P. M.; Stock, J. B.; DeRosier, D. J.; Thomas, D. R. *Proc. Natl. Acad. Sci. U. S. A.* **2004**, *101*, 17480–17485.
- (23) Levit, M. N.; Stock, J. B. *J. Biol. Chem.* **2002**, *277*, 36760–36765.
- (24) Wolanin, P. M.; Baker, M. D.; Francis, N. R.; Thomas, D. R.; DeRosier, D. J.; Stock, J. B. *Proc. Natl. Acad. Sci.* **2006**, *103*, 14313–14318.
- (25) Airola, M. V.; Sukomon, N.; Samanta, D.; Borbat, P. P.; Freed, J. H.; Watts, K. J.; Crane, B. R. *PLoS Biol* **2013**, *11*, e1001479.
- (26) Bhardwaj, A.; Walker-Kopp, N.; Wilkens, S.; Cingolani, G. *Protein Sci.* **2008**, *17*, 1475–1485.

- (27) Habazettl, J.; Reiner, A.; Kiefhaber, T. *J. Mol. Biol.* **2009**, *389*, 103–114.
- (28) Tao, Y.; Strelkov, S. V.; Mesyanzhinov, V. V.; Rossmann, M. G. *Structure* **1997**, *5*, 789–798.
- (29) Sourjik, V. *Trends Microbiol.* **2004**, *12*, 569–576.
- (30) Skou, S.; Gillilan, R. E.; Ando, N. *Nat. Protoc.* **2014**, *9*, 1727–1739.
- (31) Nielsen, S. S.; Møller, M.; Gillilan, R. E. *J. Appl. Crystallogr.* **2012**, *45*, 213–223.
- (32) Nielsen, S. S.; Toft, K. N.; Snakenborg, D.; Jeppesen, M. G.; Jacobsen, J. K.; Vestergaard, B.; Kutter, J. P.; Arleth, L. *J. Appl. Crystallogr.* **2009**, *42*, 959–964.
- (33) Konarev, P. V.; Volkov, V. V.; Sokolova, A. V.; Koch, M. H. J.; Svergun, D. I. *J. Appl. Crystallogr.* **2003**, *36*, 1277–1282.
- (34) Franke, D.; Svergun, D. I. *J. Appl. Crystallogr.* **2009**, *42*, 342–346.
- (35) Volkov, V. V.; Svergun, D. I. *J. Appl. Crystallogr.* **2003**, *36*, 860–864.
- (36) Kozin, M. B.; Svergun, D. I. *J. Appl. Crystallogr.* **2001**, *34*, 33–41.
- (37) Erbse, A. H.; Falke, J. J. *Biochemistry (Mosc.)* **2009**, *48*, 6975–6987.
- (38) Hilger, D.; Jung, H.; Padan, E.; Wegener, C.; Vogel, K. P.; Steinhoff, H. J.; Jeschke, G. *Biophys. J.* **2005**, *89*, 1328–1338.
- (39) Jeschke, G.; Abbott, R. J. M.; Lea, S. M.; Timmel, C. R.; Banham, J. E. *Angew. Chem.-Int. Ed.* **2006**, *45*, 1058–1061.
- (40) Jeschke, G.; Chechik, V.; Ionita, P.; Godt, A.; Zimmermann, H.; Banham, J.; Timmel, C. R.; Hilger, D.; Jung, H. *Appl. Magn. Reson.* **2006**, *30*, 473–498.
- (41) Sale, K.; Song, L. K.; Liu, Y. S.; Perozo, E.; Fajer, P. *J Am Chem Soc* **2005**, *127*, 9334–9335.
- (42) Chiang, Y. W.; Borbat, P. P.; Freed, J. H. *J Magn Reson* **2005**, *172*, 279–295.

- (43) Chiang, Y. W.; Borbat, P. P.; Freed, J. H. *J. Magn. Reson.* **2005**, *177*, 184–196.
- (44) Slocum, M. K.; Parkinson, J. S. *J. Bacteriol.* **1985**, *163*, 586–594.
- (45) Kort, E. N.; Goy, M. F.; Larsen, S. H.; Adler, J. *Proc. Natl. Acad. Sci.* **1975**, *72*, 3939–3943.
- (46) Woolfson, D. N.; Alber, T. *Protein Sci. Publ. Protein Soc.* **1995**, *4*, 1596–1607.
- (47) Putnam, C. D.; Hammel, M.; Hura, G. L.; Tainer, J. A. *Q. Rev. Biophys.* **2007**, *40*, 191–285.
- (48) Mertens, H. D. T.; Svergun, D. I. *J. Struct. Biol.* **2010**, *172*, 128–141.
- (49) Svergun, D. I.; Koch, M. H. *J. Rep. Prog. Phys.* **2003**, *66*, 1735.
- (50) Tawa, P.; Stewart, R. C. *Biochemistry (Mosc.)* **1994**, *33*, 7917–7924.
- (51) Surette, M. G.; Levit, M.; Liu, Y.; Lukat, G.; Ninfa, E. G.; Ninfa, A.; Stock, J. B. *J. Biol. Chem.* **1996**, *271*, 939–945.
- (52) Stewart, R. C. *Biochemistry (Mosc.)* **2005**, *44*, 4375–4385.
- (53) Eaton, A. K.; Stewart, R. C. *Biochemistry (Mosc.)* **2010**, *49*, 5799–5809.
- (54) Ninfa, E. G.; Stock, A.; Mowbray, S.; Stock, J. *J. Biol. Chem.* **1991**, *266*, 9764–9770.
- (55) Borkovich, K. A.; Kaplan, N.; Hess, J. F.; Simon, M. I. *Proc. Natl. Acad. Sci. U. S. A.* **1989**, *86*, 1208–1212.
- (56) Borkovich, K. A.; Simon, M. I. *Cell* **1990**, *63*, 1339–1348.
- (57) Stewart, R. C.; Van Bruggen, R. *J. Mol. Biol.* **2004**, *336*, 287–301.
- (58) Gegner, J. A.; Graham, D. R.; Roth, A. F.; Dahlquist, F. W. *Cell* **1992**, *70*, 975–982.
- (59) Bhatnagar, J.; Borbat, P. P.; Pollard, A. M.; Bilwes, A. M.; Freed, J. H.; Crane, B. R. *Biochemistry (Mosc.)* **2010**, *49*, 3824–3841.
- (60) Zhou, Q.; Ames, P.; Parkinson, J. S. *Mol. Microbiol.* **2009**, *73*, 801–814.

- (61) Zhou, Q.; Ames, P.; Parkinson, J. S. *Mol. Microbiol.* **2011**, *80*, 596–611.
- (62) Surette, M. G.; Stock, J. B. *J. Biol. Chem.* **1996**, *271*, 17966–17973.
- (63) Starrett, D. J.; Falke, J. J. *Biochemistry (Mosc.)* **2005**, *44*, 1550–1560.
- (64) Weis, R. M.; Hirai, T.; Chalah, A.; Kessel, M.; Peters, P. J.; Subramaniam, S. *J. Bacteriol.* **2003**, *185*, 3636–3643.
- (65) Hazelbauer, G. L.; Falke, J. J.; Parkinson, J. S. *Trends Biochem. Sci.* **2008**, *33*, 9–19.
- (66) Hazelbauer, G. L.; Engström, P. *J. Bacteriol.* **1981**, *145*, 35–42.
- (67) Wang, X. Q.; Vu, A.; Lee, K.; Dahlquist, F. W. *J. Mol. Biol.* **2012**, *422*, 282–290.
- (68) Borkovich, K. A. *Methods Enzym.* **1991**, *200*, 205–214.

CHAPTER 3: PROBING THE DYNAMICS OF *THERMOTOGA MARITIMA* HISTIDINE KINASE CHEA TO DETERMINE DOMAIN INTERACTIONS THAT REGULATE AUTOPHOSPHORYLATION ACTIVITY

3.1: Introduction

Domain movement within kinases underlies their enzymatic activity and regulation.^{1,2} The histidine kinase, CheA, is the principal enzyme in the bacterial chemotaxis pathway. The mechanism of autophosphorylation depends upon the transient interaction between the substrate-containing P1 domain and the ATP-binding P4 domain. Chemoreceptor protein interaction regions (PIRs) modulate CheA basal activity levels through a largely unknown process, but one that could involve regulation of the P1-P4 contact.

Homodimeric CheA along with its coupling protein CheW resides at the signaling tips or PIRs of the chemoreceptor complex (Figure 1-12). Each monomer of CheA contains five distinct domains (P1-P5), which have distinct functions and display variable mobility (Figure 3-1). P1 contains the substrate Histidine residues, P2 docks the response regulator CheY for final phosphotransfer from P1, P3 dimerizes the two subunits, P4 acts as the ATP-binding kinase module and P5, couples CheA to CheW and chemoreceptors.³⁻⁶

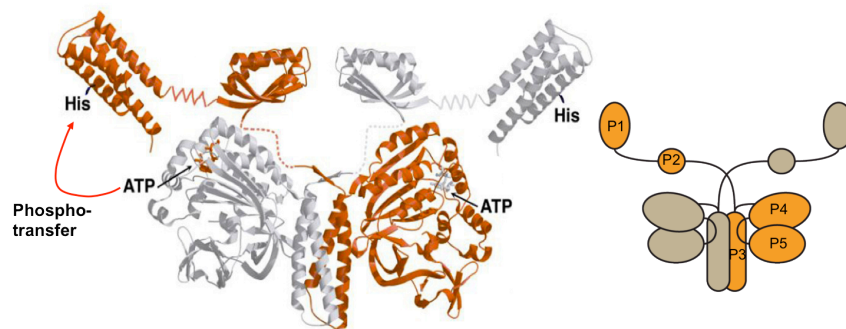


Figure 3-1: CheA. Structural prediction⁷ and cartoon of CheA_{FL} homodimer with domains labeled (P1-5) with linkers to allow for variable mobility of the domains.

CheA is unique among other known sensor histidine kinases, in that it does not have a transmembrane domain, it contains the phosphorylatable His on a separate domain (P1) instead of the dimerization domain, as in the sensor kinases, and relies on P5 and CheW for interaction with membrane components. Furthermore, sensor kinases do not contain a separate domain for docking response regulators. The *E. coli* CheA P2 domain is not required for phosphotransfer to the response regulator CheY, yet it facilitates transfer and is important for the chemotaxis response.⁸ Variants lacking the P2 domain (Δ P2) have the P1 domain directly linked to the P3 domain, exhibit a reduced phosphotransfer rate relative to CheA_{WT} but still support chemotaxis, albeit to a lower extent.^{8,9} Linker between the CheA domains have been shown to play an important role in kinase activity. For example, the Dahlquist lab has revealed the importance of P3-P4 linkers to kinase domain functionality.^{10,11} Thus, although the P2 domain itself is not critical for kinase autophosphorylation, the overall segment linking P1 to P4 may well have specific properties that are important for phosphotransfer. Notably, CheA phosphotransfer occurs exclusively in *trans*, with one subunit phosphorylating the other^{12,13} and despite the P1-P3 linker being more than long enough to access both P4 domains within the dimer. An NMR solution structure of *E. coli* CheA P1 assigns the 20 amino acid linker (residues 112-132), beginning near the C-terminus of the P1 domain as an α -helix that runs along side the primarily helical domain.¹⁴ This additional helix constrains the P1 domain, and is thought to control the movement and spatial orientation of activated CheA.

Although specific information regarding how both the P1 and P4 domains interact with ATP is known,^{15,16} the inter-domain communication and cooperativity required to transfer γ -phosphate remains unclear. Recent work has been conducted in an effort to elucidate possible contact points between these domains with one specific interaction between Glu38 and

Lys346.¹⁷⁻²¹ There has been considerable progress towards understanding the arrangement and interactions between the structural elements of CheA (Chapter 4), yet continued efforts are demanded in order to construct a comprehensive structural and biochemical model that can describe CheA autophosphorylation. Herein, the effect of the P1-P3 linker on kinase activity, transphosphorylation and regulation in the thermostable CheA kinase from *Thermotoga maritima* is investigated for the first time. The minimal linker length for trans autophosphorylation is defined and provides evidence that shorter linkers rather undergo cis phosphorylation. Shown here is targeted disulfide cross linking that kinase activity correlates with the ability of P1 to access the P4 ATP pocket. Small-angle x-ray scattering was used to describe a dramatic conformational transition in the kinase upon ATP binding that releases the P1 and P2 domains from a constrained globular arrangement to one where they sample a wide range of conformational space. Finally, it is likely that the P5 domain relays the conformational signal from MCPs to the other CheA domains.²² The worked presented here establishes this perturbation primarily affects the interaction between the phosphotransfer and kinase domains.

3.2: Materials and Methods

3.2.1: Construction and cloning of $\Delta P2$ variants. The P1 and P3P4P5 regions of *T.m.* CheA were covalently joined via a linker of varying length, composed primarily of the native P1-P2 linker residues (Figure 3-2, Table 3-1). Nonetheless, several additional residues were added to the $\Delta P2$ constructs to achieve the desired length. The constructs were cloned into pET28a vector containing the NdeI and BamHI restriction sites. Mutations were introduced via Quikchange. The nomenclature of the $\Delta P2$ variants were assigned according to their linker lengths between the P1 and P3 domains. Two, endogenous cysteine residues within in the constructs, C63 and

C208, were mutated to serine for targeted cross-linking studies. Proteins were purified to homogeneity according to protocols as described previously.²³

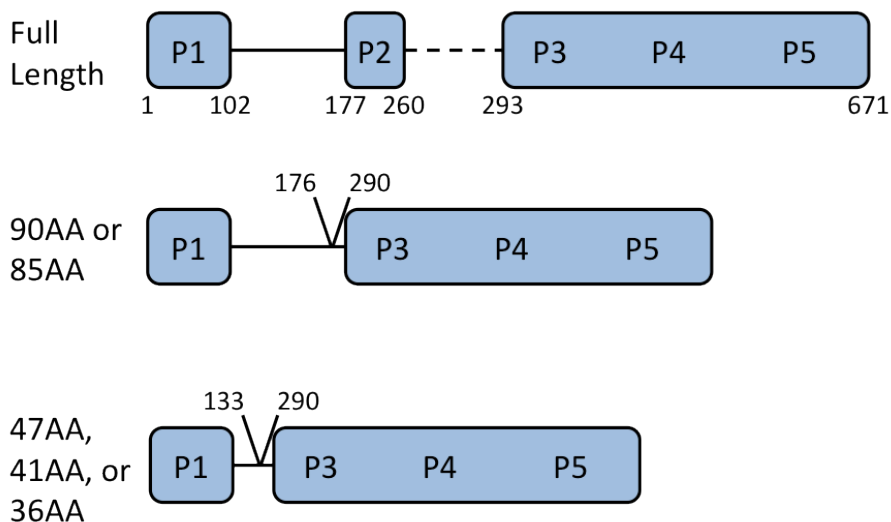


Figure 3-2: ΔP2 variants. Cartoon depiction of ΔP2 variants of *Thermotoga maritima* CheA with domain residues listed and splice point indicated.

Name	Splice point
90AA	176-PAPAAPPRASA-290
85AA	176-ASGGTG-290
47AA	133-PAPAAPPRASA-290
41AA	133-ASGGTG-290
36AA	133-290

Table 3-1: Description of ΔP2 variants. Description of ΔP2 variants, nomenclature is based upon number of amino acids in the linker. Splice point residues listed with additional amino acids added.

3.2.2: Heterodimer formation and analysis. Solutions containing 35 μM (subunit concentration) D449A *T.m.* CheA_{FL} and 35 μM *T.m.* CheA P3P4P5 were incubated for various time points in TKEDM buffer (50 mM KCl, 10 mM MgCl₂, 0.5 mM DTT, 0.5 mM EDTA, 5 mM Tris pH 7.5) to a total volume of 500 μL. Samples were heated to 55 °C for 0-18 hours prior to injection onto the analytical 200 size-exclusion sepharose column for separation.

3.2.3: *Autophosphorylation activity of $\Delta P2$ variants.* Solutions containing *T.m.* CheA $\Delta P2$ variants (10 μM monomer) were prepared overnight at 4 °C in TKEDM buffer (50 mM KCl, 10 mM MgCl_2 , 0.5 mM DTT, 0.5 mM EDTA, 5 mM Tris pH 7.5) to a total volume of 25 μL . To each sample, 2 μL of 2.3 mM cold ATP and 3-8 μL of [γ - ^{32}P] ATP (3000 Ci/mmol, 10 mCi/mL, Perkin Elmer) was added and allowed to incubate for 6 minutes at room temperature. The reaction was quenched with the addition of 25 μL of 3 \times SDS buffer supplemented with 50 mM EDTA (pH 8.0). Then 30 μL of each sample was electrophoresed on a 4-20% gradient Tris-glycine SDS-PAGE gel. The gel was stained with Coomassie blue for 10 minutes, subsequently destained with water for three hours, and then dried with a GelAir dryer for three hours. The dry gel was placed in a cassette for at least 24 hours, imaged with Storm phosphoimager (GE Healthcare), and the resulting bands representing phosphorylated protein were analyzed with ImageJ.

Phosphotransfer to CheY. Solutions of 5 μM (monomer) *T.m.* CheA (or $\Delta P2$) and 20 μM *T.m.* CheY were prepared and left overnight at 4 °C in TKEDM buffer (50 mM KCl, 10 mM MgCl_2 , 0.5 mM DTT, 0.5 mM EDTA, 5 mM Tris pH 7.5) to a total volume of 25 μL . Hot ATP solutions were added to the samples to initiate the reactions and the assays were processed as described above.

Assessment of trans vs. cis autophosphorylation. Solutions of 5 or 10 μM (monomer) *T.m.* CheA_{WT}, or *T.m.* CheA H45K and H405Y mutants (CheA_{FL} and $\Delta P2$ variants) were prepared overnight in TKEDM buffer (50 mM KCl, 10 mM MgCl_2 , 0.5 mM DTT, 0.5 mM EDTA, 5 mM Tris pH 7.5) to a total volume of 25 μL . The samples were heated for 3-18 hours at 55 °C, to allow exchange of subunits prior to being assayed for autophosphorylation according to the procedure described above. Only heterodimers containing one subunit with a P1_{WT} subunit

(H405Y) and a WT P4 subunit (H45K) can undergo autophosphorylation, and it must occur in trans.

3.2.4: Disulfide cross linking. Solutions of *T.m.* CheA single site Cys variants H45C* and S492C* were incubated for 1 hour at 55°C in the presence of freshly prepared initiator 5 mM $\text{Cu}(\text{1,10 phenanthroline})_3^{2+}$, with a total volume of 10 μL . For some samples 1 mM ADP or ATP was added. Similarly, some samples included the *T. maritima* KCM Tm14 (residues 41-254) at a 1:3 ratio (CheA monomer:Tm14 dimer), with CheW added at the same concentration as the CheA subunit. Disulfide crosslinking was quenched by the addition 8 μL of 3 \times SDS buffer supplemented with 10 mM imidazole. The samples were electrophoresed on a 4-12% gradient Bis-Tris SDS PAGE gel, run in MES or MOPS (in the case of CheA_{FL}) running buffer. The gel was stained with Coomassie blue, destained with an acetic acid/ethanol solution, and then dried overnight at room temperature.

3.2.5: Small-angle x-ray scattering (SAXS). For SAXS experiments the protein buffer was exchanged to 50 mM HEPES pH 7.5, 150 mM NaCl, 2 mM DTT, and 5% glycerol the day of the experiment then prepared at three concentrations (6, 3, and 1.5 mg/mL). Another set of samples were prepared with the same protein concentrations containing 5 mM α,β -methyleneadenosine 5'-triphosphate. The samples were centrifuged at 13,000 rpm for 20 minutes at 4 °C, then kept in the tray at 4 °C prior to exposure. Data was collected at the F2 beam line of CHESS with Pilatus 100K detector.²⁴ Each sample was exposed during continuous oscillation for 30 seconds for 10 frames. During exposures 30 μL of sample is continuously oscillated through the illuminated volume (0.125 μL) at 2-4 $\mu\text{L s}^{-1}$, thereby reducing the absorbed dose by two orders of magnitude.²⁵ RAW²⁶ and Primus²⁷ were implemented for data processing and generation of Guiner and Kratky plots. Molecular weight prediction was based upon a standard of 3 mg/mL of

lysozyme (13 kDa). Envelope reconstructions were calculated using ATSAS programs.²⁸⁻³⁰ A total of ten independent models were generated and averaged using Damaver then combined into one envelope.

3.2.6: Circular dichroism. For CD experiments the protein buffer was exchanged to 10 mM Sodium phosphate pH 7.2 and 150 mM NaCl the day of the experiment then prepared at 0.5 mg/mL. For comparison two sets of samples were generated, one of which contained 1 mM of the non-hydrolyzable ATP analog α,β -methyleneadenosine 5'-triphosphate (ADPCP) and one without. A former data set was collected on the sample with nucleotide, 24 hours later. Samples were analyzed using an AVIV Biomedical (model 202-01) spectropolarimeter. A 0.1 cm quartz cell was used. Data was collected at 1 nm intervals with 5 second averaging time at 25 °C from 260-200 nm. Degree of elipicity was plotted versus wavelength.

3.2.7: ATP-TNP binding assay by fluorescence enhancement. CheA_{FL} (2 μ M) in 2 mL of Fluoro buffer (25 mM Tris (pH 7.5), 0.5 mM Na₂EDTA, 10% glycerol, 25 mM NaCl, 54.7 mM potassium glutamate, 20 mM MgCl₂) at 25 °C. Stock TNP-ATP solutions were added in small increments (1-2 μ L) over time to final concentrations of 0-50 μ M. The emission spectra were collected 530-600 nm (545 nm specifically) using a λ_{ex} of 520 nm with 4 nm slits on a Horiba Jobin Yvon Fluorolog-3 fluorescence spectrophotometer equipped with a with 450 W Xe lamp, double excitation and emission monochromators, and a digital photon-counting multiplier.

3.3: Results

3.3.1: Generation of the Δ P2 variants. To generate CheA variants with altered linkages between the kinase core composed of, P3P4P5 (Δ 289) and the substrate P1 domain, P1 was fused to P3P4P5 with linkers in which the P2 domain and the P2-P3 linker were removed. However, various stretches of the P1-P2 linker were retained along with several short non-native sequences

added to adjust the linker length and flexibility (Figure 3-2). The $\Delta P2$ variant nomenclature was assigned according to the number of residues within the synthetic P1-P3 linker (Table 3-1). For the longer variants (85AA and 90AA), all but the last residue (K177) of the native P1-P2 linker was incorporated. The shorter variants (36AA, 41AA, and 47AA) retain the naturally occurring 33 residues after the C-terminus of the fourth helix in P1. The 41AA and 47AA also include a 5-14 residue sequence was to modulate the linker flexibility.

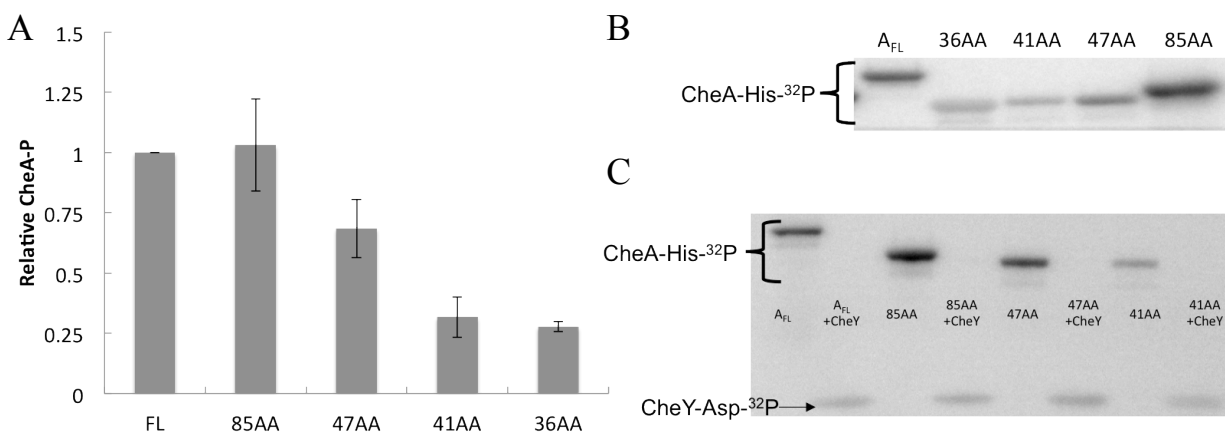


Figure 3-3: Phosphorimages and bar plot of $\Delta P2$ variants. In all assays *T. maritima* CheA_{FL} or $\Delta P2$ variants (10 μ M) and CheY (25 μ M) left at 4 °C overnight prior to exposure for 6 minutes. **A:** Bar plot of the relative amount of phosphorylated P1-His (CheA-P) of CheA_{FL} and $\Delta P2$ variants the longer linker is more active. **B:** Phosphorimage of CheA_{FL} and $\Delta P2$ variants. **C:** Phosphorimage of CheA_{FL} and $\Delta P2$ variants exhibit complete transfer of phosphate to CheY.

3.3.2: *Activity of $\Delta P2$ versus CheA_{FL}.* The $\Delta P2$ variants with longer linkers (85AA and 47AA) have similar autophosphorylation activity to *T.m.* CheA_{FL} (Figure 3-3) after 6 minutes of exposure. In contrast, the 41AA and 36AA species exhibited an ~50% reduction in autophosphorylation activity compared to *T.m.* CheA_{FL}. This reduction of activity in the shorter variants could reflect the greater steric restraint associated with the condensed linker length. More specifically, the majority of the shorter linker likely forms a fifth α -helix in the P1 domain, thus reducing its intrinsic flexibility.¹⁴ Although the $\Delta P2$ variants exhibit reduced

autophosphorylation activity, all retain the ability to transfer the phosphate from the His45 residue of P1 to *T.m.* CheY (Figure 3-3C). This result is consistent with similar studies of a Δ P2 variant of *E. coli* CheA,^{12,31–34} that also found that the P2 domain is not essential for phosphotransfer to CheY.

3.3.3: Generation of CheA heterodimers to test for trans phosphorylation. Temperature dependent subunit exchange of *T. maritima* CheA allows for heterodimers of unequal subunits to be formed and trapped.³⁵ Prolonged incubation at 55 °C of CheA_{FL}, with CheA P3P4P5 produces heterodimers containing only one P1-P2 unit that can be separated on an analytical size-exclusion column at 4 °C (Figure 3-4).³⁵ The yield of homodimers to heterodimer follows a statistical ratio of 1 CheA_{FL} dimer:2 mixed dimer:1 P3P4P5 dimer. To test for *trans* autophosphorylation a CheA_{FL} variant harboring P4 mutation (H405Y)^{13,36} was exchanged with a CheA_{FL} variant that that lacks the substrate His (H45K).^{13,36} Thus, autophosphorylation can only occur within a heterodimer when the subunit with the functional P4 domain *trans* phosphorylates the P1 domain of the opposing subunit.

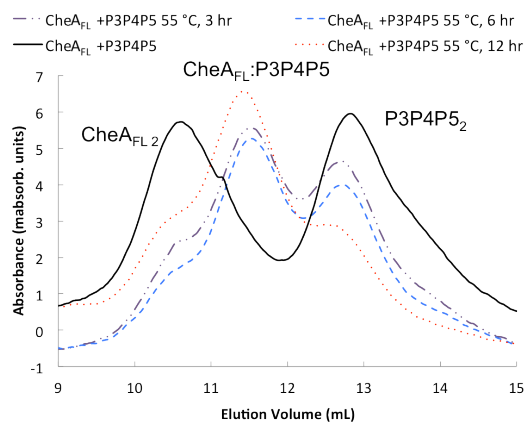


Figure 3-4: SEC profiles of CheA_{FL} and P3P4P5. SEC profiles of CheA_{FL} (35 μ M) and P3P4P5 (35 μ M) dimers during heat exchange at 55 °C over time from black (0 minutes) to purple (3 hours) to blue (6 hours) to red (12 hours). The formation of a 1:2:1 ratio of dimers CheA_{FL} 2:(CheA_{FL}:P3P4P5):P3P4P5₂ over time.

Based on the results from analytical SEC with CheA_{FL} and P3P4P5, 1:2:1 ratio is expected of the species H45K₂:(H45K:H405Y):H405Y₂ after exchange, and hence only 50% activity should be regained. In this system, CheA_{FL}, 85AA, and 47AA were able to regain the expected activity upon heat-exchange (Figure 3-5). However, the 41AA and shorter P1 and P4 mutants were unable to regain any activity in the exchange assay despite both 41AA_{WT} and 36AA_{WT} demonstrating autophosphorylation activity. Thus, it can be concluded that the variants with the shortest P1-P2 linkers autophosphorylate in *cis*, i.e. within the same subunit.

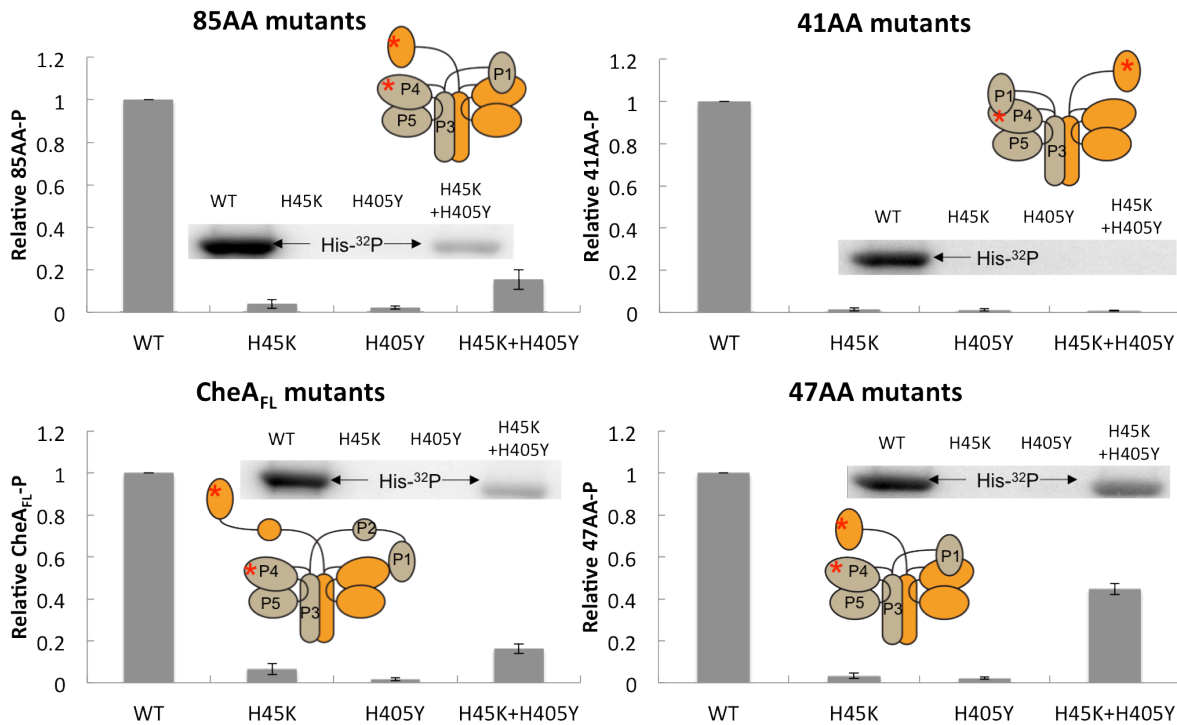


Figure 3-5: Phosphorimages and bar plots of CheA_{FL} and Δ P2 mutants.

Autophosphorylation activity of CheA_{FL}, 85AA, 47AA, and 41AA mutants relative to the wild type P1-P4 variant. All proteins are at a total concentration of 10 μ M were heated overnight at 55 $^{\circ}$ C prior to being exposed for 6 minutes at 25 $^{\circ}$ C. Intensity of autophosphorylation is relative to the wild type of each variant in the bar plots. A phosphorimage of the gels of the wild type and mutants are inset within the bar plot with each lane labeled. A cartoon depiction of the trans or cis autophosphorylation event for each variant is also inset within the bar plot a red asterisk depicts the point mutations in the mixed dimer.

Domains	Mutants*	MW (subunit)
P1*	H45C	14.7
P4*	S492C	20
P3P4*	S492C	27.1
P3P4P5*	S492C	42.5
41AA*	H45C, S492C, H45C/S492C	53
CheA _{FL} *	H45C, S492C, H45C/S492C	74

Table 3-2: Disulfide cross linking mutants defined. Description of cysteine mutants within different variants of CheA, the asterisk is used to denote the cysteine mutants in the text.

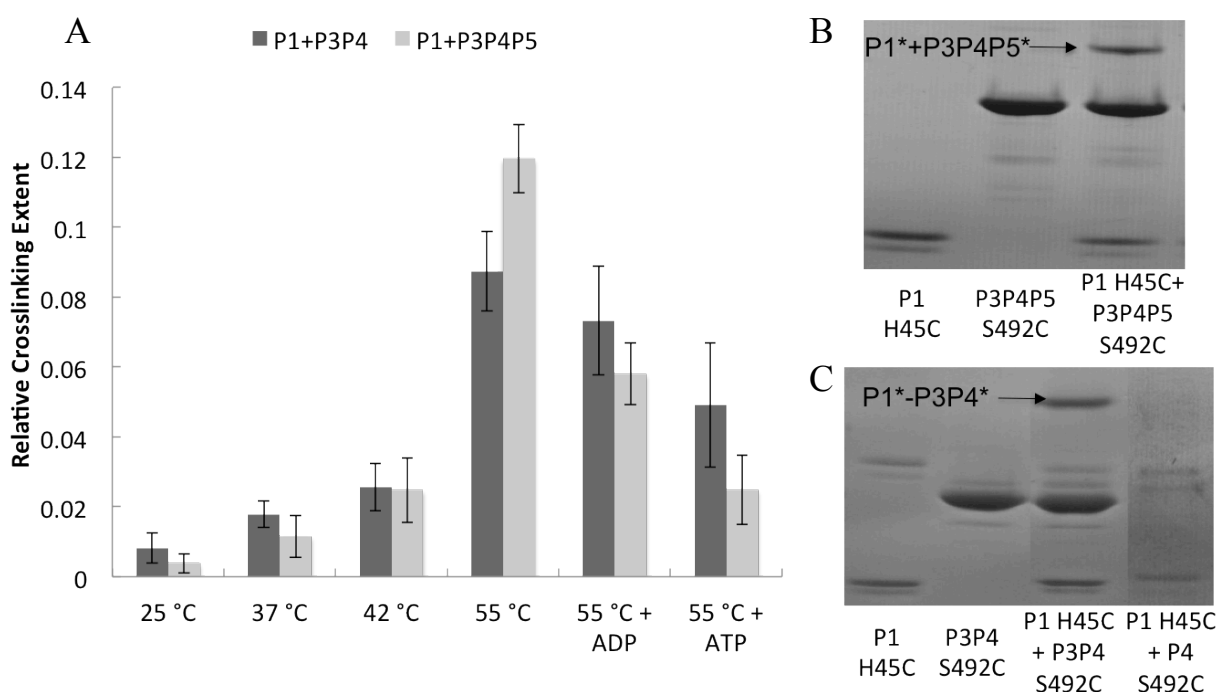


Figure 3-6: Disulfide cross linked SDS-PAGE gels and bar plot of P1*+P3P4* and P1*+ P3P4P5* over temperature and with nucleotide. P1-P4 crosslinking in various CheA species **A**: Formation of cross-linked band varying conditions, P1* (12 μ M) and P3P4 or P3P4P5* (24 μ M) at indicated temperature for 1 hour, with 2 mM ADP or ATP. **B**: SDS-PAGE gel of P1* (12 μ M) cross-linked to P3P4P5* (24 μ M) at 55 °C for 1 hour. **C**: SDS-PAGE gel of P1* (12 μ M) cross-linked to P3P4* (24 μ M) at 55 °C for 1 hour. In the 4th lane is P1* (12 μ M) and P4* (12 μ M) in identical conditions with no crosslinking apparent.

3.3.4: P1 and P4 domain interactions as a probe of kinase activity. The interaction of the P1 and P4 domains within *T.m.* CheA is essential for His phosphorylation. A cross linking assay was

devised to detect the association of these two domains, which is otherwise transient in the full-length enzyme and extremely weak in the isolated domains. Cysteine substitutions (Table 3-2) were generated in the P4 domain (S492C, P4*) and at the P1 substrate His (H45C, P1*). Ser492 is in close proximity to the Mg²⁺ ion that coordinates the γ -phosphate of ATP in the P4 active site.¹⁵ At 55 °C (but not 25 °C) P1-P4 crosslinking produces a higher MW species easily resolved on SDS-PAGE. Disulfide cross linking was observed between P1* and P3P4P5* and P1* and P3P4*, but not between P1* and P4*, even after extended heating and incubation (Figure 3-6). Thus, the interaction between the kinase (P4) and histidine phosphotransfer (P1) domains dramatically increases in the presence of the dimerization domain (P3). This conclusion is corroborated by autophosphorylation assays (see Chapter 4).

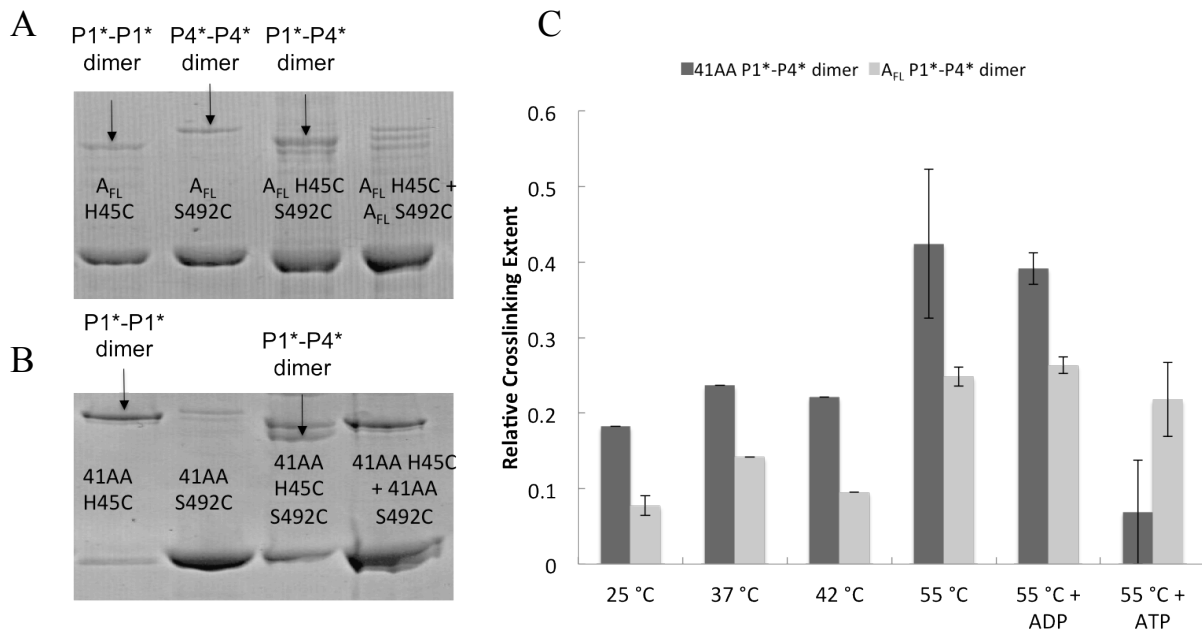


Figure 3-7: Disulfide cross linked SDS-PAGE gels and bar plot of CheA_{FL}* and 41AA* over temperature and with nucleotide. P1-P4 crosslinking within CheA_{FL}* and 41AA* dimer formation. A: SDS-PAGE gel of CheA_{FL}* (12 μ M) cross linked dimers at 55 °C for 1 hour, the mixture of the single mutants forms all three dimers. **B:** SDS-PAGE gel of 41AA* (12 μ M) cross-linked dimers at 55 °C for 1 hour, no lower band forms in the mixture of the single mutants. **C:** Formation of the CheA_{FL}* and 41AA* P1*-P4* dimers, heated at indicated temperature for 1 hour, with 2 mM ADP or ATP.

Similarly, crosslinking of CheA_{FL}* generated multiple disulfide bands on SDS-PAGE indicative of P1*-P1*, P4*-P4* and P1*-P4* disulfide-linked species (Figure 3-7). Positions of the P1*-P1* and P4*-P4* bands were confirmed in variants that only harbored the P1* or P4* cysteine substitutions, respectively. For CheA_{FL}, the P1*-P4* cross linked species runs at twice the subunit MW, between that of P1*-P1* and P1*-P4*, owing to trans cross linking. Nonetheless, the cross linking efficiency yielded in these higher molecular weight species of CheA_{FL}* and 41AA* was significantly less than that compared to the systems when P1* was supplied as separate protein, as judged by band intensity (Figure 3-7). The 41AA* double mutant P1*-P4* runs below the P1*-P1* and is not present upon mixture of the single mutants and has been assigned as cis. Thus, interactions between P1* and the P3P4P5* or P3P4* core units are stronger than between P1* and P4* in CheA_{FL}*. As described previously, the cytosolic MCP Tm14 exhibits a deactivating effect on CheA autophosphorylation.³⁷ A truncated, stable version Tm14 (residues 41-254) was used to probe the effect of inhibitory receptors on the P1*-P4* interaction (Figure 3-8). Tm14 KCM (41-254) contains the adaptation region yet is more stable to heat *in vitro* than the full length Tm14. With all species, the CheW presence inhibited disulfide formation by blocking interactions between the reactive cysteines on P1* and P4*. Addition of deactivating MCP (Tm14) further inhibited crosslinking of the 41AA* and P1*+P3P4P5* species. Less of an effect on CheA_{FL}* cross linking with Tm14 was observed however, the level of cross-linking is already low when CheW is present and further reduction is difficult to quantify. ATP also inhibited cross-linking of both the 41AA* and CheA_{FL}* variants, likely because the γ -phosphate interferes with approach of the H45C residue to S492C. Indeed, ADP causes little change to cross-linking yields.

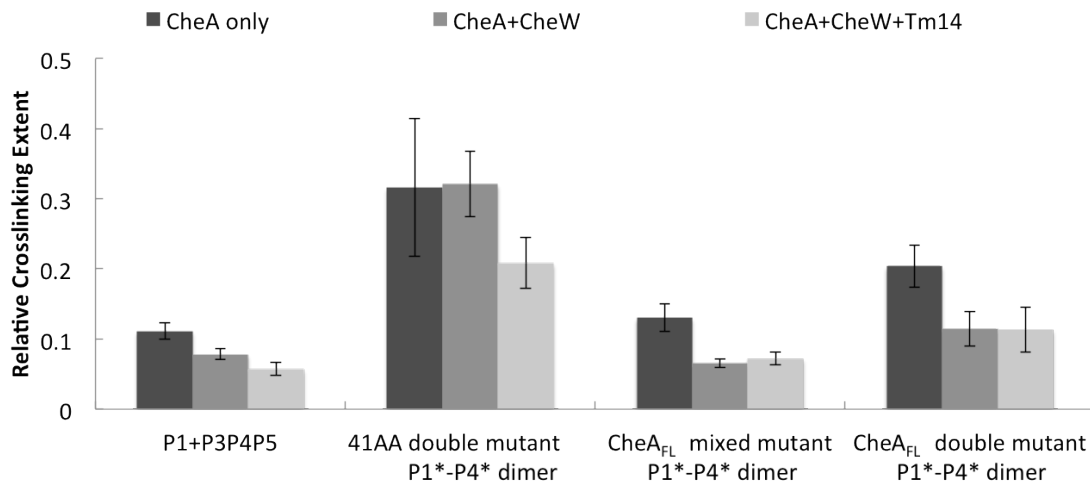


Figure 3-8: Bar plots of P1*+ P3P4P5*, CheA_{FL}*, and 41AA* with CheW and Tm14. Bar plots of the cross-linked CheA (6 μ M) with and without CheW (6 μ M) and Tm14 (18 μ M) at 55 $^{\circ}$ C for 1 hour. The CheA_{FL} mixed mutant dimer is composed of 6 μ M of both the CheA_{FL} H45C and CheA_{FL} S492C mutants. Mixture of CheA_{FL}* mutants and the double mutant both do not observe more of a reduction in cross linking when Tm14 added compared to just addition of CheW.

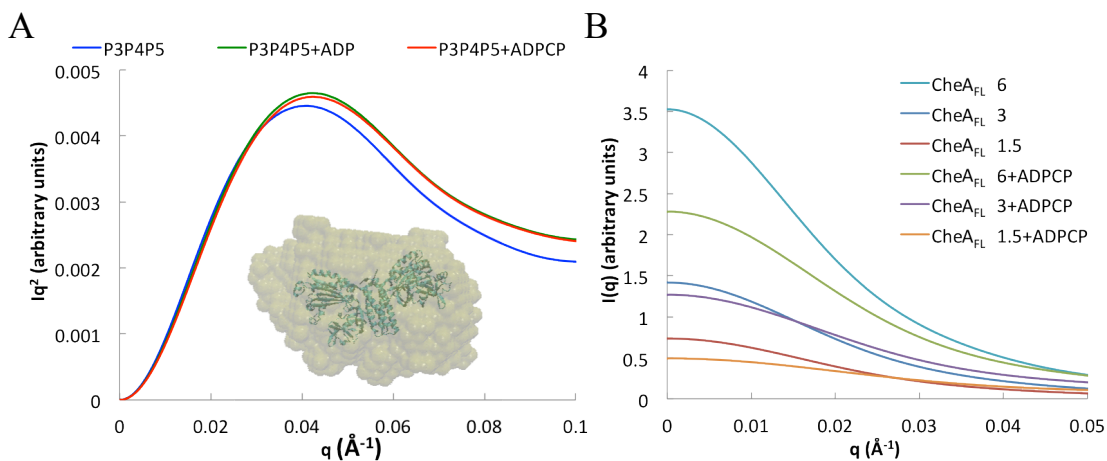


Figure 3-9: Kratky plots of P3P4P5 and Scattering plot of CheA_{FL}. **A:** Kratky profile of P3P4P5 (6 mg/mL) with and without nucleotide, ADP and ADPCP, (5 mM). **B:** Intensity vs. scattering plot of CheA_{FL} at various mg/mL concentrations indicated (6, 3, 1.5) with and without ADPCP (5 mM) to depict no aggregation.

3.3.5: ATP causes dramatic changes to the dynamics of P1-P2 within CheA_{FL}. SAXS was used to evaluate the conformational properties of CheA and its variants in solution under a variety of conditions. For all species studied, scattering data collected at several concentrations showed no evidence of aggregation (Figure 3-9B). The shape of Kratky plots ($I(q)q^2$ vs. q , where q

represents the momentum transfer, $\frac{4\pi\sin(\theta)}{\lambda}$) reports on the overall conformational properties of a polymer chain. For rod-like particles $I(q)q^2$ plateaus at large values of q , for random Gaussian chains $I(q)q^2$ increases with positive slope and for globular particles it curves down toward baseline. P3P4P5 has a resting globular shape in solution (Figure 3-9A). Upon addition of an ATP analog (ADPCP: α,β -methyleneadenosine 5'-triphosphate) or ADP, P3P4P5 has no change in the globular envelope. The subsequent Kratky plot of the variants with nucleotide exhibited a Gaussian chain-like character (Figure 3-10). The presence of ADP generated no disruptions within the globular envelope in CheA_{FL} (Figure 3-11A); and these trends were observed for both *T. maritima* and *E. coli* CheA (Figure 3-11B). To confirm the impact of ATP on CheA conformational properties SAXS data was also collected on a CheA variant with a residue substitution in the ATP binding pocket that prevents nucleotide binding. Indeed, a fluorescent ATP analog (TNP-ATP) bound the variant weakly or not at all, and as expected, no change was observed in the SAXS profile upon addition of non-hydrolyzable ATP (Figure 3-12). The changes in the molecular shape of the protein are also not a result of protein aggregation based upon the slope of the Guiner region in $\log(I)$ vs. q plots and the concentration dependence of scattering behavior (Figure 3-9B). In addition, overall secondary structure of the protein is not substantially altered by nucleotide, as evidenced by circular dichroism spectra (Figure 3-13). However, the slight change in absorbance observed is due to additional phosphate absorption as a result of nucleotide addition.³⁸ The stability of *T.m.* CheA was demonstrated, as minimal changes were observed in the CD wavelength scans after 24 hours incubation at 4 °C later (Figure 3-13). Thus, transition from globular to Gaussian chain behavior depends on the P1-P2 domains and ATP binding, suggesting that the ATP γ -phosphate displaces the CheA N-terminal domains from a restricted position within the full-length dimer.

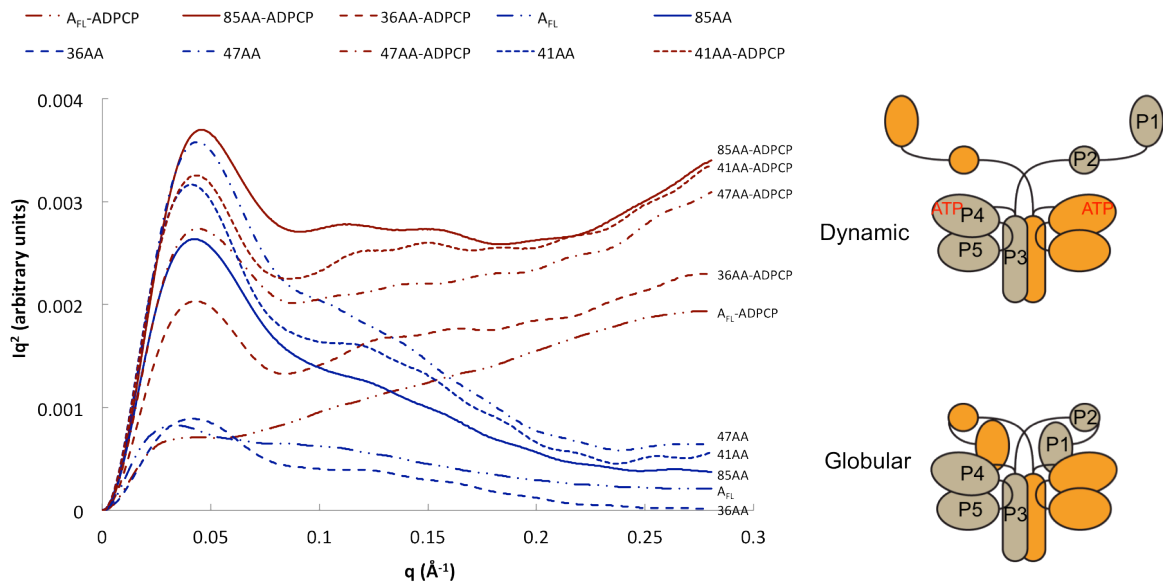


Figure 3-10: Kratky plots of CheA_{FL} and ΔP2 variants. Kratky plot of CheA_{FL} and ΔP2 variants (3 mg/mL) with and without ADPCP described to the right of each curve, with subsequent cartoon depictions of a dynamic form of CheA_{FL} with ATP bound and a globular CheA_{FL}. All variants show a globular resting state, which differs from current opinion. While addition of nucleotide (ADPCP) causes a gaussian chain behavior, that is not the formation of an aggregate or the protein unfolding.

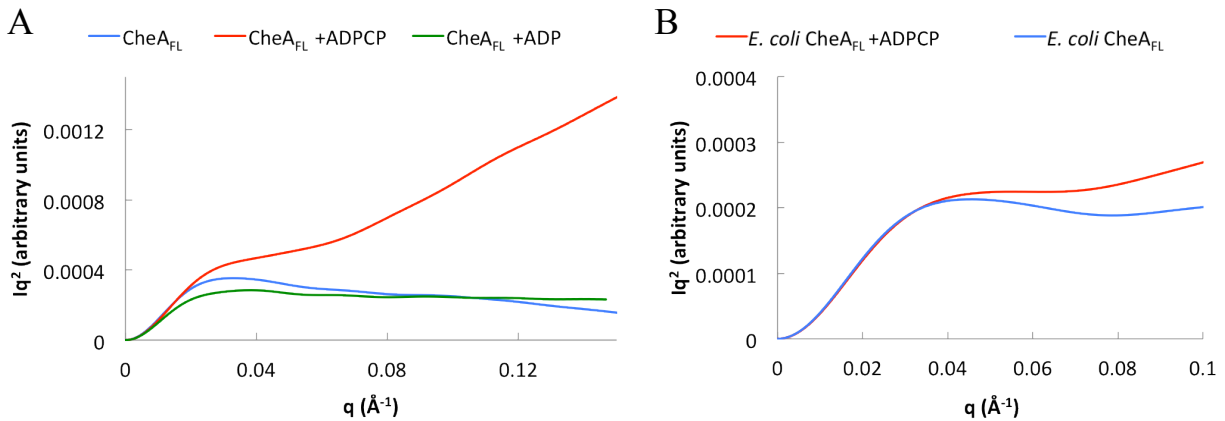


Figure 3-11: CheA_{FL} Kratky plot with nucleotide in *T. maritima* and *E. coli*. **A:** Kratky plot of *T. maritima* CheA_{FL} (3 mg/mL) with and without (blue) nucleotide at 5 mM, ADPCP (red) and ADP (green). Only when the γ -phosphate is present is there a large disruption in the globular nature of CheA. **B:** Kratky plot of *E. coli* CheA_{FL} (5 mg/mL) with (red) and without (blue) ADPCP at 5 mM. *E. coli* CheA is also globular and becomes gaussian chain-like when nucleotide is present.

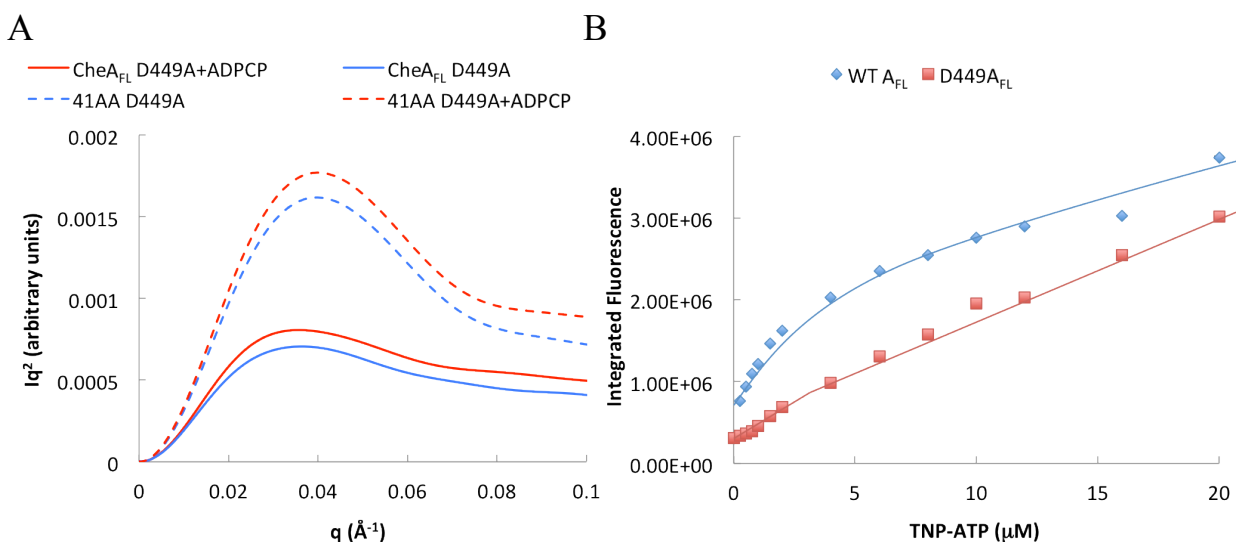


Figure 3-12: Kratky plots and Fluorescence of CheA D449A mutant. A: SAXS Kratky plots of CheA_{FL} and 41AA D449A (20 μ M) with and without nucleotide, ADPCP, (5 mM) shows no change in globular shape. **B:** Fluorescence plots of native and D449A CheA_{FL} (2 μ M) binding of TNP-ATP over increasing concentrations from 0-20 μ M.

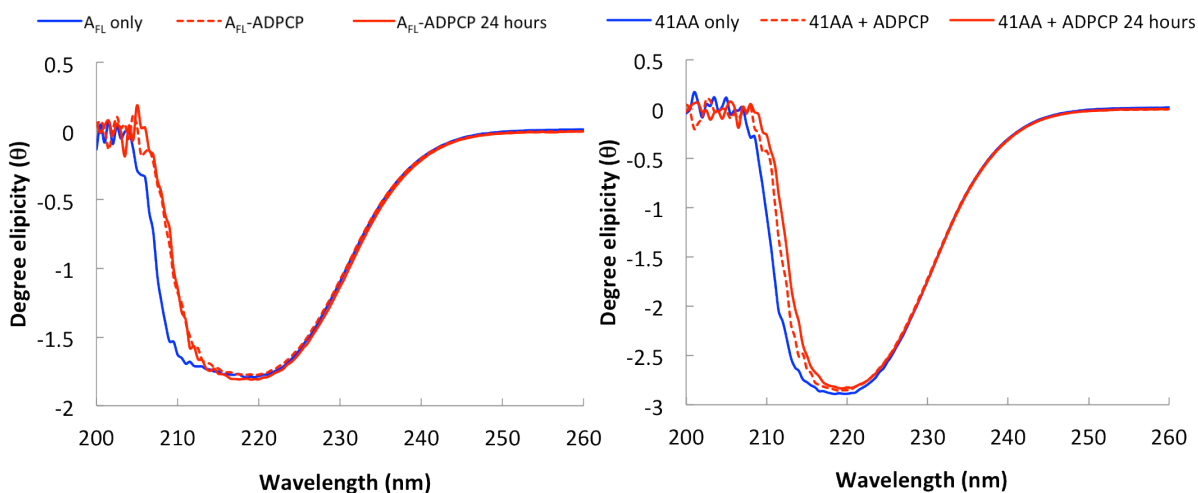


Figure 3-13: CD profiles of CheA_{FL} and 41AA with nucleotide. Circular Dichroism of CheA_{FL} and 41AA (0.5 mg/mL) before (blue) and after (red dashed) addition of ADPCP (1 mM) shows no change in helical content, however there is a baseline shift upon addition of the phosphate. Another spectrum was collected 24 hours after ADPCP was initially added (red solid). Since SAXS is sensitive to aggregation effects, multiple concentrations of all variants were subjected to scattering. These spectra confirm that the Gaussian chain behavior was observed regardless of the protein concentration and were not a result of protein aggregation

3.4: Discussion

3.4.1: *Trans autophosphorylation by CheA. E. coli* CheA have been shown to undergo trans autophosphorylation^{12,13,31-34} while other sensor kinases in this GHKL family can perform both cis or trans phosphotransfer.³⁹ *T. maritima*, CheA normally undergoes trans autophosphorylation, but is capable of both cis and trans autophosphorylation, depending on the linker length separating the P1 domain from P3P4P5 units. Trans autophosphorylation in 47AA and all longer Δ P2 variants including CheA_{FL} is demonstrated by their ability to regain activity with a mixed mutant dimer. Though both 41AA_{WT} and 36AA_{WT} are capable of some autophosphorylation, the mixed mutant dimers are inactive (Figure 3-5), thus indicating that these variants are only capable of cis autophosphorylation. The shortest linker in the 36AA variant is primarily an α -helix that runs antiparallel to the helices of the P1 domain, restricting the overall motion of P1.¹⁴ The 41AA_{WT} is considerably less active than CheA_{FL} (Figure 3-3) thus, cis autophosphorylation achieves only ~50% of the activity compared to the trans event. The inclusion of only six amino acids (41AA to 47AA) improves the flexibility of the linker, enabling trans autophosphorylation and an activity level similar to that of CheA_{FL} (Figure 3-5). Considering *T.m.* CheA autophosphorylation requires the association and subsequent interaction between the P1 and P4 domains, the smaller linker may prevent the reorganizational motion required to facilitate transfer of the γ -phosphate. The P3P4 structure (Chapter 4) poises the linker leading to the P3 domain such that the P1 domain orientation adopts a trans position, consistent with the activity data of mixed dimers (Figure 3-14).

3.4.2: *CheA_{FL} and 41AA dimers.* The 41AA* and CheA_{FL}* covalent dimers that arise due to cross linking between H45C and S492C provide insight into key interactions between the subunits (Figure 3-7A, 3-7B). In CheA_{FL} the band corresponding to the P4*-P4* dimer is the

highest, with the P1 and P2 domains free from the core. The P1*-P1* dimer band is the lowest, locking CheA into a more compact species. The trans P1*-P4* dimer band in CheA_{FL}* is between the P1*-P1* and P4*-P4* bands. While the 41AA* P1*-P4* cis dimer band is below the P1*-P1* dimer band which can be attributed to the steric restrictions associated with the reduced linker length. Similarly, both the P1*-P4* dimers are more condensed than the P4*-P4* dimer. The various levels of compaction CheA can achieve demonstrates the high dexterity imparted on the CheA structure by the P1-P2 and P2-P3 linkers.^{10,11} The mixture of the single mutants of CheA_{FL}* shows no preference between the dimers and all form relatively equally. While the mixture of the 41AA* single mutants forms only the P1*-P1* dimer, supporting the radioisotope results that the 41AA is incapable of trans autophosphorylation.

3.4.3: P1 and P4 interactions. Using targeting disulfide cross-linking phosphorylation competent interaction between P1* and P4* was probed. The cysteine substitutions were chosen to report on the close approach of the P1 substrate position and the ATP γ -phosphate. The specificity of this contact was confirmed by the ability of ATP, but not ADP to diminish crosslinking. This can be attributed to the γ -phosphate blocking the His45 and Ser492 sites from interacting with one another (Figure 3-6A, Figure 3-7C). In these studies, an optimal temperature was used³⁵ to promote cross linking, maximize activity and avoid degradation of the nucleotide or the receptor. Importantly, it was found that the interactions between P1* and P4* are diminished in CheA_{FL}* compared to the case where P1* is separated from P3P4* or P3P4P5*. Furthermore, there is virtually no interaction between the P1* domain and the isolated P4*, which is consistent with inability of P4 to phosphorylate isolated P1 to any appreciable extent. Thus, the P3 dimerization domain plays a key role in promoting interactions between P1 and P4. The presence of CheW and deactivating Tm14 receptor³⁷ decreased disulfide formation (Figure 3-8) by inhibiting the P1

and P4 interaction. This was observed only for the species that contained the P5 domain (P1*+P3P4P5*, CheA_{FL}*, and 41AA*) as the P5 domain serves as the regulatory domain facilitating communication with Tm14 and CheW.

3.4.4: Dynamics of the CheA P1-P2. The P3P4P5 portion of the CheA_{FL} structure (also known as Δ 289) composes the globular core of the enzyme,⁷ which has now been confirmed in solution by SAXS studies. Both *T. maritima* and *E. coli* CheA_{FL} were found to be essentially globular (Figure 3-10, Figure 3-11) in their nucleotide free states.⁴⁰ This is also true for Δ P2 variants. The P3P4P5 core undergoes little to no change upon addition of nucleotide thus, any changes in conformational properties remains under the detection limit of SAXS (Figure 3-9A). However, in the presence of non-hydrolyzable ATP analog (ADPCP), CheA_{FL} and the Δ P2 variants show a dramatic change in conformational state, in which a substantial portion of the molecule behaves as a Gaussian chain (Figure 3-10). Conformation of nucleotide binding causing changes in the SAXS profiles of CheA_{FL} and Δ P2 was achieved by the inability of the ATP-binding potent D449A to undergo such a conformational transition (Figure 3-12). Circular dichroism wavelength scans show no loss in helical content of the CheA_{FL} or the Δ P2 in the presence of the same ATP analog (Figure 3-13), thereby signifying that the changes observed in the SAXS data are not attributed to protein unfolding. CheA_{FL} has a more drastic change due to the presence of the P2 domain, which exhibits an intrinsic flexibility independent of the CheA core. This can perhaps be rationalized as conversion of an ordered globular P1-P5 unit to a species with a smaller globular core (P3P4P5) and a conformationally flexible region that samples a large range of spatial coordinates.

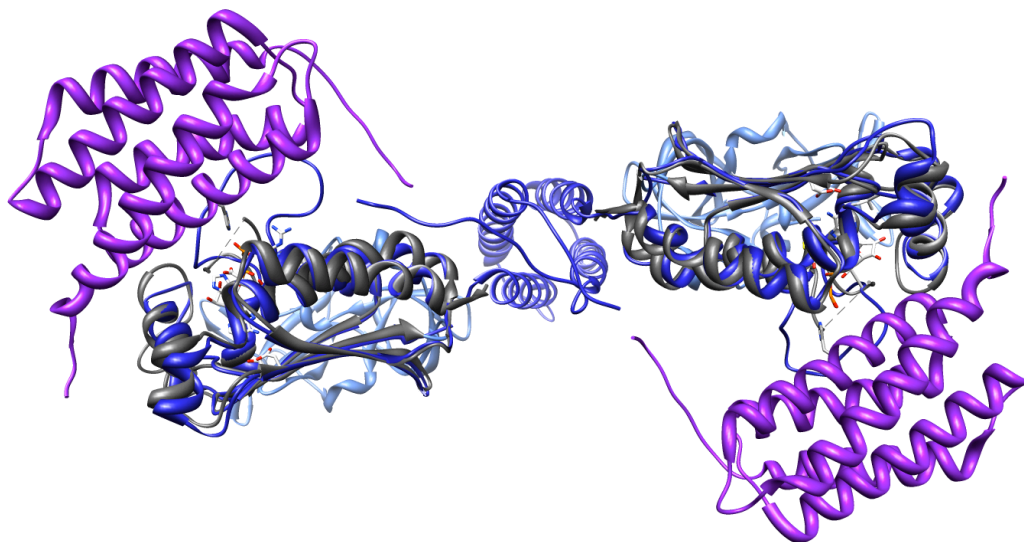


Figure 3-14: Model of 41AA variant. 41AA variant structure prediction with P1 active sites near the P4 active sites. The extra helix from the C-terminus of the P1-P2 linker is oriented to be near the P2-P3 linker. While displayed with the P1 in a trans orientation, the gaps in the linkers are positioned such that the 41AA would cause the linker to be taut and incapable of trans autophosphorylation unlike that of the 47AA variant.^{7,14}

In summary CheA in *T. maritima* undergoes trans autophosphorylation, as in *E. coli* CheA. For *T. maritima* CheA cis autophosphorylation is possible yet less preferred. CheA has a natural basal activation *in vitro*, where upon addition of nucleotide, the enzyme becomes dynamic to allow association of the P1 domain and the P4 domain of the other subunit. Importantly, the P3 dimerization domain is essential for promoting interactions between P1 and P4. Furthermore, disconnection of the P1 domain from the P3P4P5 core increases the P1-P4 contact. Given that a disconnected P1 requires a second order reaction for P1-P4 contact, it is surprising this process diminishes when the domain is tethered to P4. This finding suggests that P1 is somehow prevented from accessing P4 in the context of the full-length enzyme. Because the Δ P2 variants have the same behavior, this internal steric inhibition does not involve P2. Importantly, relief of this constraint may contribute to CheA regulation by receptors. Finally, locking the P1 and P4 domains together through cross linking provides a means to trap their interaction and thereby

study imperative contact residues required to achieve autophosphorylation through crystallographic or other structural approaches.

REFERENCES

- (1) Casino, P.; Miguel-Romero, L.; Marina, A. *Nat. Commun.* **2014**, *5*.
- (2) Yamamoto, K.; Hirao, K.; Oshima, T.; Aiba, H.; Utsumi, R.; Ishihama, A. *J. Biol. Chem.* **2005**, *280*, 1448–1456.
- (3) Adler, J. *Annu. Rev. Biochem.* **1975**, *44*, 341–356.
- (4) Koshland, D. E. *Annu. Rev. Biochem.* **1981**, *50*, 765–782.
- (5) Falke, J. J.; Bass, R. B.; Butler, S. L.; Chervitz, S. A.; Danielson, M. A. *Annu. Rev. Cell Dev. Biol.* **1997**, *13*, 457–512.
- (6) Wadhams, G. H.; Armitage, J. P. *Nat. Rev. Mol. Cell Biol.* **2004**, *5*, 1024–1037.
- (7) Bilwes, A. M.; Alex, L. A.; Crane, B. R.; Simon, M. I. *Cell* **1999**, *96*, 131–141.
- (8) Stewart, R. C.; Jahreis, K.; Parkinson, J. S. *Biochemistry (Mosc.)* **2000**, *39*, 13157–13165.
- (9) Jahreis, K.; Morrison, T. B.; Garzón, A.; Parkinson, J. S. *J. Bacteriol.* **2004**, *186*, 2664–2672.
- (10) Wang, X.; Vallurupalli, P.; Vu, A.; Lee, K.; Sun, S.; Bai, W.-J.; Wu, C.; Zhou, H.; Shea, J.-E.; Kay, L. E.; Dahlquist, F. W. *Biochemistry (Mosc.)* **2014**, *53*, 855–861.
- (11) Wang, X.; Wu, C.; Vu, A.; Shea, J.-E.; Dahlquist, F. W. *J. Am. Chem. Soc.* **2012**, *134*, 16107–16110.
- (12) Swanson, R. V.; Bourret, R. B.; Simon, M. I. *Mol. Microbiol.* **1993**, *8*, 435–441.
- (13) Gloor, S. L.; Falke, J. J. *Biochemistry (Mosc.)* **2009**, *48*, 3631–3644.
- (14) Mo, G.; Zhou, H.; Kawamura, T.; Dahlquist, F. W. *Biochemistry (Mosc.)* **2012**, *51*, 3786–3798.
- (15) Bilwes, A. M.; Quezada, C. M.; Croal, L. R.; Crane, B. R.; Simon, M. I. *Nat. Struct. Mol. Biol.* **2001**, *8*, 353–360.

- (16) Quezada, C. M.; Hamel, D. J.; Grădinaru, C.; Bilwes, A. M.; Dahlquist, F. W.; Crane, B. R.; Simon, M. I. *J. Biol. Chem.* **2005**, *280*, 30581–30585.
- (17) Natale, A. M.; Duplantis, J. L.; Piasta, K. N.; Falke, J. J. *Biochemistry (Mosc.)* **2013**, *52*, 7753–7765.
- (18) Bass, R. B.; Butler, S. L.; Chervitz, S. A.; Gloor, S. L.; Falke, J. J. In *Two-Component Signaling Systems, Pt B*; Methods In Enzymology; 2007; Vol. 423, pp. 25–51.
- (19) Nishiyama, S.; Garzón, A.; Parkinson, J. S. *J. Bacteriol.* **2014**, *196*, 257–264.
- (20) Zhang, J.; Xu, Y.; Shen, J.; Luo, X.; Chen, J.; Chen, K.; Zhu, W.; Jiang, H. *J. Am. Chem. Soc.* **2005**, *127*, 11709–11719.
- (21) Shi, T.; Lu, Y.; Liu, X.; Chen, Y.; Jiang, H.; Zhang, J. *J. Phys. Chem. B* **2011**, *115*, 11895–11901.
- (22) Piasta, K. N.; Ulliman, C. J.; Slivka, P. F.; Crane, B. R.; Falke, J. J. *Biochemistry (Mosc.)* **2013**, *52*, 3866–3880.
- (23) Ninfa, E. G.; Stock, A.; Mowbray, S.; Stock, J. *J. Biol. Chem.* **1991**, *266*, 9764–9770.
- (24) Skou, S.; Gillilan, R. E.; Ando, N. *Nat. Protoc.* **2014**, *9*, 1727–1739.
- (25) Nielsen, S. S.; Møller, M.; Gillilan, R. E. *J. Appl. Crystallogr.* **2012**, *45*, 213–223.
- (26) Nielsen, S. S.; Toft, K. N.; Snakenborg, D.; Jeppesen, M. G.; Jacobsen, J. K.; Vestergaard, B.; Kutter, J. P.; Arleth, L. *J. Appl. Crystallogr.* **2009**, *42*, 959–964.
- (27) Konarev, P. V.; Volkov, V. V.; Sokolova, A. V.; Koch, M. H. J.; Svergun, D. I. *J. Appl. Crystallogr.* **2003**, *36*, 1277–1282.
- (28) Franke, D.; Svergun, D. I. *J. Appl. Crystallogr.* **2009**, *42*, 342–346.
- (29) Kozin, M. B.; Svergun, D. I. *J. Appl. Crystallogr.* **2001**, *34*, 33–41.
- (30) Volkov, V. V.; Svergun, D. I. *J. Appl. Crystallogr.* **2003**, *36*, 860–864.

- (31) Borkovich, K. A.; Simon, M. I. *Cell* **1990**, *63*, 1339–1348.
- (32) Ellefson, D. D.; Weber, U.; Wolfe, A. J. *J. Bacteriol.* **1997**, *179*, 825–830.
- (33) Hess, J. F.; Bourret, R. B.; Simon, M. I. *Nature* **1988**, *336*, 139–143.
- (34) Wolfe, A. J.; Stewart, R. C. *Proc. Natl. Acad. Sci.* **1993**, *90*, 1518–1522.
- (35) Park, S.-Y.; Quezada, C. M.; Bilwes, A. M.; Crane, B. R. *Biochemistry (Mosc.)* **2004**, *43*, 2228–2240.
- (36) Hirschman, A.; Boukhvalova, M.; VanBruggen, R.; Wolfe, A. J.; Stewart, R. C. *Biochemistry (Mosc.)* **2001**, *40*, 13876–13887.
- (37) Bhatnagar, J.; Borbat, P. P.; Pollard, A. M.; Bilwes, A. M.; Freed, J. H.; Crane, B. R. *Biochemistry (Mosc.)* **2010**, *49*, 3824–3841.
- (38) Kelly, S. M.; Jess, T. J.; Price, N. C. *Biochim. Biophys. Acta* **2005**, *1751*, 119–139.
- (39) Dutta, R.; Inouye, M. *Trends Biochem. Sci.* **2000**, *25*, 24–28.
- (40) Briegel, A.; Ames, P.; Gumbart, J. C.; Oikonomou, C. M.; Parkinson, J. S.; Jensen, G. J. *Mol. Microbiol.* **2013**, *89*, 831–841.

CHAPTER 4: STRUCTURE AND ACTIVITY OF A CHEA KINASE VARIANT THAT UNDERGOES ENHANCED AUTOPHOSPHORYLATION

4.1: Introduction

Kinases play an essential role in a multitude of intracellular processes by acting as sensors, processors, modulators, and transducers of signals.¹⁻³ Bacterial chemotaxis signaling pathway depends on the propagation of the extracellular signals through membrane incorporated chemoreceptor arrays containing methyl-accepting chemotaxis protein receptors (MCP), the histidine kinase CheA, and the coupling protein CheW. CheA is a multi-domain dimeric histidine kinase that acts as the primary enzyme in the phospho-relay pathway. A central question in chemotaxis is how the autophosphorylation activity of CheA is regulated and what conformational transitions convert its inactive and active states. Despite extensive crystallographic characterization of its various modules a structure of the full length protein has yet to be determined due to the long flexible linker regions between the domains. Recent studies have revealed the importance of these CheA linker regions to kinase regulation.^{4,5}

Several biochemical and crystallographic studies have been conducted to elucidate the organization of the receptor arrays,⁶⁻¹⁰ as well as identify the specific interactions between the MCPs, CheA, and CheW in the extended lattice (Figure 1-13). Communication between these proteins is essential for the initiation of the phospho-relay leading to flagellar rotor rotational switching.¹¹⁻¹³ Previously determined *T. maritima* CheA structures have furthered our understanding of the P4 and the P5 domain arrangements within the lattice.¹⁴⁻²⁰ Electron cryo tomography (ECT) images⁹ of the hexagonal lattice defines a protein organization that can be interpreted in terms of the crystal structure of the P5/CheW ring in complex with a Tm14 MCP

dimer.¹⁶ However, the domain arrangements in the most complete structure of CheA to date, which composes the core P3P4P5 domains ($\Delta 289$)¹⁵ is not consistent with the array model. Here, the minimal unit of *T. maritima* CheA with enhanced autophosphorylation activity is characterized: the dimer formed from the P3P4 domains (see Chapter 3). The dimerization (P3) and kinase (P4) activity together produce a highly activated species, thus proving essential for CheA activation. The structure exhibits a planar arrangement of the domains, consistent with the orientation of CheA in the receptor arrays seen by electron microscopy. Employing ³²P radiolabeled biochemical assays and crystallographic methods; a model was generated of the active P3P4 domain arrangements within CheA that mimics the *in vivo* configuration in the lattice. Coupling crystallographic and biochemical data, to account for variation in CheA enzymatic activity, and identify key structural features for signal transduction in bacterial chemotaxis.

4.2: Materials and Methods

4.2.1: Cloning and protein purification. Various constructs were PCR cloned into the pET28a vector with NdeI and BamHI restriction sites. Proteins were purified as described previously.²¹

4.2.2: Activity of CheA_{FL} and separated histidine phosphotransfer and kinase domains. CheA_{FL} or isolated domains (10 μ M monomer) were prepared overnight in TKEDM buffer (50 mM KCl, 10 mM MgCl₂, 0.5 mM DTT, 0.5 mM EDTA, 5 mM Tris pH 7.5) and made up to a total volume of 25 μ L. After 12 hours preincubation at 4 °C the samples were incubated with 2 μ L of a hot solution containing 2.3 mM cold ATP and 3-8 μ L of [γ -³²P] ATP (3000 Ci/mmol, 10 mCi/mL, Perkin Elmer) for 6 minutes at indicated temperature, then quenched with 25 μ L of 3 \times SDS containing 50 mM EDTA pH 8.0. Then 30 μ L of the samples were subjected to gel electrophoresis on a gradient 4-20% Tris-glycine SDS-PAGE gel. The gel was stained with

Coomassie blue, destained with water, and dried with GelAir dryer. The dried gel was placed in a cassette for at least 24 hours, imaged with Storm phosphoimager (GE Healthcare), and then analyzed with ImageJ and the kinetic data was fit to $P_t = A_0(1 - e^{-kt})$ or $P_t = A_0'e^{-k(t-t_0)}$.

4.2.3: Crystallization and Data collection. The P3P4 domain structure of *T. maritima* CheA was determined to 2.83 Å resolution in space group P2₁2₁2₁. The P3P4 crystals were obtained by vapor diffusion by mixing 1 µL of protein (700 µM monomer and 1.3 mM α,β-methyleneadenosine 5'-triphosphate) and 1 µL of well solution, against a reservoir containing 0.5 M Ammonium sulfate, 0.1 M sodium citrate tribasic dihydrate pH 5.6, and 1.0 M lithium sulfate monohydrate (Hampton) research at 4 °C. Diffraction data were collected at the Cornell High Energy Synchrotron Source (CHESS) A1 beam line on an ADSC Quantum 210 CCD detector. The crystal was flash frozen with 25% glycerol. Data were processed with HKL2000.²² Molecular replacement using individual domains P3 residues 293-353 and P4 residues 354-540 from the search model 1B3Q was performed using Phenix (LLG=329, TFZ=16).²³ Model Refinement was carried out with Phenix²³ and model building performed with Coot.²⁴

4.2.4: Modeling. Models were generated using supramolecular overlap function in Coot.²⁴ The placement of the P5 domain was altered from the original overlay using 1B3Q as the arrangement of the domains were based upon crystal packing in the original structure. Through the rotation of the domains, steric clash was still avoided, yet this allowed for a more planar orientation of the P5/CheW alternating rings to one another. The crystal structures used were from *T. maritima* (1B3Q, 4JPB)^{15,16} and *E. coli* (2LP4)²⁵

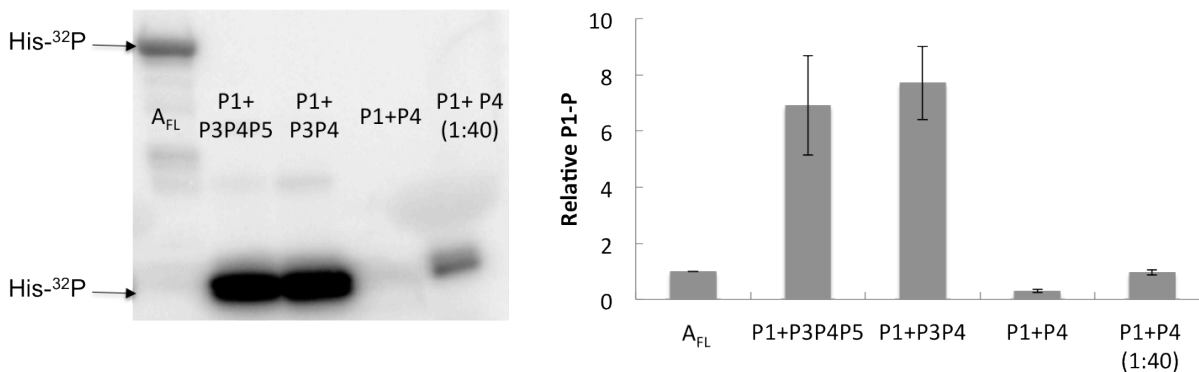


Figure 4-1: Activity of CheA_{FL} and separated domains. Phosphorimage of a radioisotope gel and bar plot of CheA_{FL} vs. separated domains (10 μM) at 55 °C, 6 minutes after incubation shows that separation of the P1 from the P4 domain increases activity, but only if the P3 domain is also present.

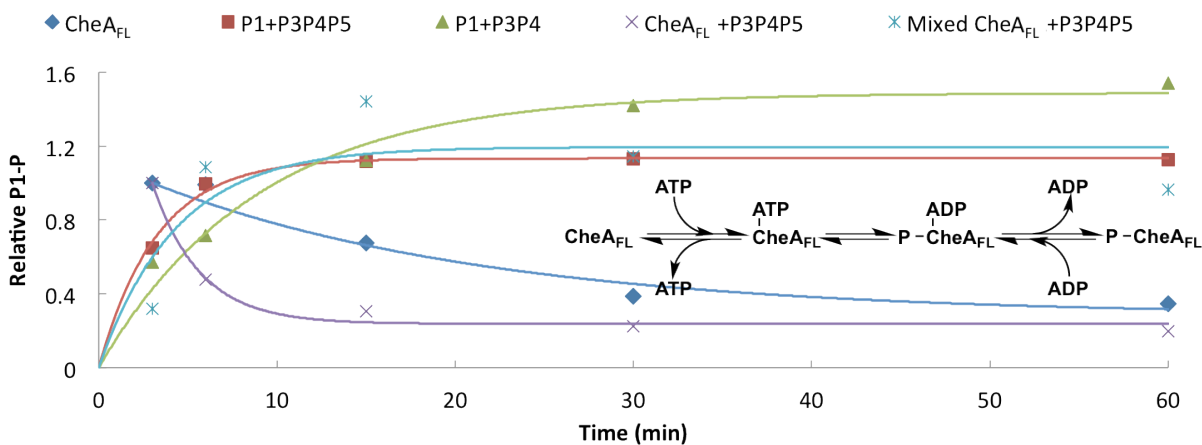


Figure 4-2: CheA_{FL} and separated domains activity over time. Activity over time of CheA (10 μM) and separated domains, all are at 55 °C over time, all CheA listed is made relative to 1 initially. The separated domains and CheA_{FL}:P3P4P5 mixed dimer increase in activity over time. While CheA_{FL} or CheA_{FL} with extra P3P4P5 present decrease in activity over time when heated. The *in vitro* phosphorylation of CheA_{FL} equilibrium reaction (inset) describes each step and how the reverse reaction can be forced.

4.3: Results

4.3.1: Separated P1+P3P4 has higher activity than CheA_{FL}. It has been previously shown that P3P4P5 can phosphorylate P1 with an activity similar to that of CheA_{FL}.²⁶ However, here both P1+P3P4P5 and P1+P3P4 were found to show higher transfer yields of the γ-phosphate from

ATP to P1 compared to CheA_{FL}, (Figure 4-1).²⁷ Over time, the separated domains dimerization domain reach elevated saturation levels compared to CheA_{FL} (Figure 4-2 and Table 4-1) which was fit to $P_t = A_0(1 - e^{-kt})$. In contrast, P1+P4 produced very little P1-P, thereby establishing P3P4 as the minimal unit required for high levels of CheA activity. The separated domains produced increased P1-P over time whereas, CheA_{FL} activity decreased was fit to $P_t = A_0'e^{-k(t-t_0)}$. Addition of P3P4P5 to CheA_{FL} did not increase the activity of CheA_{FL}, thereby indicating that P3P4P5 cannot phosphorylate the P1 domain of CheA_{FL}. However, heat induced subunit exchange of CheA_{FL} and P3P4P5 produced nearly as much CheA-P as in the case of the isolated domain. To ensure that the separated domains can participate in the same phosphatase reactions as CheA_{FL}, excess ADP was added to shift the equilibrium to favor production of ATP. In all cases ADP addition after an initial 6 minutes of exposure, diminished the presence of P1-P (Figure 4-3 and Table 4-1).

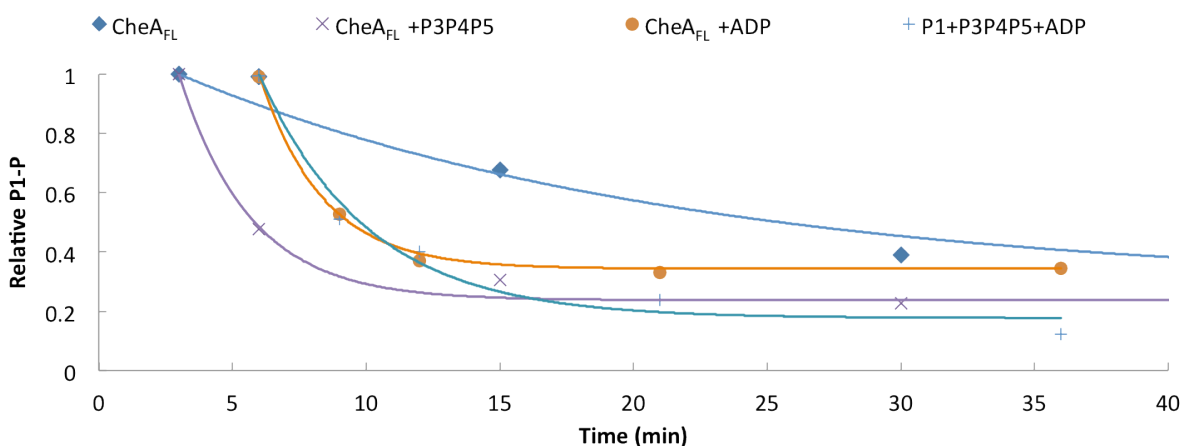


Figure 4-3: Addition of ADP to CheA_{FL} and separated domains deplete P1-P. Activity of CheA (10 μ M) and separated domains, all are at 55 $^{\circ}$ C except when indicated over time. After 6 minutes of initial exposure to hot ATP, cold ADP (2 mM) was added to force the reverse reaction. Addition of kinase in the form of P3P4P5 to CheA_{FL} does not increase activity. Both CheA_{FL}-P and P1-P of the separated domains decrease after addition of cold ADP as expected.

Components	A_0 (P1-P formation)	k (minutes ⁻¹)	R^2
P1+P3P4P5	1.13 ± 0.05	0.30 ± 0.05	0.99
P1+P3P4	1.4 ± 0.2	0.11 ± 0.05	0.97
Mixed CheA _{FL} +P3P4P5	1.1 ± 0.4	0.2 ± 0.1	0.79
CheA _{FL}	$0.7 \pm 0.3^*$	0.05 ± 0.04	0.95
CheA _{FL} +P3P4P5	$0.7 \pm 0.1^*$	0.3 ± 0.2	0.98
CheA _{FL} +ADP	$0.65 \pm 0.03^*$	0.42 ± 0.06	0.99
P1+P3P4P5+ADP	$0.8 \pm 0.1^*$	0.2 ± 0.1	0.97

Table 4-1: Kinetic parameters for CheA autophosphorylation assays. Rate constant and prefactor values from relative activity plots. The * denotes A_0' in the equation: $P_t = A_0' e^{-k(t-t_0)}$.

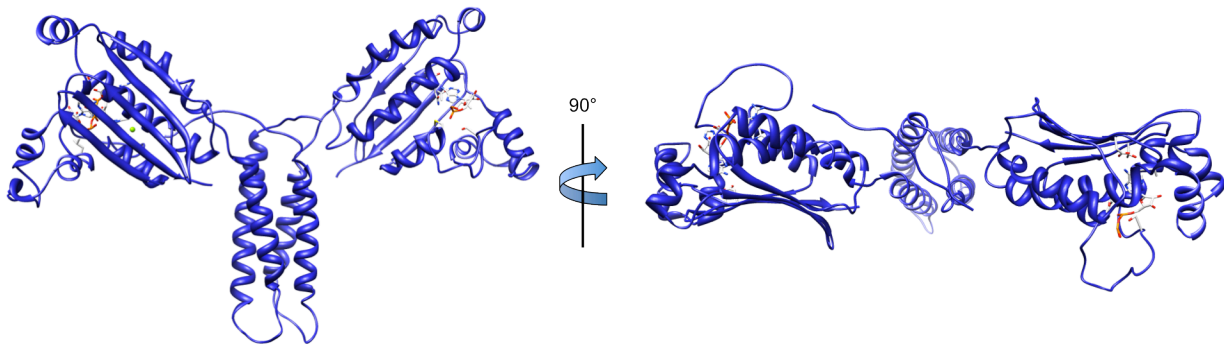


Figure 4-4: P3P4 crystal structure. Ribbon structure of P3P4 depicted in blue obtained with nucleotide present in binding pocket. The structure is planar and has residues 289-293 of one of the P3 domains elucidated.

4.3.2: *Structure of CheA P3P4.* The crystal structure of the P3P4 domains was determined to 2.8 Å resolution (Figure 4-4). The P3 domain is composed of two α -helices that form a coiled coil dimer. The P4 domain has a characteristic Bergerat ATP binding fold.² Unlike the previously crystallized P3P4P5 structure the P4 domains reside in a narrow plane with their β -sheets roughly aligned with the helical axis of the P3 domain and their ATP pockets facing 180° from each other (Fig. 4-4). Where the P4 domains are roughly perpendicular with respect to each other within the dimer,¹⁵ the P3P4 structure retains a planar conformation of the P4 domains. The unit cell and space group differs significantly from the P3P4P5 structure, reflecting the substantial differences in crystal contact geometry (Table 4-2) caused by the P5 domain contact points in

P3P4P5. Due to the large solvent channels present in the lattice, soaking the P3P4 crystal with the histidine phosphotransfer domain (P1) was attempted. Upon incorporation into the crystal, the lattice was destroyed thus, indicating conformation rearrangements within the lattice structure as a result of integration of P1.

Data Collection Statistics	
Space Group	P2 ₁ 2 ₁ 2 ₁
Unit Cell:	
Length (Å)	Angle (°)
a = 66.4	α = 90
b = 131.4	β = 90
c = 147.0	γ = 90
Unique Reflections	30783
Resolution (Å)	49.2-3.0
Redundancy	5.2/5.4
Completeness (%)	98 (97.4)
I/σ	14.5/8.8
R _{pim} (3.0 Å)	0.075 (0.659)
CC ½ (3.0 Å)	0.511
Refinement Metrics	
R _{work}	0.2322
R _{free}	0.2860
No. atoms	4014
RMSD from ideal bond lengths (Å)	0.011
RMSD from ideal bond angles (Å)	1.7
B-factors (Å ²)	
Main chain	44.3
Side Chain	52.5
Nucleotide	133

Table 4-2: Data collection and refinement statistics for the P3P4 structure.

4.3.3: *Comparison of P3P4 to the structure of P3P4P5.* Superimpositions of the kinase domain from either P3P4P5¹⁵ or P4¹⁴ onto the P3P4 structure show little difference in the main chain of the kinase domain outside of the ATP lid region (Figure 4-5). Electron density in the binding pocket reveals the presence of an adenosine nucleotide in a similar conformation as that found in the P4 crystal structure (Figure 4-6).¹⁴ However, a portion of the ATP lid (493-503)⁷ is

characteristically disordered thus precise structure is difficult to discern for this region, although a backbone conformation is depicted in the structural figures. Unlike previously published structures of the CheA P3 domain, the electron density corresponding to the terminal linker region preceding the P3 domain (residues 289-292) remains visible in one of the monomers (Figure 4-7).¹⁵ These residues are oriented adjacent to the α -helices of the P4 domain in an arrangement that supports the bias of the P1P2 domains to adopt a trans configuration with respect to the intra-monomer P4 domain. This P1-P4 configuration derived from this data can rationalize the observation that *T.m.* CheA undergoes trans autophosphorylation across the dimer (Chapter 3).

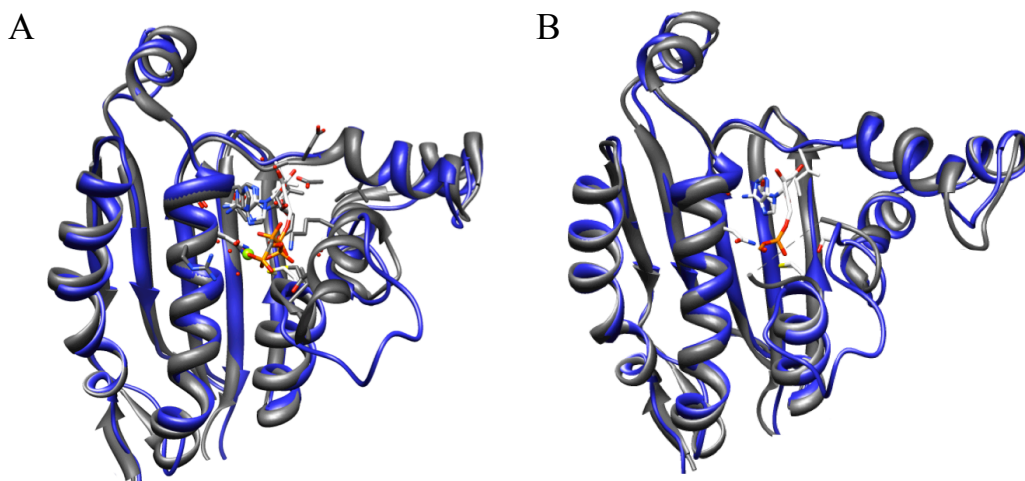


Figure 4-5: Overlay of P3P4 kinase domain with existing crystal structures. Kinase domain overlays of P4¹⁴ (A) and P3P4P5¹⁵ (B) crystal structures on P3P4 (blue).

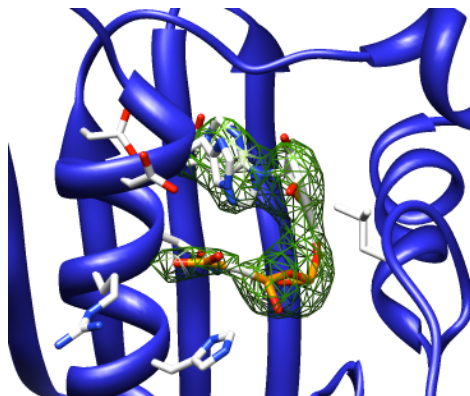


Figure 4-6: Electron density of nucleotide within the P4 domain. ADPCP is placed in the density within the ATP binding pocket.

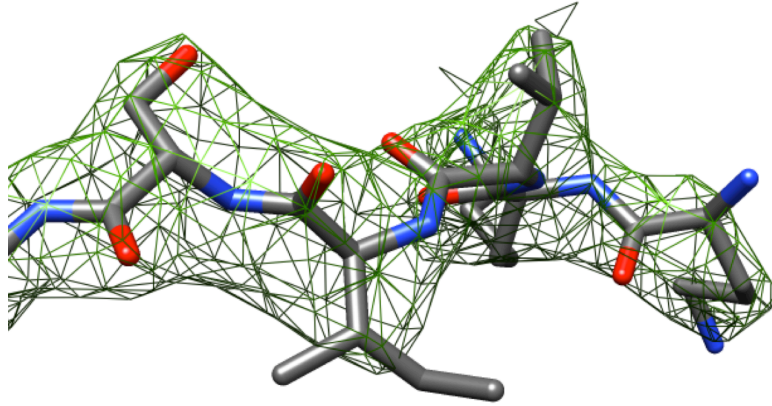


Figure 4-7: Electron density of the linker. Residues 289-293 from the C-terminus end of the P2-P3 linker electron density with residues placed that have not been previously visualized.

4.3.4: *Extrapolating the P3P4 structure to a full length CheA:CheW complex.* In order to generate a model of CheA_{FL}, bound to CheW, the P4P5 modules from the *T.m.* P3P4P5 (Δ 289) structure were superimposed separately onto the respective kinase domains of the P3P4 structure (Figure 4-8).¹⁵ If the dimerization domains are overlain, the P3-P4 linker N-terminus residues Arg354 and Met355 are in a different orientation leading the rest of the linker to orient the P4 domains perpendicular to one another in the P3P4P5 crystal structure. In the kinase superposition, the P5 domains reside directly underneath the P4 domains and do not clash with the P3 domain. In the resulting P3P4P5 structure the P5 domains lie in a plane, roughly perpendicular to the P4 domains. The complex of P5 domain and the coupling protein CheW¹⁶ were then superimposed based on alignment of the respective P5 modules and the resulting structure was again free of any steric clashes (Figure 4-9). To further develop the model the P1 domain²⁵ was docked in a conformation productive for autophosphorylation. The *E. coli* CheA P1 domain²⁵ substrate His48 was placed 7 Å from the exposed His405 residue in the P4 domain.²⁸ The P1 domain such that its C-terminus would join to the P3 N-terminus and direct the substrate His for trans phosphorylation from the adjacent subunit (Figure 4-10). The His405 on the exterior of the *T.m.* P4 active site, as the 405 residue indicated by Bilwes¹⁴ is near the γ -

phosphate of ATP when bound in the P4 binding pocket. The P1 C-terminal region forms another α -helix that aligns antiparallel relative to the terminal helix of the P1 4-helix bundle. This ordered connection constrains P1, especially when the linker is shortened to the minimal length that allows trans phosphorylation (47AA, see Chapter 3). Taking into consideration this minimal linker length there are no steric conflicts between any of the other CheA domains or CheW.

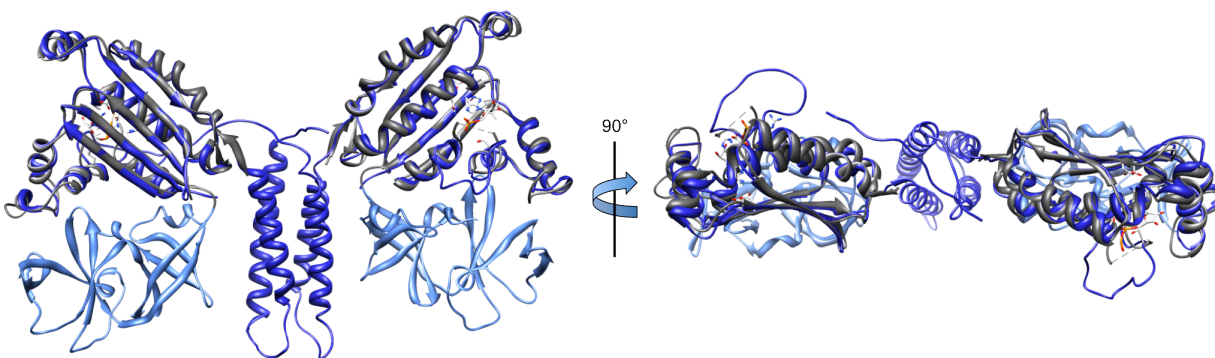


Figure 4-8: Grafting P4 unto the P3P4 structure. Superposition of the respective P4 domains places P5 from the P4P5:CheW complex onto the P3P4 structure without the introduction of steric clashes. P4 is in gray and P5 is in pale blue.¹⁵ The P5 domain was rotated in the plane by less than 5° toward the P4 domain and away from the P3 domain to enable the formation of a planar arrangement of the CheW/P5 rings.

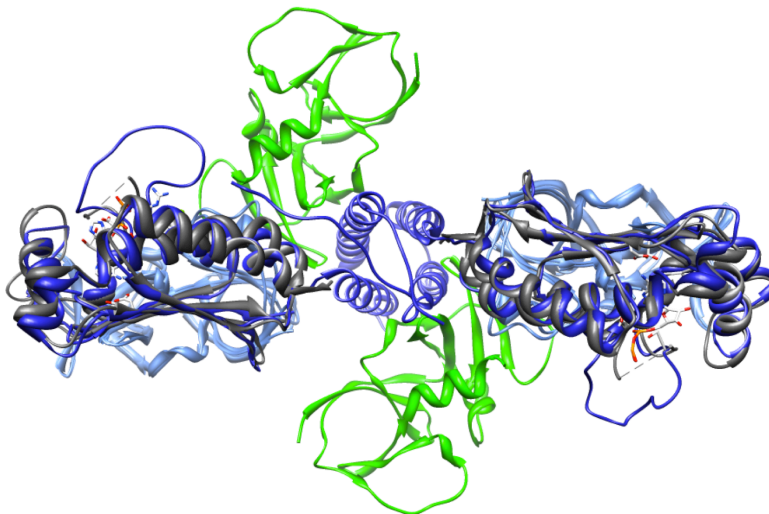


Figure 4-9: Grafting CheW onto the P3P4P5 structure. CheW (green) in complex with P5 (pale blue) are overlaid onto the P3P4 structure with P4P5 from Figure 4-8.¹⁶

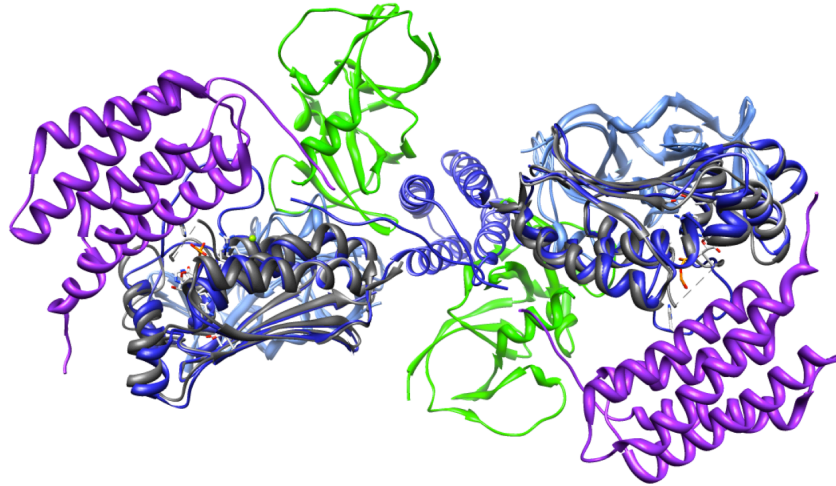


Figure 4-10: Modeling the 41AA variant with intact P1 domain. P1 NMR structure²⁵ added to depict structure CheA with CheW within the array. The His48 (*E. coli*) residue is near His405 (*T. maritima*). The linker is oriented in a position for the 41AA variant, the gaps are a result of this variant is not capable of trans autophosphorylation.

4.3.5: *A full array model based on the P3P4 structure.* Previous modeling of the CheA chemoreceptor array based on cryoEM and crystal structures required rotations about the P3-P4 linker regions to orient the two P5 units in a planar arrangement required by the extended P6 symmetry of the lattice (Figure 4-11).⁷ As shown, the new P3P4 structure has the appropriate juxtaposition of the P3 and P4 domains to form the planar lattice, thus demonstrating that the linker can achieve this conformation. The new CheA:CheW model was easily overlaid onto the hexagonal P5/CheW ring depicted by Li et al (Figure 4-11).⁵ This generated a model of CheA in the array that is similar in topology to the honeycomb lattice present in the EM images.⁹ The MCP trimer-of-dimers resides at the vertices of the hexagon and interact directly with CheW and P5 domain of CheA based upon the location of MCP Tm14 in the ternary crystal structures.¹⁶ Overall, the planarity of the P3P4P5 structure allows the CheW/P5 rings to extend in a hexagonal two-dimensional lattice. The P4 domains reside below in a position that can accommodate their interaction with P1.

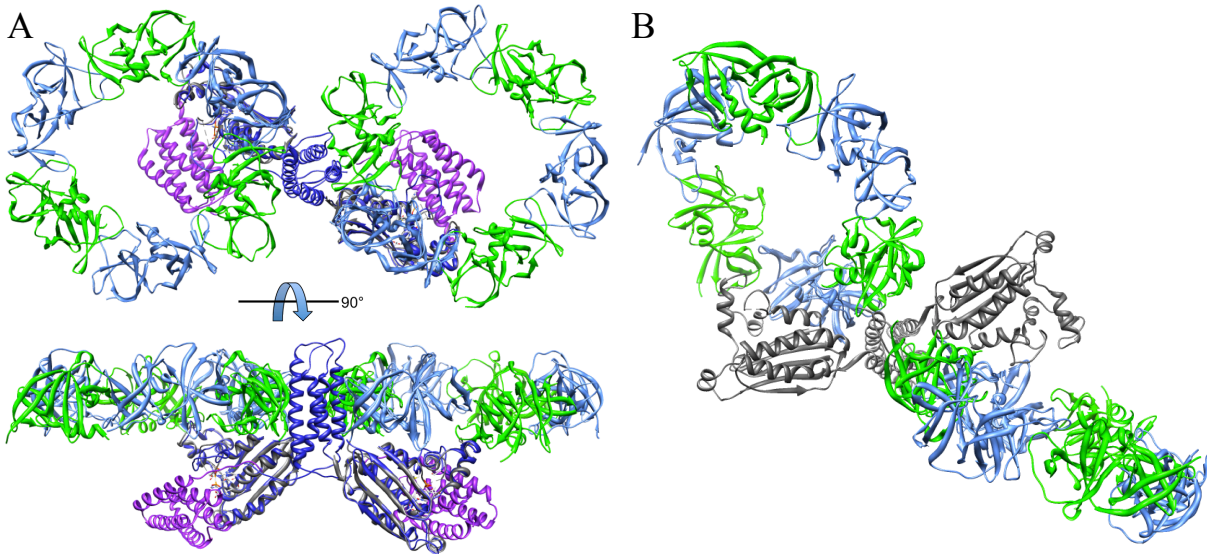


Figure 4-11: Planar vs. orthogonal CheW/P5 ring structures. **A:** Planar CheA structure with CheW/P5 ring overlay.¹⁶ **B:** P3P4P5 structure of the CheW/P5 rings almost perpendicular to one another is not compatible with an extended array.

4.4: Discussion

4.4.1: *CheA* activity. Due to the thermophilic nature of, *T. maritima*, the enzymatic activity of the multi-domain histidine kinase CheA is optimum at elevated temperatures.²⁹ This dependence could be due to the increased rate of intermolecular interactions at higher temperatures, which is closer to the physiological environment of the bacterium or related to increased active site dynamics necessary for catalysis. As the thermal energy of the system increases, the P1 and P4 domains come into contact more frequently, enabling interdomain phosphotransfer or increase the strength of hydrophobic contacts which can also modulate activity. When separated from P1 the P4 domain alone exhibits very low kinase activity, even when P4 is present in large excess (a 40 P4:1 P1 molar ratio is needed to observe any autophosphorylation).¹⁴ However, when the dimerization domain (P3) is fused to P4, there is a large increase in activity, thus indicating a P3 dependence for kinase activity (Figure 4-1). Both $\Delta 289$ and P3P4 in the presence of the P1 domain surpass the activity seen in full length CheA when incubated at 55 °C (Figure 4-2). This

may in part be due to the P3-P4 linker effecting the conformational state of the P4 domain⁴ and the spatial orientation of the kinase domains when P3 is present (Figure 4-4).⁵ It is also possible that P3 increases the affinity of P1 for P4 by interacting directly with P1, or that a second kinase domain facilitates phosphorylation by the first. CheA_{FL}-P decreases over long incubation times due to the prevalence of the reverse reaction, there are a couple possibilities for this observation. 1) The degradation of ATP to ADP increases with temperature, 2) there is a distinct difference between CheA in *E. coli* and *T. maritima* where the back reaction is more prevalent for *T. maritima*, and 3) the tethering of the P1 and P4 domains restricts both domains function. ATP is known to degrade over time. Both the sequence and structure of CheA is highly conserved across species.³⁰ When the P1 domain is tethered to the CheA core, there is a higher probability of the P1-P interacting with the kinase domain to generate ATP. Similarly, the reverse reaction can be increased for both CheA_{FL} and the separated domains by the addition of ADP.¹⁴ Both the CheA_{FL} and the separated domains show similar phosphatase activity, thus differences in this processes cannot explain the enhanced activity of the separated domains. Addition of P3P4P5, which is itself quite active for P1 phosphorylation cannot increase formation of P-CheA_{FL}. This finding suggests that the P1 domains may be sequestered within the full length enzyme. Indeed, when the CheA_{FL} subunits are exchanged with those of P3P4P5 autophosphorylation obtains levels similar to the separated domains. Thus, the two P1 domains within the CheA dimer may act to sequester each other. Removal of one P1 in the CheA_{FL}:P3P4P5 heterodimer (mixed dimer) removes this inhibition freeing the remaining P1 domain for access to the P4 domain. This result corroborates recent cryoEM studies on active and inactive receptor mutants that suggests the P1-P2 unit of CheA is more ordered in the inhibited state⁶ and prior studies that found negative subunit cooperativity in CheA activation.³¹

4.4.2: *CheA Domain Flexibility*. A complete structure *T. maritima* CheA structure has yet to be elucidated. In an effort to compensate for the deficiency, a nearly complete model of CheA was generated by superimposing existing crystal structures of the various domains with the core of the P3P4 structure determined in this study. Such an investigation has yielded a model of CheA that displays the appropriate spatial orientation of CheA within the array when compared to EM images.

In the structure¹⁵ of CheA P3P4P5 (Δ 289), the P4P5 domains are positioned almost orthogonally within the dimer. However, this structure did not contain nucleotide and most likely represents an inactive form of the enzyme. Interestingly, the conformation of the kinase domain within the structures of both the Δ 289 structure¹⁵ and the P4 domain¹⁴ also hold similar conformations as observed in the P3P4 forms (Figure 4-5). The P4P5 domains described by Bilwes¹⁵ were separately superimposed onto each kinase domain in P3P4 (Figure 4-8). From this overlay, the P5 and P3 domains show no steric conflict and the P5 domains reside directly beneath the P4 domains in a perpendicular retaining planarity of all the domains that comprise the CheA core. This is a drastically different structure than P3P4P5, and the domain orientations observed may be important for understanding kinase activity, particularly since they appear consistent with the constraints on the membrane arrays¹⁵

Taking this planar version of the CheA core, CheW was incorporated using the P5/CheW structure from Li.¹⁶ After overlay, P5 and CheW surround the P3 dimerization domains; yet avoiding any discernable steric clash (Figure 4-9). This enables the CheA dimer to span two honeycombs sections within the array, an arrangement that supported by other crystallographic and EM data.⁶⁻⁹ To have a more complete picture of CheA in the array, the *E. coli* P1 domain²⁵ (72% sequence identity to *T. maritima*) was oriented adjacent to the kinase domain. The addition

of the P1 domain creates no steric conflict with the rest of the CheA dimer (Figure 4-10). The specific location of the P1 domain was based on possible contact points between the P1 and P4 domain described by Natale,³² as well as taking into consideration the proximity of the active histidine (His48) to the γ -phosphate location in the P4 crystal structure.¹⁴ The solution structure of the P1 domain²⁵ is composed of four α -helices, with a fifth helix running antiparallel to the last helix of the P1 domain that is part of the linker between the P1 and P2 domains. The P1 is oriented next to a P4 domain of the opposite monomer with a 41-residue linker between the P1 and P3 domains, which appears to be quite taut (Chapter 3). While it remains to be established if the P1 is in its biologically relevant orientation necessary to achieve the transfer of the γ -phosphate, it is evident that a shorten linker would make be unable to accomplish trans-phosphorylation. Indeed, it was found that although the 47AA linker allows trans phosphorylation, a 41AA linker can only facilitate cis phosphorylation.

4.4.3: A molecular model for the chemoreceptor arrays. Based on the data generated in this investigation, the most complete structure of CheA and CheW in the array currently available was determined. Overlaying the P5/CheW ring onto the P3P4P5 structure,¹⁵ the rings would exist in a perpendicular disposition with respect to one another, similar to the configuration observed in the P4P5 domains which are not biologically relevant (Figure 4-11). In contrast, our structure of the P3P4 unit defines a P3-P4 linker conformation that allows for a planar arrangement and hence anchors a 2D hexagonal lattice. With the addition of the trimer-of-dimers receptors (Chapter 2), the array approaches what would be expected from the electron density visible from the ECT images (Figure 4-12).^{9,33} This architecture also accommodates a trans association between P1 and P4 with the minimal P1-P3 linker length. While different in domain juxtaposition, the P4 portion of the Δ 289 structure superimposes readily with the P4 portion of

the P3P4 structure. Because there are no obvious differences in internal domain structure, the increased activation of P3P4 is not likely an allosteric effect of P3 on P4. Instead, it is more likely that relief of internal inhibition generated through interactions of the two P1 domains causes activation of P3P4 and P3P4P5 relative to the full length enzyme. How changes in receptor conformation are able to alter P1 interactions remains to be established.

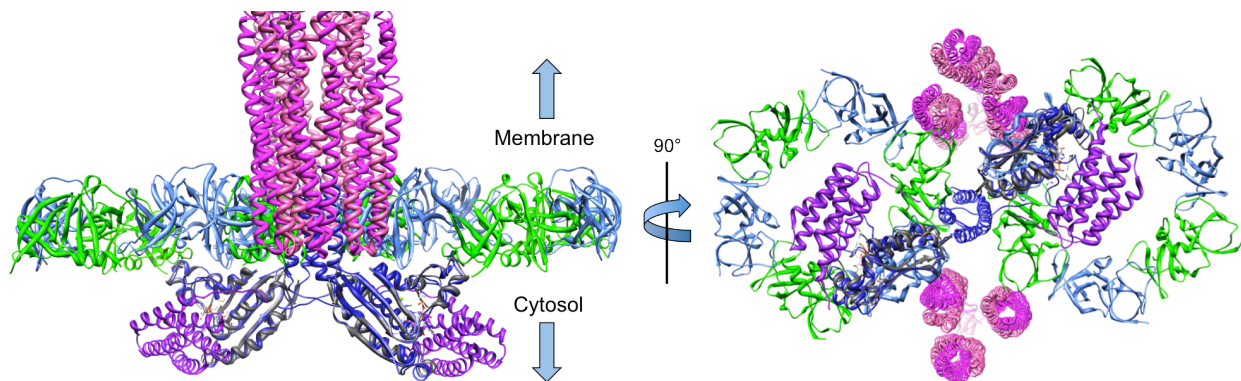


Figure 4-12: Depiction of the array *in vivo*. Model of CheA within the array with receptors³⁴ located at the vertices of the hexagonal P5/CheW ring from the side and below.

In summary, the high activity of the P3P4 domains, compared to P4 alone suggests that the regulation of the P4 kinase is P3 dependent. It remains to be established unclear whether this is an allosteric or structural effect. Furthermore, it was established that heterodimers of CheA containing only one P1 domain are much more active than symmetric dimers. Thus, in CheA_{FL} the P1 domains interfere with each other. Control of this inhibition may lie at the core of regulating CheA activity state. Recently, Li and Hazelbauer proposed a model of signal propagation in the array that the P3 domain plays a crucial role in amplification of the signal in the lattice.³⁵ Thus, the findings here and by others illuminate the importance of the dimerization domain for assembling the chemoreceptor arrays and also conferring high levels of autophosphorylation activity on CheA. Additionally, the crystal structure of P3P4 in the active conformation of the dimerization and kinase domains retains a planar orientation, a configuration

that was previously undetermined. Ultimately, a 3D model of CheA, CheW, and receptor was generated that agrees with the ECT density of the *in vivo* array. Overall, our current understanding of CheA has been advanced by defining new structures compatible with current array models and establishing key functions of modules within the multi-domain kinase.

REFERENCES

- (1) Casino, P.; Miguel-Romero, L.; Marina, A. *Nat. Commun.* **2014**, *5*.
- (2) Dutta, R.; Inouye, M. *Trends Biochem. Sci.* **2000**, *25*, 24–28.
- (3) Hoch, J. A.; Silhavy, T. J. *Two-component signal transduction*; ASM Press: Washington, D.C., 1995.
- (4) Wang, X.; Vallurupalli, P.; Vu, A.; Lee, K.; Sun, S.; Bai, W.-J.; Wu, C.; Zhou, H.; Shea, J.-E.; Kay, L. E.; Dahlquist, F. W. *Biochemistry* **2014**, *53*, 855–861.
- (5) Wang, X.; Wu, C.; Vu, A.; Shea, J.-E.; Dahlquist, F. W. *J. Am. Chem. Soc.* **2012**, *134*, 16107–16110.
- (6) Briegel, A.; Beeby, M.; Thanbichler, M.; Jensen, G. J. *Mol. Microbiol.* **2011**, *82*, 748–757.
- (7) Briegel, A.; Li, X.; Bilwes, A. M.; Hughes, K. T.; Jensen, G. J.; Crane, B. R. *Proc. Natl. Acad. Sci.* **2012**, *109*, 3766–3771.
- (8) Briegel, A.; Ortega, D. R.; Tocheva, E. I.; Wuichet, K.; Li, Z.; Chen, S.; Müller, A.; Iancu, C. V.; Murphy, G. E.; Dobro, M. J.; Zhulin, I. B.; Jensen, G. J. *Proc. Natl. Acad. Sci.* **2009**, *106*, 17181–17186.
- (9) Briegel, A.; Wong, M. L.; Hodges, H. L.; Oikonomou, C. M.; Piasta, K. N.; Harris, M. J.; Fowler, D. J.; Thompson, L. K.; Falke, J. J.; Kiessling, L. L.; Jensen, G. J. *Biochemistry (Mosc.)* **2014**, *53*, 1575–1585.
- (10) Shimizu, T. S.; Le Novère, N.; Levin, M. D.; Bevil, A. J.; Sutton, B. J.; Bray, D. *Nat. Cell Biol.* **2000**, *2*, 792–796.
- (11) Aizawa, S.-I.; Harwood, C. S.; Kadner, R. J. *J. Bacteriol.* **2000**, *182*, 1459–1471.
- (12) Blair, D. F. *Annu. Rev. Microbiol.* **1995**, *49*, 489–520.
- (13) Scharf, B. E.; Aldridge, P. D.; Kirby, J. R.; Crane, B. R. *Mol. Microbiol.* **2009**, *73*, 5–19.

- (14) Bilwes, A. M.; Quezada, C. M.; Croal, L. R.; Crane, B. R.; Simon, M. I. *Nat. Struct. Mol. Biol.* **2001**, *8*, 353–360.
- (15) Bilwes, A. M.; Alex, L. A.; Crane, B. R.; Simon, M. I. *Cell* **1999**, *96*, 131–141.
- (16) Li, X.; Fleetwood, A. D.; Bayas, C.; Bilwes, A. M.; Ortega, D. R.; Falke, J. J.; Zhulin, I. B.; Crane, B. R. *Biochemistry* **2013**, *52*, 3852–3865.
- (17) Park, S.-Y.; Beel, B. D.; Simon, M. I.; Bilwes, A. M.; Crane, B. R. *Proc. Natl. Acad. Sci. U. S. A.* **2004**, *101*, 11646–11651.
- (18) Park, S.-Y.; Borbat, P. P.; Gonzalez-Bonet, G.; Bhatnagar, J.; Pollard, A. M.; Freed, J. H.; Bilwes, A. M.; Crane, B. R. *Nat. Struct. Mol. Biol.* **2006**, *13*, 400–407.
- (19) Quezada, C. M.; Grădinaru, C.; Simon, M. I.; Bilwes, A. M.; Crane, B. R. *J. Mol. Biol.* **2004**, *341*, 1283–1294.
- (20) Vu, A.; Hamel, D. J.; Zhou, H.; Dahlquist, F. W. *J. Biomol. NMR* **2011**, *51*, 49–55.
- (21) Ninfa, E. G.; Stock, A.; Mowbray, S.; Stock, J. J. *Biol. Chem.* **1991**, *266*, 9764–9770.
- (22) Otwinowski, Z.; Minor, W. In *Methods in Enzymology*; Charles W. Carter, J., Ed.; Macromolecular Crystallography Part A; Academic Press, 1997; Vol. Volume 276, pp. 307–326.
- (23) Adams, P. D.; Afonine, P. V.; Bunkoczi, G.; Chen, V. B.; Echols, N.; Headd, J. J.; Hung, L. W.; Jain, S.; Kapral, G. J.; Kunstleve, R. W. G.; McCoy, A. J.; Moriarty, N. W.; Oeffner, R. D.; Read, R. J.; Richardson, D. C.; Richardson, J. S.; Terwilliger, T. C.; Zwart, P. H. *Methods* **2011**, *55*, 94–106.
- (24) Emsley, P.; Lohkamp, B.; Scott, W. G.; Cowtan, K. *Acta Crystallogr. D Biol. Crystallogr.* **2010**, *66*, 486–501.
- (25) Mo, G.; Zhou, H.; Kawamura, T.; Dahlquist, F. W. *Biochemistry* **2012**, *51*, 3786–3798.

- (26) Quezada, C. M.; Hamel, D. J.; Grădinaru, C.; Bilwes, A. M.; Dahlquist, F. W.; Crane, B. R.; Simon, M. I. *J. Biol. Chem.* **2005**, *280*, 30581–30585.
- (27) Surette, M. G.; Levit, M.; Liu, Y.; Lukat, G.; Ninfa, E. G.; Ninfa, A.; Stock, J. B. *J. Biol. Chem.* **1996**, *271*, 939–945.
- (28) Hirschman, A.; Boukhvalova, M.; VanBruggen, R.; Wolfe, A. J.; Stewart, R. C. *Biochemistry* **2001**, *40*, 13876–13887.
- (29) Park, S.-Y.; Quezada, C. M.; Bilwes, A. M.; Crane, B. R. *Biochemistry* **2004**, *43*, 2228–2240.
- (30) Wuichet, K.; Zhulin, I. B. *Sci Signal* **2010**, *3*, ra50.
- (31) Levit, M.; Liu, Y.; Surette, M.; Stock, J. *J. Biol. Chem.* **1996**, *271*, 32057–32063.
- (32) Natale, A. M.; Duplantis, J. L.; Piasta, K. N.; Falke, J. J. *Biochemistry* **2013**, *52*, 7753–7765.
- (33) Liu, J.; Hu, B.; Morado, D. R.; Jani, S.; Manson, M. D.; Margolin, W. *Proc. Natl. Acad. Sci.* **2012**, *109*, E1481–E1488.
- (34) Kim, K. K.; Yokota, H.; Kim, S.-H. *Nature* **1999**, *400*, 787–792.
- (35) Li, M.; Hazelbauer, G. L. *Proc. Natl. Acad. Sci. U. S. A.* **2014**, *111*, 15940–15945.

APPENDIX

CONCLUSIONS

This thesis focused upon CheA enzymology, structure, and the influence chemotaxis receptors have on CheA. The pre-formed trimer-of-dimers (Tar_{FO}) enabled formation of *in vitro* ternary complexes containing the CheA dimer and CheW monomers in the absence of crowding agents, nanodisks, or membranes. These variants were utilized to probe the structural interaction and regulation of CheA autophosphorylation. The Tar_{FO} 4Q and short both stimulated CheA autophosphorylation by increasing the population of kinase in an active form and facile conversion from the inactive conformation. The change in CheA conformation may be similar to the states of those achieved in the native membrane array. However, this increase in CheA phosphorylation activity is not translated downstream to the CheY-P formation. This could be evidence of a slight phosphatase activity the ternary complex components exhibit when not bound in the array. Further work will be accomplished by Alise Muok and Dipanjan Samanta to ascertain what features of the ternary complex contribute to the stability of each state and the subsequent generation of CheY-P. Overall, the Tar_{FO} modules provide useful tools for delineating key factors involved in the regulation of CheA activity.

CheA is also inherently active on its own *in vitro*, thus its structure and function can be probed. Interestingly, *T. maritima* CheA activity is highly dependent upon temperature although it is not a factor of protein unfolding. However, as temperature increases the generation of CheA-P is subjected to a phosphatase activity, possibility by bound ADP or the opposing P1 domain. This biexponential activity can be overcome by a mixed dimer comprised with only one P1 domain. Separation of the P1 and P3P4P5 domains resulted in no observable phosphatase activity compared to $CheA_{FL}$. Therefore, it is evident that the dimerization of the core is essential

for promoting the interaction between the kinase (P4) and histidine phosphotransfer (P1) domains. Recently, Li and Hazelbauer proposed a model of signal propagation in the array that the P3 domain plays a crucial role in amplification of the signal in the lattice.¹

It has been determined with the use of Δ P2 variants that *T. maritima* CheA naturally undergoes trans autophosphorylation, similar to that as *E. coli* CheA, although it is capable of cis but not preferred. Even without the P2 domain, CheA in both *T. maritima* and *E. coli*, exists as a globular protein in its resting state. Upon addition of nucleotide, CheA becomes highly dynamic with the release of the P1 domain from the globular core. Yet, it is the receptors that regulate CheA in the array and has been shown to limit the interaction between the P1 and P4 domains.

A disulfide bond formation occurs between the P1 His45 and P4 Ser492 residues, which supports the hypothesis of an association site existing between the P1 and P4 domains at these residues. Employing this P1-P4 contact point, a CheA model was generated using the obtained P3P4 crystal structure, thus producing a planar arrangement of the CheA core. Overlays of array components produced a model of CheA in the array, which agrees with the EM and ECT images of the *in vivo* arrays.²⁻⁵ Overall, our current understanding of CheA has been significantly advanced by confirming the planar arrangement of P3P4P5 in the array. Furthermore, inter-domain interactions has been elucidated, where the release of the P1 domain is triggered by nucleotide binding or an activating MCP a result that is contradictory to what is currently thought in the field.

REFERNCES

- (1) Li, M.; Hazelbauer, G. L. *Proc. Natl. Acad. Sci. U. S. A.* **2014**, *111*, 15940–15945.
- (2) Briegel, A.; Li, X.; Bilwes, A. M.; Hughes, K. T.; Jensen, G. J.; Crane, B. R. *Proc. Natl. Acad. Sci.* **2012**, *109*, 3766–3771.
- (3) Briegel, A.; Ding, H. J.; Li, Z.; Werner, J.; Gitai, Z.; Dias, D. P.; Jensen, R. B.; Jensen, G. J. *Mol. Microbiol.* **2008**, *69*, 30–41.
- (4) Zhang, P.; Khursigara, C. M.; Hartnell, L. M.; Subramaniam, S. *Proc. Natl. Acad. Sci.* **2007**, *104*, 3777–3781.
- (5) Liu, J.; Hu, B.; Morado, D. R.; Jani, S.; Manson, M. D.; Margolin, W. *Proc. Natl. Acad. Sci.* **2012**, *109*, E1481–E1488.